# CEMENT-BASED SENSORS
## FOR STRUCTURAL HEALTH MONITORING

by

**FAEZEH AZHARI**

B.Sc., Isfahan University of Technology, 2003

A THESIS SUBMITTED IN PARTIAL FULFILLMENT OF THE REQUIREMENTS FOR THE DEGREE OF

MASTER OF APPLIED SCIENCE

in

THE FACULTY OF GRADUATE STUDIES

(Civil Engineering)

THE UNIVERSITY OF BRITISH COLUMBIA

(Vancouver)

May 2008

# Abstract

The purpose of structural health monitoring is to continuously and accurately assess the performance of structures using a sensory system.

Recently introduced, cement-based sensors are piezoresistive and therefore can be used to sense stress/strain, simply by monitoring their electrical resistivity. These sensors, also known as smart (self-monitoring) structural materials can be used as a part or total component of structures and provide both structural capability and response to applied stress and damage.

In this study cement-based sensors are developed using two types of carbon fibres, as well as both single-walled and multi-walled carbon nano-tubes. A wide range of experiments were conducted to pinpoint the most efficient fibre content, frequency, electrode type and resistivity measurement technique. The influence of different parameters such as curing, temperature, moisture and chloride were also investigated.

The resistivity of the specimens increased with curing time, but became almost constant after a certain amount of time. The resistivity values decreased with increasing temperature and increased with the decrease in temperature at a rate of about 22-35 ohm-cm/°C. It was further found that moisture and chloride have a considerable influence on the electrical resistivity of these sensors.

Next, the response of the developed cement-based sensors to compressive, tensile and flexural loading was explored. The resistivity values from the sensors were compared with load and displacement values as well as strain data acquired from conventional strain gauges.

The results indicate that electrical resistivity of the sensors increases reversibly upon tension and decreases reversibly under compression provided that substantial cracking does not occur and the sensor remains in the elastic range.

Once a dense field of micro-cracking followed by macro-cracking occurs, these sensors respond distinctly, possibly even prior to the appearance of visible cracks, providing an early prediction of any upcoming failure.

The resistivity measurements under both compressive and tensile stress demonstrated an excellent correlation with strain. The developed sensors offer gauge factors well above those of electrical strain gauges.

It is concluded, therefore, that cement-based sensors can be the future alternative for conventional sensors in the structural health monitoring of concrete structures.

# Table of Contents

# List of Tables

# List of Figures

# List of Symbols

A: amperes; cross-sectional area

B: susceptance

C: capacitance

G: conductance

H: henrys

$f$ : frequency

$|Z|$ : magnitude of impedance

$\pi$ : pi: 3.14159

°: degrees

Hz: hertz

I: current intensity

L: inductance

ℓ: length

nm: nanometre

Q: quality factor

R: resistance (ohmic resistance)

Rad/sec: radians per second

$S.m^{-1:}$ siemens per metre

S: siemens

V: voltage

V: volts

X: reactance

$X_C$: capacitive inductance

$X_L$: inductive reactance

Y: admittance

Z: impedance

θ: phase angle

ρ: resistivity

σ: conductivity

ω: angular frequency

Ω: ohms

$Ω^{-1}$: mho

Ω-m: ohm-meters

# List of Abbreviations

AC: Alternating Current

CF: Carbon Fibre

CFCM: Carbon Fibre Cement Mortar

CFRC: Carbon Fibre Reinforced Cement-Based Composites

CNT: Carbon Nano-Tube

CNTCM: Carbon Nanotubes Cement Mortar

CPCF: Coal tar Pitch-based Carbon Fibres

C-S-H: Calcium-Silicate-Hydrate

DAQ: Data Acquisition system

DC: Direct Current

ECC: Engineered Cementitious Composites

FCR: Fractional Change in Resistivity

FOS: Fibre Optic Sensor

FRP: Fibre Reinforced polymer

GGBFS: Ground Granulated Blast Furnace Slag

GPIB: General Purpose Interface Bus

LCR: Inductance, Capacitance, Resistance

LCR: Inductance/Capacitance/Resistance

LVDT: Linear Voltage Differential Transducer

MC: Methylcellulose

MEMS: MicroElectroMechanical Systems

MWCNT: Multi-Walled Carbon Nano-Tube

NSM: Near-Surface Mounted

PE: Polyelectrolytes

PPCF: Petroleum Pitch-based Carbon Fibres

RLC: Resistor-Inductor-Capacitor

SCM: Supplementary Cementing Materials

SEM: Scanning Electron Microscopy

SHM: Structural Health Monitoring

SWCNT: Single-Walled Carbon Nano-Tube

$V_f$ : Volume Fraction

W/C: Water-to-Cement ratio

# Acknowledgements

It is a pleasure to thank the many people who made this thesis possible.

I would like to express my utmost gratitude to my supervisor, Professor Nemy Banthia whose guidance, support and patience helped me in all the time of research. I could not have imagined having a better advisor and mentor.

I am deeply indebted to Maman and Baba, whose love is boundless, for all their emotional support. I take this opportunity to thank my family in Iran for giving me happiness and joy.

My thanks and appreciation goes to everyone in the Civil Engineering Materials group at UBC for their help and interest in my work. I am especially grateful to my officemates Manote, Sudip and Aidin for providing an inspiring and fun environment in our lab. I am also thankful to Ms. Terry Moser for all her help during my studies.

I wish to express my warm and sincere thanks to Mr. Doug Smith, Mr. Harald Schrempp, Ms. Susan Harper, Ms. Paula Parkinson, Mr. JohnWong, Mr. Scott jackson and Mr. Bill Leung who were always there to help me out and made my work so much smoother.

Thanks are extended to Dr. John Madden and his students Arash and Tina at the department of Electrical Engineering for allowing me to use their laboratory equipment and assisting me in my experiments.

I express my gratitude to the ISIS Canada network for providing me with invaluable information on structural health monitoring and sensing systems. I would especially like to thank Dr. Mufti and Dr. Thomson whose knowledgeable guidance and ideas have had a remarkable influence on conducting my research.

Finally, special thanks to my best friend and husband Mohsen whose patient love helped me through the difficult times and enabled me to complete this work.

# CHAPTER 1

# Introduction

## 1.1 Structural Health Monitoring

Bridges, buildings and many other structures are susceptible to deficiencies due to different loading and environmental conditions such as corrosion, material aging, fatigue and the coupling effects with long-term and extreme loads (Ou 2006). These structures, when damaged or deteriorated, no longer meet the required standards and need to be repaired and rehabilitated or even rebuilt. These procedures can be very costly and time consuming if damage or deterioration is not detected shortly after occurrence.

In order to catch any deficiency in the structures performance before any serious loss of capacity occurs, a technology has recently emerged known as Structural Health Monitoring (SHM).

The purpose of SHM is to accurately monitor the behaviour of a structure, constantly assessing its performance and providing continuous data on its current conditions. Similar to the way a doctor would point out when an organ is malfunctioning in a patient's body during regular check-ups, an SHM system is able to diagnose and locate any anomalies in the structure. By means of this technique, engineers are now able to accurately monitor the health of structures under various environmental conditions and service loads. Some of the parameters that can be monitored using SHM are the corrosion rate, alkali reaction, moisture, ph, stresses, accelerations, strains and cracks.

Most structures have always been inspected from time to time using conventional assessment practices, but the need for continuous and more accurate monitoring solutions has led to the development of today's sophisticated SHM systems. These SHM systems not only record the required data, but are also able to provide on demand statistics and information on the prevailing conditions of the structure.

In the event of a damage, deterioration or abnormal condition, the engineer will be notified and appropriate course of actions can be taken to prevent damage from occurring or further propagating. Since this notification would be at a very early stage, the remedial procedure will usually be trouble-free with minimal cost.

The recorded data from a structure during its service life may also be used in modifying design codes for that specific type of structure, leading to more efficient and economical designs for future structures.

The following sensing and ancillary devices are integrated into an SHM diagnostic configuration:

- a sensory system
- a data acquisition system (DAQ)
- a data processing system
- a communication system
- a damage detection system and modelling system (Mufti 2001)

By means of these devices and a systematic procedure, SHM is able to determine the existence of any damage, locate it and estimate its magnitude. Subsequently, appropriate repair and rehabilitation of the structure can take place in a timely manner, preventing any catastrophic failure. In the case of structures like bridges, while monitoring the bridge performance and detecting damage, SHM can also be used to monitor the traffic and weigh the passing vehicles.

### 1.1.1 Applications of SHM

The number of applications for Structural Health Monitoring is increasingly growing. Nowadays, since the world is moving towards having stricter safety regulations, buildings, bridges and other structures are expected to always be in perfect condition. On the other hand, it takes a certain amount of time before any damage becomes visible or inspected and by that time the repair and rehabilitation process will be both costly and time consuming, not to mention the safety risks and losing the serviceability of the structure for quite some time. This is why engineers are now employing SHM to ensure the safety and integrity of structures. By receiving continuous and on-demand data on the well-being of structures, they are able to perform any necessary repair and maintenance in a timely manner. This procedure would be done long before any serious or even visible damage has occurred, therefore the repairing process will cost the least amount of time, money and loss of serviceability.

SHM systems can be integrated into almost any type of structure, from buildings, bridges, highway systems, tunnels, power plants, dams, pipelines and foundations to automobiles, trains and ships to various aircraft and space structures.

Whenever an innovative construction method is developed, questions arise on the efficiency and competence of these techniques. One application of SHM is to confirm the effectiveness of such new and innovative design and construction techniques. A perfect example of this application is assessing the performance of steel-free bridge decks with fibre reinforced polymer (FRP) replacing steel reinforcement (Mufti 2001). Another example could be assessing the performance and durability of sprayed FRPs applied for bridge strengthening (Banthia et al. 2002)

As mentioned before, data collected during the SHM of a structure, may be used to evaluate the efficiency of current design methods. SHM provides the physical parameters of the structure, which in turn demonstrate how the structure is

performing in service. If the performance does not satisfy the required regulations, the design codes for that specific type of structure should be modified.

### 1.1.2 Benefits of SHM

Implementing Structural Health Monitoring has recently become a significant consideration in the construction and maintenance of civil engineering structures because of the numerous advantages it brings about.

The ability to monitor the health of structure in real-time using wireless communication is one of the main assets of SHM, providing a reliable way for the owner and engineers to ensure the safety of our infrastructure at any given time without having to go through regular conventional inspections.

Knowing that their infrastructure is being constantly monitored for its safety, offers the public more comfort when it comes to using both old and new, innovative types of structures.

In the case of any damage in a structure, the SHM system would detect and locate it at a very early stage and therefore the repair process is usually very simple and quick, significantly reducing the down time and the maintenance costs.

By detecting the deficiencies in a timely manner, SHM also optimizes resources for repair, rehabilitation, or replacement of in-service structures. Collected data from the SHM system provides information about the performance of the structure on the inside, which can be useful in estimating the life-cycle costs of structural components as well as optimizing the design and construction of future structures (Mufti 2001).

## 1.2 Civionics

It has become imperative that Structural Health Monitoring is practiced to ensure the safety and well being of in-service structures. In addition, for major

modifications in the design and construction of innovative structures to be accepted, SHM plays a key role in developing the required data banks (Mufti et al. 2007).

In order to integrate SHM into civil engineering structures, a major contribution of electronics is required. To facilitate this requirement, the discipline of Civionics has emerged, which is derived from the application of electronics/electrophotonics to civil engineering (Klowak et al. 2005). The expression Civionics is a derivative of civil engineering and electronics, in the same way Avionics arose from aviation electronics.

An SHM system comprises of a control room, different types of sensors, wires, conduits and junction boxes. The science and technology of electronics along with the knowledge of civil engineering has, under the combined term Civionics, led to the development of the required electronic devices for SHM.

With the help of Civionics, engineers are able to fully utilize all the capabilities and benefits of SHM. The function of Civionics is to assist in building smart structures and ensure that the design and installation of SHM systems is such that they continue to accurately perform over time (Rivera et al. 2007).

A Civionics Specification manual (Rivera and Mufti 2004) was developed by ISIS Canada Research Network in 2004, with the purpose of assisting engineers and contractors in the implementation of civionics in the SHM of civil engineering structures, outlining the technical requirements for fibre optic sensors, cables, conduits and junction boxes.

## 1.3 Sensors

The sensory system is the most important component of Structural Health Monitoring. Sensing devices comprising the sensory system are responsible for

measuring parameters such as time, load, displacement, strain, acceleration, temperature, moisture, etc.

Some of the commercially available sensors include linear variable differential transducers (LVDT), accelerometers, foil strain gauges, vibrating wire strain gauges, fibre optic sensors (FOS), and ferro-magnetic sensors.

For strain measurements, foil strain gauges and fibre optic gauges are the most widely used sensors. Foil gauges, being less expensive and easier to install, are more commonly used than FOS systems. However, sensitivity to moisture and humidity, in addition to the fact that they become less reliable when increasing the distance between the gauge and the readout unit is increased (Mufti 2001), makes foil strain gauges less favourable. Fibre optic sensors, on the other hand, do not have these problems and since they are small in diameter, they are appropriate for numerous sensing applications. Yet, FOS systems have their own drawback: the high cost of the sensors and their readout units (Mufti 2001).

A distributed network of sensors is usually installed in selected areas of a structure to monitor its health when in service. The feasibility of this SHM system depends on whether the sensors can be integrated securely within the host structure and changes in sensor measurements can be reliably correlated to the physical changes of the structure (Wang et al. 2001).

A new type of sensors has recently emerged, known as cement-based sensors. These sensors are also described as smart (self-monitoring) structural materials because they are made of structural material and thus can be used as a part or total component of structures, providing both structural capability and measurable response to applied stresses, strains, cracks and other flaws.

## 1.4 Organisation of the thesis:

In this research, smart cement-based materials are introduced as sensors for SHM. These cementitious composites containing either carbon fibres or carbon nano-tubes (or a hybrid of both) as the conductive phase are piezoresistive in which the electrical resistivity varies in response to any changes in the applied stress or strain. Taking into account the piezoresistive property of these sensors, they can be used to sense stress/strain, simply by monitoring their electrical resistivity. The influences of other parameters such as chlorides, moisture and temperature variation are also investigated in this study.

Due to their extremely fine size, carbon fibres provide a very effective inter-fibre continuity and therefore improve the conductivity of cement composites to a large extent (Banthia et al. 1992). Two types of carbon fibres, petroleum pitch-based carbon fibres (PPCF) and coal tar pitch-based carbon fibres (CPCF), are used in this project.

The size and distribution of the fibres are important issues in the development of these sensors. Depending on the fibre size, a minimum amount of conductive fibre has to be used in order to obtain a conductive composite (Xie et al. 1996). Various volume fractions of carbon fibre are used in the samples for this project and comparing their electrical resistivities has led to defining the best volume fraction.

In addition, the effectiveness of using of both single-walled and multi-walled carbon nano-tubes (CNT) with and without the presence of carbon fibres in cement paste is investigated.

Various types of small size specimens are prepared, each containing two or four electrodes as electrical contacts for measuring their resistivity. Different types of electrodes as well as two-probe and four-probe resistivity measurements are examined to find the best test procedure.

Prior to commencing the main series of tests, a set of preliminary tests were performed using a hand made resistance measurement system prepared by the lab technicians. These experiments are carried out to confirm previous research and create a reference point for the later, more sophisticated experiments.

For the core set of tests conducted during this study, an Inductance/Capacitance/Resistance (LCR) meter is employed. A wide range of experiments are carried out using different fibre contents, in order to identify the most efficient fibre content. Since alternating current is used, the influence of frequency is also looked at to find the most appropriate frequency. The effect of different parameters such as curing, temperature variation, and moisture and chloride presence are also investigated.

Specimens are tested under several monotonic and cyclic loading conditions including compression, tension and flexure to evaluate their effectiveness in monitoring stress/strains and detecting cracks. The resistivity values from these sensors are compared with load and displacement values as well as strain data acquired from conventional strain gauges.

Due to their low cost, good durability, compatibility with concrete structures and superb mechanical properties, which enable them to in fact perform as a load-bearing structural component as well, these sensors would be a very efficient replacement for currently conventional sensors. This type of sensor can be easily embedded into the host structure, and since it is made of structural material, the sensor can be regarded almost as an aggregate because it does not alter the properties or appearance of the structure.

Following a short background on the electrical concepts and a comprehensive literature review in Chapters 2 and 3, the experimental program for both preliminary and main set of experiments is explained in Chapters 4 and 5, respectively. The influence of fibre volume fraction, frequency, electrode type and curing is described in Chapters 6 to 9. Results obtained from employing

these cement-based sensors in different environmental conditions including, temperature, moisture and chloride presence as well as loading conditions such as compressive, tensile and flexural loading, is discussed in Chapters 10 to 14. Chapters 15 and 16 offer some concluding remarks and suggestions for future research, respectively.

# CHAPTER 2

# Electrical Concepts

## 2.1 Ohm's Law

How strongly a material opposes the flow of electrical current through it, is defined by its electrical resistance.

According to Ohm's law, at a constant temperature, the resistance of a material is equal to the applied voltage divided by the current flowing through it, mathematically formulated as:

$$R = \frac{V}{I} \tag{2-1}$$

Where,

R: electrical resistance in ohms (Ω)
V: voltage in volts (V)
I: intensity of the current in amperes (A)

The above equation holds true for direct current (DC) circuits. In the case of alternating current (AC) circuit, with the presence of both resistance and reactance, Ohm's law is amended to:

$$Z = \frac{V}{I} \tag{2-2}$$

Where, Z is the total opposition to the current, ohmic resistance and reactance combined, known as impedance. Impedance (Z) is also measured in ohms (Ω).

This law holds true for all ohmic materials. There are materials, however, in which the flowing current is not proportional to the applied voltage. These materials which do not obey Ohm's law are acknowledged as non-ohmic. The current-voltage graphs in these materials are nonlinear. A few examples of non-ohmic materials are diodes, battery acid and alkaline solutions. Diodes, for example have different resistances depending on the direction of the current flowing through them.

## 2.2 Resistivity

Resistance values not only depend on the material, but also on its geometry. In order to omit the geometrical factor, another quantity is introduced, called resistivity (ρ) that represents the ability of a material to resist electrical conduction independent of its geometry. Electrical resistivity, also known as specific electrical resistance, is an intrinsic property and therefore can be used to compare different materials based on their ability to conduct electricity. The higher the resistivity values, the more resistant the materials is to the flow of electrical current and the lower the values, the more and easier the material transmits electrical current. For conductors, resistivity depends on the composition and temperature of the material.

The electrical resistivity (ρ) of a material with a uniform cross section is measured as its resistance per unit length:

$$\rho = R\frac{A}{\ell} \qquad (2\text{-}3)$$

Where:

ρ: electrical resistivity in ohm-meters (Ω-m)
R: electrical resistance of a uniform specimen in ohms (Ω)
A: cross-sectional area of the specimen in square metres ($m^2$)

ℓ: length of the specimen (or length between the measurement electrodes) in metres (m)

To obtain an idea of what the resistivity of different materials would be, the following is a list of materials with their electrical resistivity values at a temperature of 20°C:

Silver: $1.59\times10^{-8}$ Ω-m

Copper: $1.7\times10^{-8}$ Ω-m

Carbon: $3.5\times10^{-5}$ Ω-m

Glass: $10^{10}$ to $10^{14}$ Ω-m

Concrete: 5 to15 Ω-m

Resistivity may also be defined as the inverse of the electrical conductivity (σ) of a material:

$$\rho = \frac{1}{\sigma} \qquad (2\text{-}4)$$

Where σ (electrical conductivity) is the material's ability to conduct an electric current and has the SI units of siemens per metre ($S.m^{-1}$).

## 2.2 Polarization

The phenomenon, in which the centers of positive and negative charges do not coincide, is expressed with the term electric polarization and generally occurs in dielectric materials exposed to an electric field (Wen and Chung 2001). In simpler words, there are many positively charges and negatively charges ions (such as $Na^+$, $Ca^+$, $OH^-$, etc) in materials like carbon fibre reinforced cement based materials. When applying an external voltage through electrodes attached to the material, the negative ions move toward the positive electrode and the positive ions move toward the negative electrode, which generates a potential opposite to the applied voltage. This opposite voltage is referred to as polarization potential. If polarization occurs during resistivity measurements, it

will cause the measured resistivity values to increase with time, complicating the procedure and causing difficulties in correlating the changes in resistivity to strain or other sought-after parameters. There are a number of ways to somewhat prevent this undesirable phenomenon from happening, one of which is to make the material more conductive. The tendency to polarize becomes less when the material is more conductive, thus the addition of carbon fibres to cement paste diminishes polarization (Wen and Chung 2001). Carbon fibre reinforced cement-based sensors are also slightly capacitive and charge build-up is possible. Thus they are still susceptible to polarization and appropriate measures need to be taken to prevent it.

The simplest method to measure resistivity is to use direct current (DC). However, the DC measurement of electrical resistivity has proven to be technically difficult due to the polarization effect causing exponential rise in the measured resistivity (Tsung-Chin Hou and Lynch 2005). There are two methods to cancel out the polarization phenomenon when measuring resistivity using DC signal, one of which is to measure the changes in electrical resistivity of a control specimen over time and then subtract those values from the measurements on the actual specimen under loading conditions. The second technique would be to apply a DC voltage well ahead of loading the specimen in order for the resistivity to reach a plateau due to complete polarization; but since polarization depends on the specimen geometry, large specimens take more time to fully polarize (Tsung-Chin Hou and Lynch 2005). Moreover, this approach is not very convenient in practice.

Alternatively, resistivity measurements can be made using alternating current (AC) signals with equal magnitudes of positive and negative peaks. Figure 2-1 illustrates a comparison between the polarization effect of cementitious materials when DC and AC signals are applied. As observed from this figure, even though some polarization still exists when using AC signals, by increasing

the applied AC frequency, it is narrowed to a tolerable range (Tsung-Chin Hou and Lynch 2005).

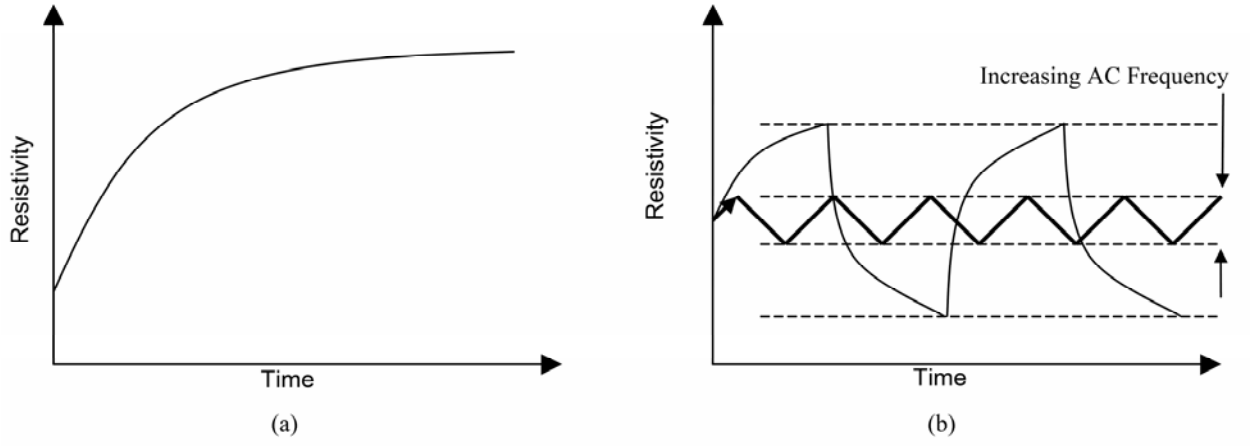


Figure 2- 1: Polarization effect of cementitious materials when (a) DC and (b) Ac signals are applied (Tsung-Chin Hou and Lynch 2005)

## 2.3 Impedance

The total opposition to the flow of an alternating current (AC) at a certain frequency is defined as impedance, which is the combination of ohmic resistance and reactance. Impedance (Z) is generally represented using complex notation (Equation 2-5) or the polar form (Equation 2-6) and is expressed with the ohm (Ω) unit.

$$Z = R + jX \tag{2-5}$$

Where,

Z: impedance in ohms (Ω)

R: ohmic resistance, known as the real part of the impedance, in ohms (Ω)

$j$ : imaginary unit

X: reactance, known as the imaginary part, in ohms (Ω)

$$Z = |Z| \angle \theta \qquad (2\text{-}6)$$

Where,

$$|Z| = \sqrt{R^2 + X^2}$$

$$\theta = \tan^{-1}\left(\frac{X}{R}\right)$$

$|Z|$ and $\theta$ are the magnitude and phase angle of impedance, in ohms (Ω) and degrees (°), respectively.

### 2.3.1 Ohmic Resistance

When working with DC signals, resistance is the only opposing parameter of concern. In AC circuits, however, the concept of resistance is extended to a more complicated form, referred to as impedance.

Impedance (Z) consists of two parts; ohmic resistance (R) and reactance (X). Due to the effects of reactance, the DC resistance is by and large not the same as AC impedance.

Resistance (or ohmic resistance) is known as the real part of impedance. The resistance portion of impedance has the following relationship with the phase angle:

$$R = |Z| \cos\theta \qquad (2\text{-}7)$$

Where,

R: resistance in ohms (Ω)

$|Z|$: magnitude of impedance in ohms (Ω)

θ: phase angle (phase difference between voltage and current) in degrees (°)

According to equation 2-7, purely resistive impedance occurs when the phase angle is zero.

### 2.3.2 Reactance

In an AC circuit, reactance (X) is referred to the imaginary part of impedance. Reactance, which may in turn be in the form of inductive reactance ($X_L$) or capacitive reactance ($X_C$) or a combination of the two, also opposes the flow of alternating current and like resistance is expressed in ohms (Ω).

The resistance portion of impedance has the following relationship with the phase angle:

$$X = |Z| \sin\theta \qquad (2\text{-}8)$$

Where,

X: reactance in ohms (Ω)

$|Z|$: magnitude of impedance in ohms (Ω)

θ: phase angle in degrees (°)

Often a by-product of certain material in the cement-based sensors, reactance is not desirable in the experiments and measures are taken to reduce the effects of this parameter.

When the reactance is positive (X>0), it is said to be more inductive, whereas a negative reactance (X<0) implies that the reactance is more capacitive. A reactance of zero (X=0), clearly means that there is no reactance and the impedance is merely resistive.

The ratio of the reactance portion to the resistance portion of electrical impedance, known as the quality factor (Q), represents how close the impedance is to having no resistance, being purely reactance:

$$Q = \left| \frac{X}{R} \right| \tag{2-9}$$

Where,

Q: quality factor

X: reactance in ohms (Ω)

R: resistance in ohms (Ω)

### 2.3.2.1 Capacitive Reactance

By definition, capacitive reactance ($X_C$) is the part of reactance that arises from the presence of a capacitor within the circuit. $X_C$ is known to be inversely proportional to the AC signal frequency ( $f$ ) and the capacitance (C):

$$X_C = -\frac{1}{\omega C} = -\frac{1}{2\pi f C} \tag{2-10}$$

Where,

$X_C$: capacitive reactance in ohms (Ω)

ω: angular frequency in radians per second (rad/s)

C: capacitance of the capacitor in farads

$f$ : signal frequency in hertz (Hz)

### 2.3.2.2 Inductive Reactance

By definition, inductive reactance ($X_L$) is the part of reactance that arises from the presence of an inductor within the circuit. $X_L$ is known to be directly proportional to the AC signal frequency ( $f$ ) and the inductance (L):

$$X_L = \omega L = 2\pi f L \tag{2-11}$$

Where,

$X_L$: inductive reactance in ohms (Ω)

ω: angular frequency in radians per second (rad/s)

L: inductance of the inductor in henrys (H)

$f$ : signal frequency in hertz (Hz)

### 2.3.3 Phase Angle

The sinusoidal current and voltage oscillations in an AC circuit are not necessarily in phase, meaning they do not peak at the same time. Although they oscillate with the same frequency, one generally leads and the other lags. This phase shift between the voltage and current is caused by the capacitance and inductance within the AC circuit. Since the voltage and current are out of phase with each other, resistance and reactance cannot be simply added together to obtain impedance. The Pythagorean Theorem should be used to add them as vectors at right angles to each other.

The angle, by which the voltage sine curve lags or leads the current sine curve, is known as the phase angle (θ) and is expressed in degrees (°) (θ≤90°). If the phase angle is positive, the voltage leads the current and the reactance is more inductive. If the voltage is leading by 90° (π/2), then the device has pure inductive reactance. Conversely, if the phase angle is negative, the voltage lags the current and the reactance is more capacitive, with the device having pure capacitive reactance if the voltage is lagging by 90° (π/2).

For a circuit consisting of a resistor (R), an inductor (L) and a capacitor (C), connected in series or in parallel (an RLC circuit), the phase angle can be determined from the following equation:

$$\tan\theta = \frac{X_L - X_C}{R} \qquad (2\text{-}12)$$

Where,

θ: phase angle in degrees (°)

$X_L$: inductive reactance in ohms (Ω)

$X_C$: capacitive reactance in ohms (Ω)

R: resistance in ohms (Ω)

There is an exception where there is no phase shift between the voltage and currant of an AC circuit, which happens when the circuit is in resonance (the reactive impedance components $X_L$ and $X_C$ cancel each other out) or if there is only a resistor in the circuit.

### 2.3.4 Frequency

The effects of capacitance and inductance vary with the frequency of the alternating current. Thus reactance and consequently impedance vary with frequency. According to equations 2-10 and 2-11, for a capacitive mechanism, higher frequency leads to lower capacitive reactance and for an inductive mechanism, the lower the frequency, the lower the inductive reactance.

In order to reduce the effects of reactance and use only the resistive component of cement-based materials for sensing purposes, one needs to find out whether the material is capacitive or inductive and then use high or low frequencies, respectively.

It is generally assumed that resistance is always constant and independent of frequency. Yet this is not always true. In reality, the resistance of a circuit to AC is found to be greater than its resistance to DC. This effect is small at low frequencies. At high frequencies, however, this difference is very pronounced (Robbins and Miller 2003).

One of the factors that lead to the increase in the effective resistance in AC with frequency is the skin effect. The skin effect is the tendency of an alternating current to flow in the periphery, or the skin, of conductors. Thus the effective

cross-section of the conductor is reduced, leading to an increase in the effective resistance.

## 2.4 Admittance

When the connection between resistance and reactance is serial (Figure 2-2 a), impedance is expressed as a simple summation which makes it a convenient parameter to use. In some cases, however, such as for a parallel connection between the real and imaginary components (Figure 2-2 b), impedance tends to be rather complex to express. In such cases, the reciprocal of impedance (Equation 2-13), admittance (Y), is usually considered to be a better parameter to use. The unit of admittance is the siemens (S), equal to one ampere per volt, or mho ($\Omega^{-1}$), the reciprocal of an ohm.

$$Y = \frac{1}{Z} = \frac{1}{(R + jX)} = G + jB \qquad (2\text{-}13)$$

Where,

Y: admittance in siemens (S)
G: conductance, known as the real part of the admittance
B: susceptance, known as the imaginary part of the admittance

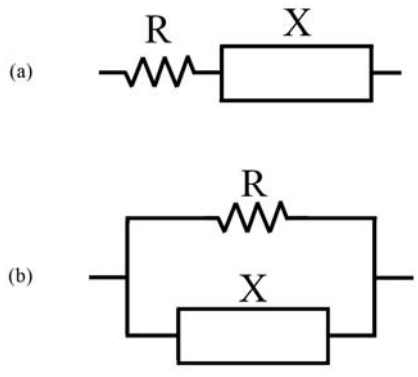


Figure 2- 2: (a) Series and (b) parallel combinations of resistance and reactance

# CHAPTER 3

# Previous Research

## 3.1 Electrical Resistivity of Concrete

The electrical resistivity of concrete has long been an issue of concern due to the fact that it affects a variety of concrete applications and specifications.

The resistance of concrete to the flow of electrical current becomes a very important factor when it comes to applications such as electrically powered rapid transit lines, where high resistivities are required, and hospital operating room floors and cathodic protection systems, where there is a need for low resistivities (Whiting and Nagi 2003). Another issue that is concerned with concrete resistivity is the corrosion of steel reinforced concrete structures which can be reduced by using a highly resistive concrete material.

There are various parameters that affect concrete resistivity. In a report by Whiting and Nagi (Whiting and Nagi 2003), a literature review has been conducted on the effects of paste content, water-to-cement (w/c) ratio, moisture content, time of moist curing, chemistry of cement, use of supplementary cementing materials (SCM), the presence of chemical admixtures and environmental conditions on the electrical resistivity of concrete.

On the effects of cement type and chemistry, it is stated that high-alumina cements exhibit higher resistivities than portland cements in concretes with similar mix proportions and curing process. It is also mentioned that high $C_3A$ contents in cements have the tendency to increase concrete resistivity as well. It should be noted, however, that since electrical current is carried primarily by the cement paste phase, and not the aggregates, as the total amount of cement in

the concrete mixture is increased, the resistivity decreases (Whiting and Nagi 2003). The electrical resistivity of concrete increases with an increase in the concrete aggregate volume (Shi 2004).

As far as the influence of w/c ratio is concerned, Monfore (Monfore 1968) found that as the w/c is decreased, the resistivity increases. In fact, resistivity can be doubled by a decrease in w/c ratio from 0.60 to 0.40. Also, at lower moisture contents, changes in concrete resistivity affected by w/c ratio tend to be greater than that at saturated conditions (Gjørv et al. 1977).

Using SCM such as fly ash, ground granulated blast furnace slag (GGBFS), and silica fume have all proven to increase electrical resistivity of concrete. In the case of chemical admixtures, the presence of chloride salts was considered and was confirmed that due to higher conductivity of chloride solutions, chloride salts such as calcium chloride, decrease electrical resistivity (Monfore 1968; Whiting and Nagi 2003).

Various environmental conditions have serious effects on the electrical resistivity of concrete. Concrete, as an electrolytic conductor, displays lower resistivities at higher temperatures. Since current is mainly carried through the pore solution in concrete, the more porous and saturated the concrete is, the lower the resistivity of the concrete. Therefore, moisture content is prone to have the most significant effect on concrete resistivity. Finally, there is the time factor. The influence of time depends on whether concrete is moist cured or air cured. If the concrete is moist cured, the electrical resistivity generally increases over time and may even double within the first 90 days of curing. Resistivities also increase with time for air dried concrete, although this increase is due more to the loss of moisture content with time (Whiting and Nagi 2003). Thus, although both moist and air cured concretes gain higher resistivities with time, this effect may emanate from different mechanisms.

Numerous applications are proposed for electrically conductive concrete, such as the electrical grounding, lightning protection, deicing, electromagnetic interference shielding and electrostatic discharge protection (Wen 2006).

## 3.2 Smart Concrete

The aforementioned knowledge of the electrical properties of concrete and the achievability of highly conducting concrete material has been the primary foundation of developing smart concrete structures. Smart concrete would be able to sense strain through measuring its electrical resistivity. This would call for the ability in concrete to exhibit reversible changes in the electrical resistivity upon deformations or strains in the elastic phase. There are strain gauges and fibre optic sensors available that are able to measure strain when they are embedded in or attached to a concrete structure. These sensors, however, have limitations such as high cost, low durability, complexity of installation and most importantly the fact that they are not made of structural material and therefore degrade the structural performance of the concrete structure. Realizing the capability of smart concrete to not only perform as a structural material with desired mechanical properties, but also to sense its own strain and stress, prompted scientists to develop smart or better yet self-sensing concrete.

Self-monitoring concrete containing short carbon fibres have proven to be effective for traffic monitoring and weighing in motion, through a series of laboratory tests by Shi and Chung (Zeng-Qiang and D.D.L 1999). The DC electrical resistance decreased reversibly with increasing stress up to 1 MPa and was independent of speed up to 55 mph.

In a study by Mo et al. (Mo et al. 2005), an electrically conductive asphalt concrete is developed where the stress-strain relation is similar to piezoresistivity, providing a basis on monitoring the deformation of asphalt

pavements through its electrical properties, and sensing cracks instantly and non-destructively.

It is usually impractical and unnecessary to use this self-sensing material to construct the concrete structure, but relatively small-sized cement-based sensors are imbedded in the structure or mounted to the surface. Without affecting the structural performance of the host structure in the slightest, these sensors will provide the stress/strain information of structural elements. Cement-based sensors are rather inexpensive, very easy to manufacture, much simpler to install compared to conventional sensors and best of all they are made of real structural material and possess mechanical properties similar to their host structure. There is usually a gauge factor, defined as the fractional change in resistance per unit strain, associated with strain gauges. These sensors have gauge factors of up to 700 and are hence highly sensitive, whereas a typical commercial strain gauge has a gauge factor of 2.

In order to produce more conductive cement-based composites, capable of sensing, a conductive phase must be added to the cement paste. This conductive phase is usually carbon fibres, carbon nanotubes, carbon black, or a combination of these materials.

It should be noted that smart behaviour can be observed in concrete as well as mortar and cement paste, but since fibres are less effective in controlling crack opening when a course aggregate is present, the changes in electrical resistance are much larger for mortar and paste than concrete (Chen and Chung 1996). Therefore, cement paste or mortar are generally used as matrices for cement-based sensors.

Steel fibres also provide electrical conductivity. In fact in 1991, Banthia et al. (Banthia et al. 1992) conducted electrical resistivity measurements on cement pastes reinforced with various volume fractions of carbon and steel micro-fibres as well as on several hybrid specimens containing different amounts of both

carbon and steel fibres. The addition of fibres significantly reduced the electrical resistivity of cement pastes. Although steel fibres on their own are a lot less resistive than carbon fibres, it was found that when incorporated in cement paste, the composite specimens containing carbon fibre are less resistive. It was concluded that this effect is due to the extremely fine size of carbon fibres, providing more and better inter-fibre continuity. Thus, it should be noted that the size and distribution of fibres in the composite can be even more influential in the resistivity than the conductivity of the fibre itself. The same analogy explains the results from the steel-carbon fibre hybrid composites, which indicate that the addition of carbon fibres are very effective in improving the electrical conductivity of the hybrid composites and that there is an optimum amount of carbon fibres required to produce an inter-fibre connectivity network mobilizing the outstanding conductivity of steel fibres (Banthia et al. 1992).

## 3.3 Piezoresistivity and Sensing

Piezoresistivity is defined as the dependence of electrical resistivity on strain, and material in which the electrical resistance changes in response to changes in the applied strain are referred to as piezoresistive material. The electrical resistivity of a material depends on the positions and motions of the internal atoms. Applied stress/strain changes these internal atomic arrangements and this leads to small changes in the resistivity of the material to the applied current. In the past, the piezoresistive effect has been formulated in terms of stress rather than strain. In act, the piezo prefix comes from the Greek word *peizin*, which means to press (Senturia 2001).

### 3.3.1 Cement-Based Piezoresistive Sensors

Cement-based sensors are designed to function based on the principle of piezoresistivity. Even a small change in the strain would change the electrical resistivity of the sensor accordingly.

In order to obtain a piezoresistive cement-based material capable of sensing strain, a conductive phase is included in the cement paste or mortar mix design. The conductive phase may be carbon fibres, carbon black, carbon nanotubes or a combination of them. A hybrid of carbon fibre and carbon nanotubes is of particular interest; the efficiency of this type of sensor is investigated for the first time in this thesis.

The objective of developing cement based sensors is to provide a more durable, compatible, and cost effective alternative for conventional sensors. By surface mounting or embedding a network of these sensors in a structure and continuously acquiring and recording the resistivity values, the performance of the structure can be accurately monitored.

Developing a wireless system to acquire data from cement-based sensors would, without doubt, augment the vast capabilities of these sensors for SHM, enabling automated online monitoring and screening of data for signs of structural damage. Moreover, since extensive wiring is no longer required between sensors and the DAQ system, wireless sensors are inexpensive to install, less labor-intensive and offer better flexibility and adaptability in the design of the SHM system (Lynch 2006; Lynch et al. 2004; Wang et al. 2007). Nevertheless, developing wireless sensors requires novel system architectures and modes of operation. A low-cost wireless active sensing unit is proposed by Hou and Lynch (Tsung-Chin Hou and Lynch 2005; Hou and Lynch 2005) to explore the piezoresistive properties of various engineered cementitious composites (ECC). ECC is referred to cementitious composites containing short fibres (polymer, steel, or carbon). These composites not only possess enhanced mechanical properties, but are piezoresistive as well; and are categorized as smart self-sensing structural materials.

### 3.3.2 Piezoresistivity vs. Piezoelectricity

The concept of piezoresistivity is often mistakenly referred to as piezoelectricity although these terms have completely different definitions. Piezoelectricity is referred to the coupling between internal dielectric polarization and strain (Senturia 2001). Since in piezoresistivity there is no stored energy component that depends on strain and thus no opportunity for actuation, it can only be used for passive sensing of stress/strain. The internal polarization in piezoelectricity, on the other hand, contributes to the stored energy, which means that piezoelectrics can be used for both sensing and actuation. Unfortunately, because of the parasitic effects of small DC leakage currents, piezoelectrics are not good at quasi-static sensing of strain; but they are highly effective for time-varying sensing applications, such as sensing vibratory or resonant motions (Senturia 2001). In piezoelectric materials, an electric field, detectable as voltage, is produced as a result of applied mechanical stress. The reverse also takes place, where an applied electric field generates mechanical deformation in the material.

Piezoelectric cement-based composites have also been under investigation for use as sensors in the civil engineering field of smart structures and SHM(Li and Dong 2003; Shen et al. 2006; Li and Yang 2005). Extensive research has been conducted in order to develop a self-sensing actuator exclusively for use in civil engineering intelligent structures (Li 2001; Zhang et al. 2002). Several applications of cement-based piezoelectric sensors for SHM have been studied. Some of these applications include monitoring traffic flows (Li et al. 2006), health assessment of pipeline structures (Park 2000), monitoring the real stress conditions of structures under earthquake (Li and Yang 2005), monitoring the dynamic strain of bridges, pinpoiting the location of damage and identifying the fatigue damage of nano-concrete beams (Ou 2006).

## 3.4 Carbon Fibre Cement-Based Sensors

The most common material used as the conductive phase in cement-based sensors is carbon fibre.

It has long been recognized that the addition of fibres to plain concrete offers convenient and practical improvements in various mechanical properties of this structural material such as enhanced toughness, fatigue resistance, impact resistance, tensile strength, flexural strength, reduced creep and shrinkage and improvements in the post-cracking behaviour (McCarter et al. 2007). Although these enhanced mechanical properties are a bonus to the sensing ability of carbon fibre reinforced cement-based composites (CFRC), it is the fact that these fibres create electrical conductivity and piezoresistivity in the material that is of major importance in the development of cement-based sensors. The addition of even a small amount of carbon fibres to cement paste significantly reduces the resistivity of the material.

CFRC sensors are generally prepared without inducing any pressure. Yet, in a study by Shifeng et al (Shifeng et al. 2007) these sensors were fabricated under 2 MPa and 10 MPa of compressive pressing. It was found that the sensors formed under 10 MPa are more suitable for SHM purposes because the larger the forming pressure is, the more compact the structure of the specimen and accordingly the better and easier formed conduction network with cyclic loading. The amplitude of the fractional change in resistance in the 10 MPa pressured specimens was larger than that of the composites formed under 2 MPa (see Figure 3-1).

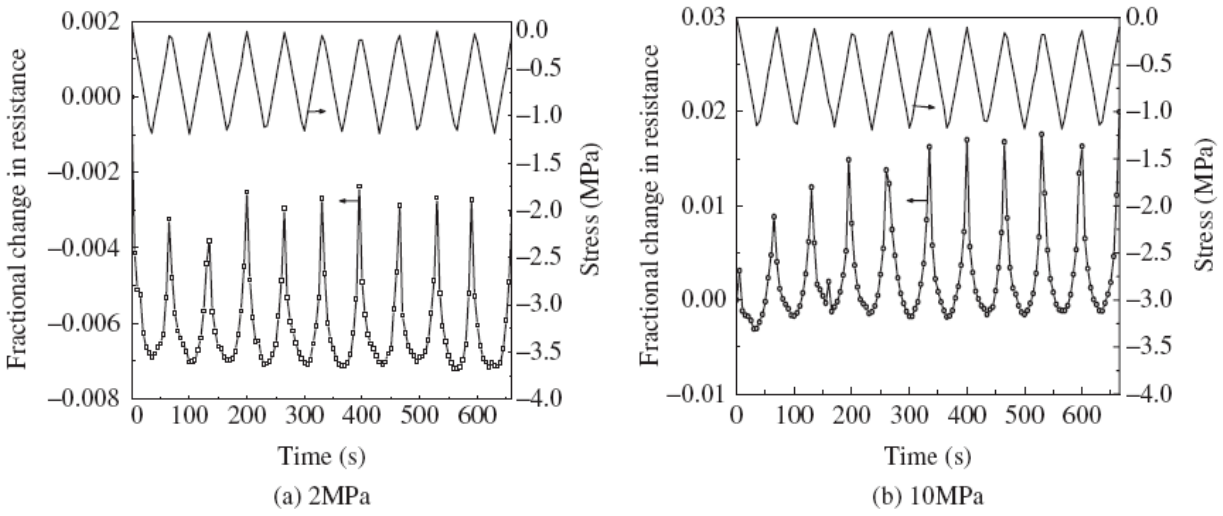


Figure 3- 2: Piezoresistivity properties of CFRC (carbon fibre content is 0.6%) under 2 and 10 MPa (Shifeng et al. 2007)

### 3.4.1 Effect of Fibre Content

The inclusion of carbon fibres makes cement composites more conductive, in other words it reduces the electrical resistivity. It is obvious that this effect will further advance with the addition of more carbon fibres to the composite. However, it has been proven that volume fractions higher than a certain threshold are no longer effective in increasing electrical conductivity. In other words, there is a relationship between conductivity and connectivity of conductive fibres, known as the percolation phenomena, illustrated in Figure 3-2. This theory deals with the effects of random variation on the number and quality of the existing interconnections (Xie et al. 1996).

Xie et al. (Xie et al. 1996) describe these phenomena using the threshold and post-threshold expressions. Conductivity boosts by several orders of magnitude, when the volume fraction of carbon fibre reaches a certain critical value, referred to as the percolation threshold. Increasing the fibre content beyond this threshold, entering the post-threshold region, will only result in marginal increase in electrical conductivity of the composite (Xie et al. 1996).

Based on Equation 3-1 (Zallen 1983) expressing the percolation theory in composites, Xie et al. (Xie et al. 1996) have proposed Equation 3-2 for a broad range of cement paste and mortars with different water/cement ratio and sand/cement ratios:

$$\sigma\alpha(\varphi-\varphi_c)^t \qquad (3-1)$$

Where,

$\sigma$: conductivity of the composite

$\varphi$: volumetric fraction of conductive fibre

$\varphi_c$: threshold value of the volumetric fraction

*t*: a positive constant that is independent of the microstructure of the composite

$$\sigma = 4.10(\varphi-0.01)^{1.65} \qquad (3-2)$$

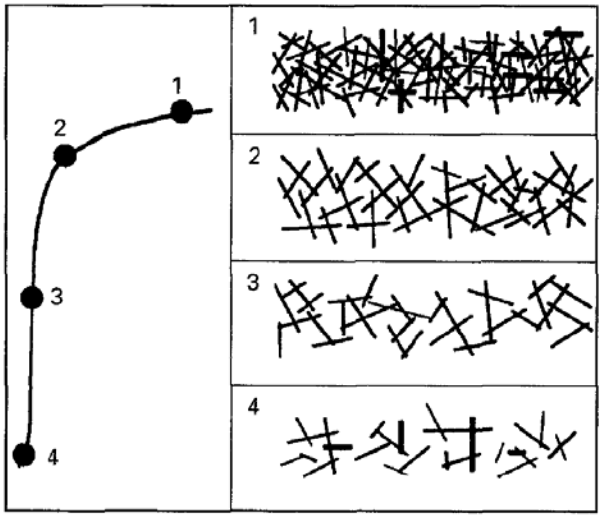


Figure 3- 3: Percolation phenomena (Xie et al. 1996)

It should also be noted that fibre size and shape are also important factors in determining the percolation threshold; for example, the longer the fibres (to a certain extent), the lower the threshold.

### 3.4.2 Effect of Fibre Length

The longer the carbon fibres, the more continuous the fibre network and hence the more effective they are in reducing the electrical resistivity of the cement paste. However, longer fibres exhibit practical difficulties when mixing; in terms of workability and obtaining a uniform distribution of fibres.

In a study by Chiarello and Zinno (Chiarello and Zinno 2005) the effect of fibre length on the electrical conductivity of carbon fibre reinforced mortar was investigated by comparing the conductivities of specimens with three different fibre lengths (Figure 3-3).

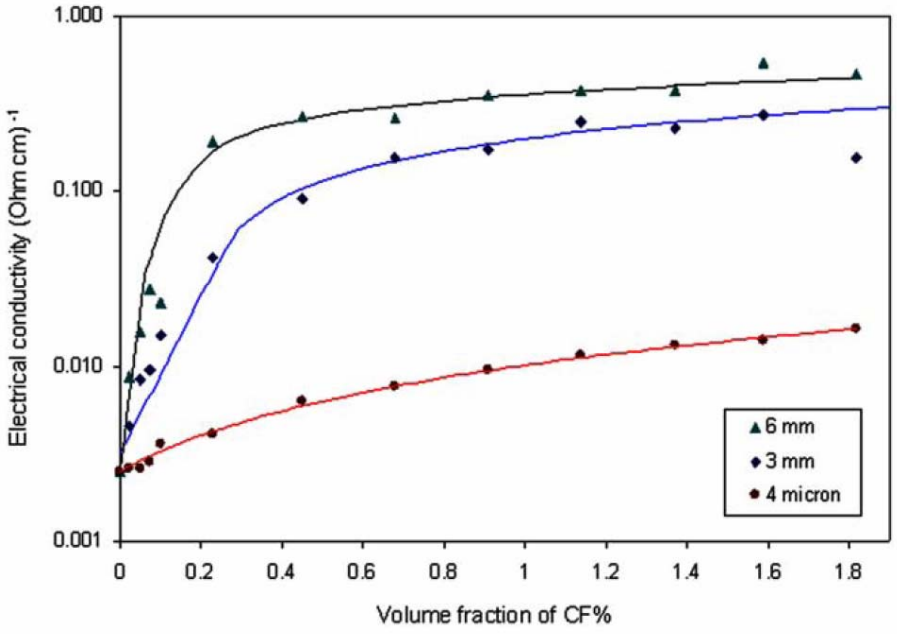


Figure 3- 4: Effect of fibre length on conductivity of CFRC at 1 day hydration (Chiarello and Zinno 2005)

Figure 3-3 confirms that specimens with longer fibres attain higher electrical conductivity at a given fibre volume fraction, while the conductivity of specimens

containing very short fibres, increases very gradually with volume fraction. In other words the percolation threshold is at much higher volume fractions for the very short fibres. Longer fibres cause inadequate workability and therefore difficulty in mixing. This graph shows that with an optimum fibre length, less fibre content is needed to form a fibre network capable of achieving the threshold conductivity without compromising the workability of the mixture.

### 3.4.3 Effect of Curing

As a result of hydration, the microstructure of cement paste changes as it cures and its resistivity increases. This holds true for both fibre reinforced and plain samples, although at higher fibre dosages, this increase is more gradual. Figure 3-4 shows the results of a study by Chako at al. (Chacko et al. 2007) on the effect of curing time on the electrical resistivity of CFRC with various fibre contents.

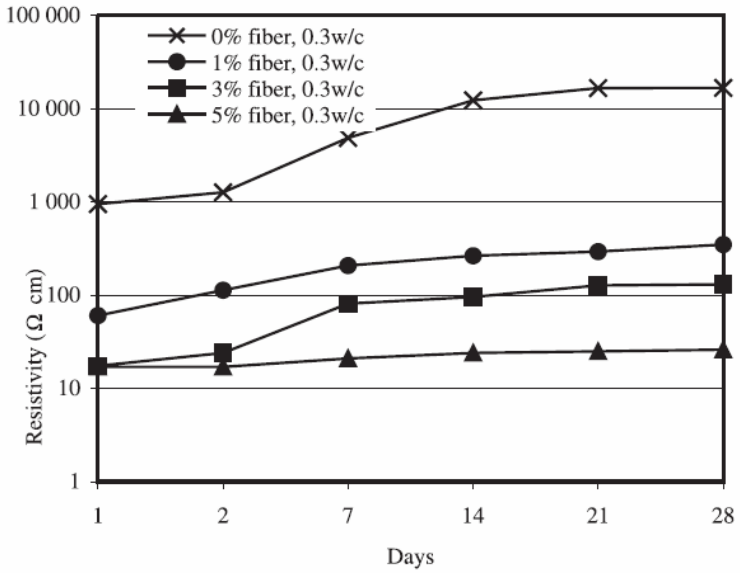


Figure 3- 5: Resistivity as a function of curing time at different fibre contents (Chacko et al. 2007)

Comparing the resistivity values of CFRC specimens and the plain sample it is noticed that although carbon fibre increases the conductivity at all ages, this improvement in conductivity appears to be more pronounced at later ages (Banthia et al. 1992).

Chako et al (Chacko et al. 2007) also investigated the effects of w/c ratio and curing method on the electrical resistivity of CFRC and concluded that w/c ratio of 0.3 shows the least amount of resistivity and that the increase in resistivity over time is greater when moist curing is employed, which is the opposite of what plain concrete demonstrates (Whiting and Nagi 2003).

At high volume fractions of carbon fibre, the w/c ratio of CFRC does not significantly affect the electrical resistivity because in this case the carbon fibres provide the primary conduction path and therefore the amount of un-hydrated water in the composite does not have a large impact on the overall resistivity (Farhad et al. 2001).

### 3.4.4 Effect of Temperature

While there has been a considerable amount of research conducted on the sensing ability of carbon fibre cement-based material, very little work has been done on the influence of temperature on the electrical resistivity of CFRC and the effect it has on the sensing feature of this material.

A letter publication by McCarter et al. (McCarter et al. 2007) focuses entirely on this issue. Experiments were conducted on carbon fibre cement mortars over the temperature range of 10–60 °C. The specimens were cured for 12 months, ensuring that the influence of age on the electrical resistivity were negligible. The results of this study show that resistivity is related inversely to the temperature, decreasing with an increase in temperature (Figure 3-5). It was also concluded that CFRC specimens are not as sensitive to changes in temperature as the plain mortar specimens (McCarter et al. 2007). It is evident from Figure 3-5 that at a certain temperature, the resistivity of the CFRC samples decreases with the increase in frequency while that of the plain specimens remains almost unchanged. This implies that carbon fibres in the composite are introducing significant scattering in conductivity (McCarter et al. 2007).

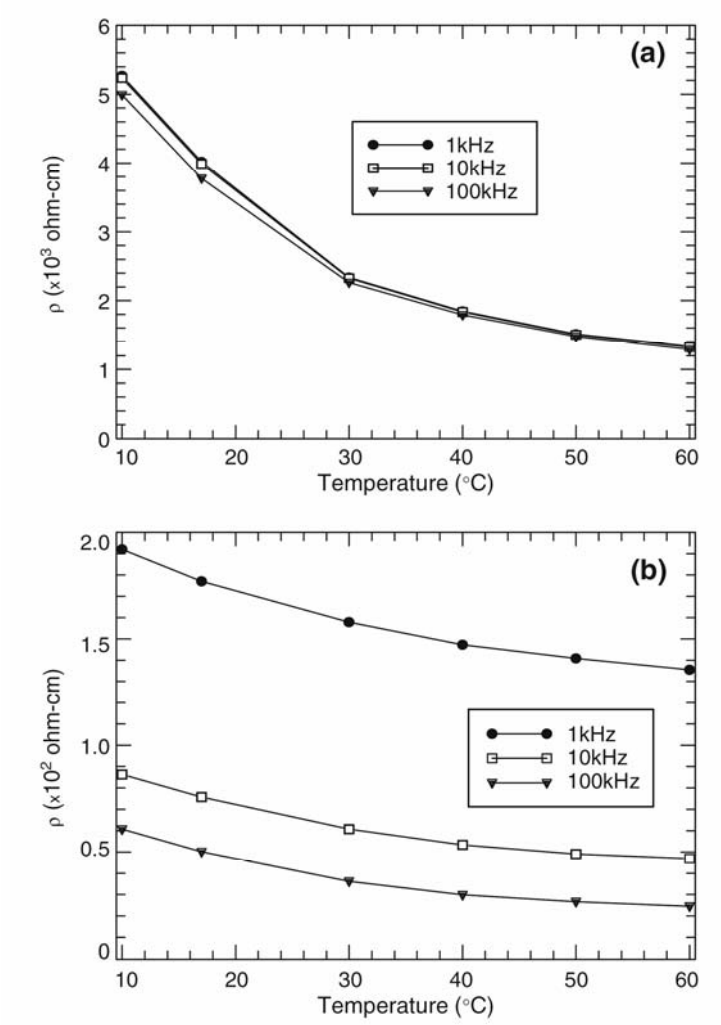


Figure 3- 6: Resistivity (ρ) variation with temperature at different frequencies for (a) plain cement mortar; (b) mortar containing 3 mm carbon fibres (McCarter et al. 2007)

It has also been proven that the effect of temperature on cement-based material is reversible which means that not only resistivity values decrease with the increase in temperature; they also increase with the decrease in temperature (Chacko et al. 2007).

It has become apparent that temperature variation during SHM influences the resistivity values acquired from cement-based sensors. Therefore, appropriate measures should be taken to reduce the effect of temperature on the sensing ability of these sensors; otherwise temperature correction must be provided.

### 3.4.5 Effect of Electrode Type and Spacing

It is important that proper electrode type is used in producing cement-based sensors. There are some basic rules that need to be considered when selecting electrodes. Electrodes should:

- Have excellent electrical conductivity themselves;
- Possess high durability towards aging, corrosion and other environmental effects;
- Have minimum influence on the mechanical properties of the sensors; and,
- Should be easy to embed in or mount on cement-based sensors and connect to the data acquisition system (DAQ).

Copper products such as foil (plate), wire and mesh (gauze) as well as silver paint or paste are the common electrode materials used in cement-based sensors. Since the cement-base sensors will be predominantly embedded in concrete structures, it is preferable that the electrodes be embedded in the sensor to ensure that the connection between the electrodes and the sensing material remains satisfactory throughout the monitoring period. However, electrodes may be surface bonded to the sensor using conductive silver paint or paste.

Han et al. (Han et al. 2007) carried out an extensive study on the electrode design and measuring methods of CFRC sensors. The results from this investigation showed that copper gauze is the ideal electrode material for CFRC sensors. With the increase in current, the polarization of specimens with gauze electrodes was proven to be weaker than that of specimens with foil electrodes. In general, compared to the other types of electrodes, copper gauze showed high durability, better compatibility with carbon fibre cement paste, low polarization, small contact resistance, and much better adaptability to the embedment style and the four-pole configuration.

It can be observed in Figure 3-6 that the fractional change in resistivity (FCR) of the sensors with embedded electrodes is quite smooth, but that of sensors with

pasted electrodes is not as smooth. Moreover, the FCR values of the specimens with pasted or surface bonded electrodes are comparatively higher and show a sharp drop at the initial loading step, which is attributed to the poor bond between the electrodes and the cement paste. Overall, embedded gauze electrodes are recommended (Han et al. 2007).

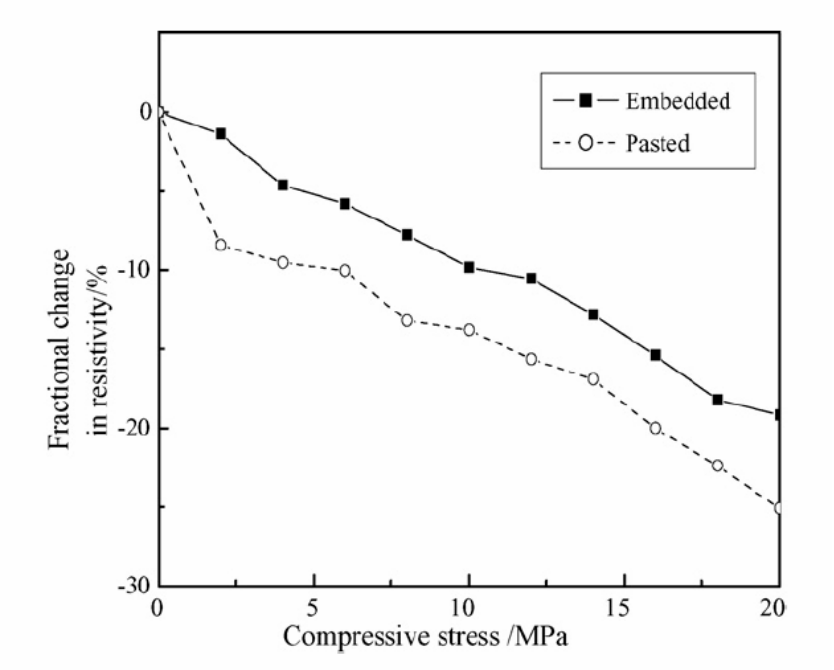


Figure 3- 7: Comparison between the response of CFRC sensors with embedded and pasted electrodes under compressive loading (Han et al. 2007)

Another important factor in the design of cement-base sensors is the effect of inter-electrode spacing. This effect was researched by Banthia et al. (Banthia et al. 1992) with a series of two-probe resistivity measurements on CFRC specimens (with dimensions of 19mm x 19mm x 150mm) containing different fibre volume fractions. The outcome, plotted in Figure 3-7, shows that the dependency of resistivity on inter-electrode spacing is somewhat more pronounced for the composites with higher fibre content than for the plain cement paste samples. It was suggested by the authors that this may be due to the heterogeneity caused by the fibres and, consecutively, related to the length of the carbon fibres. It is also concluded from Figure 3-7 that for CFRC specimens,

the resistivity values decrease with an increase in the distance between electrodes. The cause of this outcome is associated with the fact that the specimen capacitance becomes more influential at smaller inter-electrode spacing. However, for specimens with an electrode spacing of over 6 cm the resistivity values appeared to be almost constant. Hence, an inter-electrode spacing of 7 cm was recommended for this type of specimens (Banthia et al. 1992).

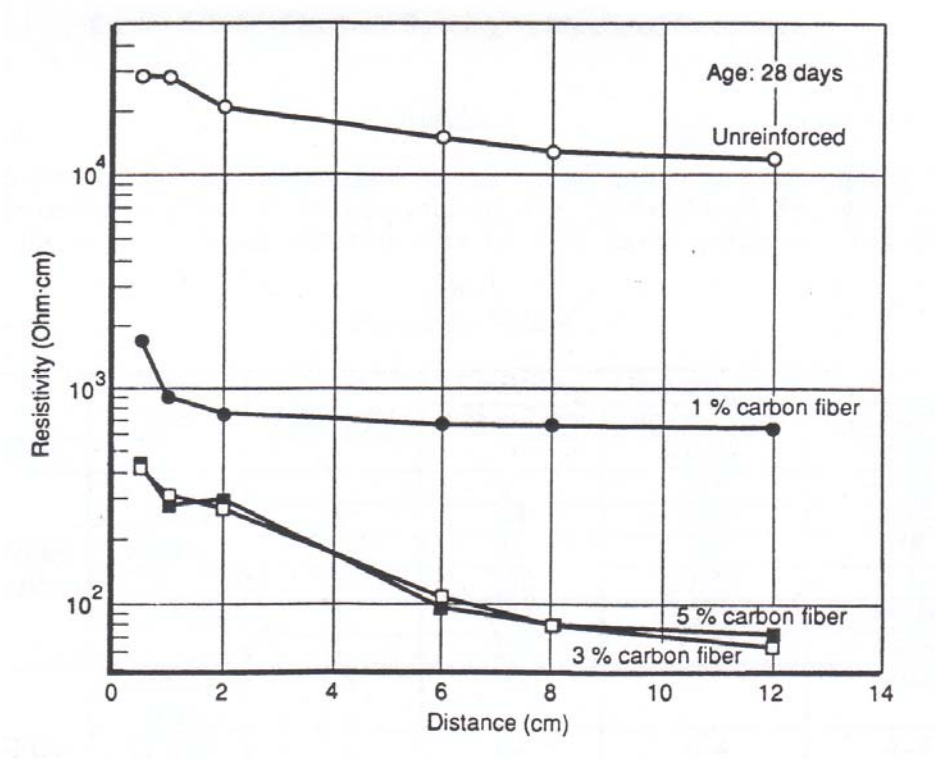


Figure 3- 8: effect of inter-electrode spacing on the resistivity of CFRC (Banthia et al. 1992)

Han et al. (Han et al. 2007) state that the resistivity of CFRC sensors is not affected by the area of voltage electrodes and the mesh size of gauze electrodes. Thus, by decreasing the area of voltage electrode along with increasing the mesh size of gauze electrodes, the influence of the gauze electrodes on the mechanical properties of CFRC sensors can be reduced to a minimum, without sacrificing the accuracy of resistivity measurements. It has also been found that the spacing between the current and voltage electrodes in the four-probe method does not

influence the resistivity when more than a critical value of 0.75 cm (Han et al. 2007).

### 3.4.6 Effect of Testing Configuration

There are two main configurations for resistivity measurements; two-probe and four-probe methods. In the four-probe method, current flows between the two outer probes and the voltage between the inner electrodes is measured, whereas in the two-probe method, only two electrodes are used for both current flow and potential measurement.

Figure 3-8 compares the resistance values obtained using two- and four-probe methods.

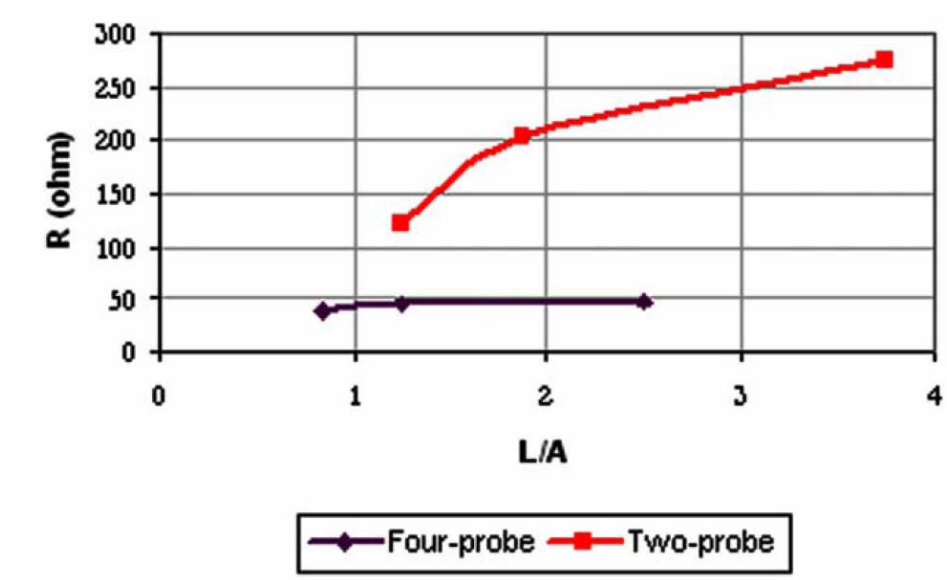


Figure 3- 9: Comparison between the two and four-probe configurations (Chiarello and Zinno 2005)

As it is clear from this figure, two-probe resistance measurements increase dramatically as L/A (electrode spacing/electrode contact area) ratio increases whereas the four-probe configuration seems to be relatively unaffected by the specimen design.

The four-probe method has also proven to provide higher gauge factors than the two probe method. In addition, the gauge factor from four-probe measurements tends to vary less with the strain amplitude (Wen and Chung 2007).

The four probe method is, by and large, preferred for the electrical resistivity measurements of cement-based sensors.

The possibility of arranging the electrodes so that measurements are taken in a direction perpendicular to the direction of the applied load was also investigated by Reza et al. (Reza et al. 2003b). Under compressive loading, no indication of internal stress is sensed when the electrical resistance is measured in the direction perpendicular to the loading direction; nevertheless the resistance values measured in this manner are much more sensitive to the propagation of large cracks.

### 3.4.7 Carbon Fibre Cement-Based Sensors upon Loading Conditions

A great number of studies have been carried out to confirm the sensing ability of carbon fibre cement-based sensors under various loading conditions (Chacko et al. 2007; Wen and Chung 2007; Wen and Chung 2005; Chen and D.D.L 1993; Chen and Chung 1993; Dragos-Marian et al. 2000).

The sensing ability of CFRC is based on its piezoresistive behaviour. The carbon fibres in CFRC bridge the micro-cracks inside the material. Under tensile loading, these fibres tend to undergo strain, causing the electrical resistivity to increase accordingly. Under compressive loading, the reverse takes place, leading to a reduction in the resistivity. This course of action is reversible under both tension and compression (in the elastic regime), which validates the stress/strain sensing concept of CFRC sensors.

Theoretical models have also been provided (Wen and Chung 2006; Zhu and Chung 2007) to gain a better understanding of the piezoresistive phenomenon in CFRC sensors under compression, tension and flexure. Figure 3-9 demonstrates

the agreement between the developed theoretical models and the experimental results from CFRC sensors under uniaxial compressive and tensile loading.

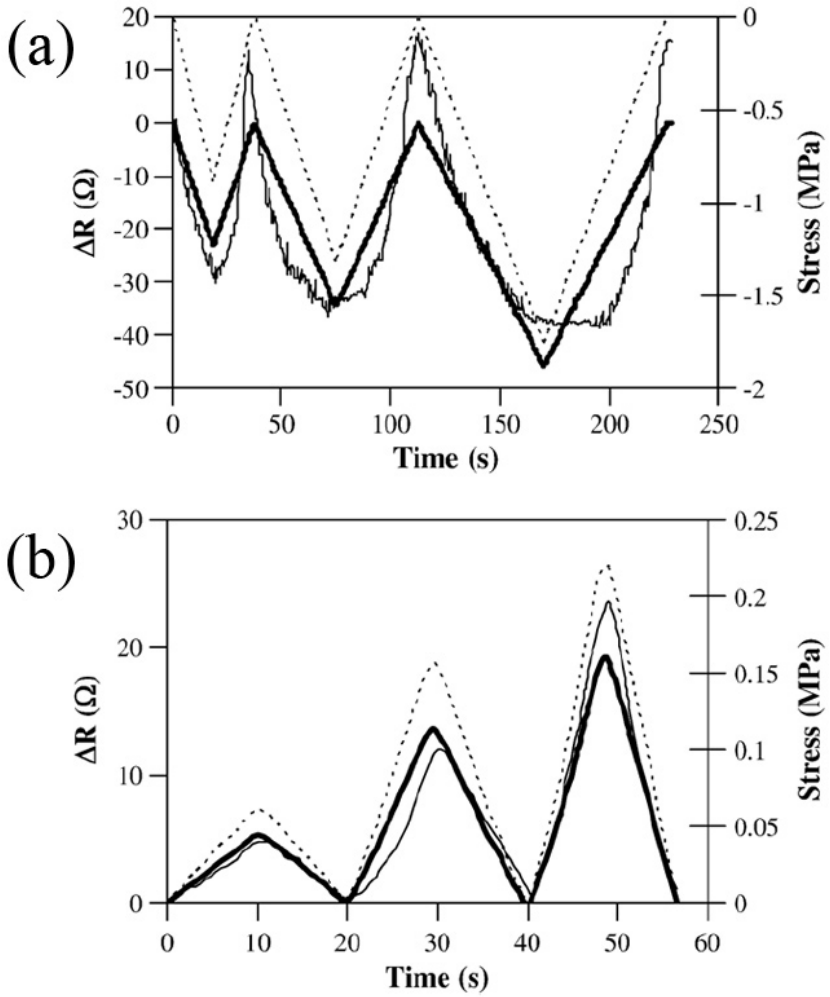


Figure 3- 10: Comparing the measured and theoretical values of change in electrical resistance under (a) uniaxial compression, and (b) uniaxial tension (Wen and Chung 2006)

It has been confirmed by every research carried out, that CFRC sensors are a perfect alternative for monitoring the stress/strain in concrete structures.

Furthermore, results from compact tension tests on carbon fibre-reinforced mortar specimens (Reza et al. 2003a) have shown that smart CFRC could potentially be used as an aid in the fracture mechanics studies of concrete.

### 3.4.8 Carbon Fibre Cement-Based Sensors for Corrosion detection

It is also believed by some researchers (Chacko et al. 2007) that CFRC sensors may be used to monitor the corrosive environment in the vicinity of steel reinforcement. In order to confirm this claim, Chako et al. (Chacko et al. 2007) carried out a set of experiments, comparing the resistivity values of CFRC specimens prepared with normal water and NaCl solution. The results, shown in Table 3-1, indicate that samples prepared with chloride solution exhibit lower resistivity values than the equivalent samples prepared with plain water.

Table 3- 1: Resistivity values for CFRC samples with and without the presence of chloride ions (Chacko et al. 2007)

| | Resistivity at 28 d (Ω·cm) | Difference (%) |
|---|---|---|
| 30 mm sample with NaCl | 33 | — |
| 30 mm sample without NaCl | 69 | 52 |
| 70 mm sample with NaCl | 34 | — |
| 70 mm sample without NaCl | 46 | 26 |

## 3.5 Carbon Black Cement-Based Sensors

The sensing ability of carbon fibre reinforced cement-based materials becomes even more enhanced when carbon black is also added to the material as electrical fillers. Researchers in China (Han and Ou 2007; Ou 2006) have found that the sensing properties of cement-based material containing both carbon fibres and carbon black are more stable with better repeatability and sensitivity than that of only containing carbon fibres.

In a recent study by Han and Ou (Han and Ou 2007), the piezoresistivity of cement-based material with carbon fibre and carbon black was investigated. Cubic specimens, shown in Figure 3-10, were tested under single compressive loading and repeated compressive loads at different loading amplitudes.

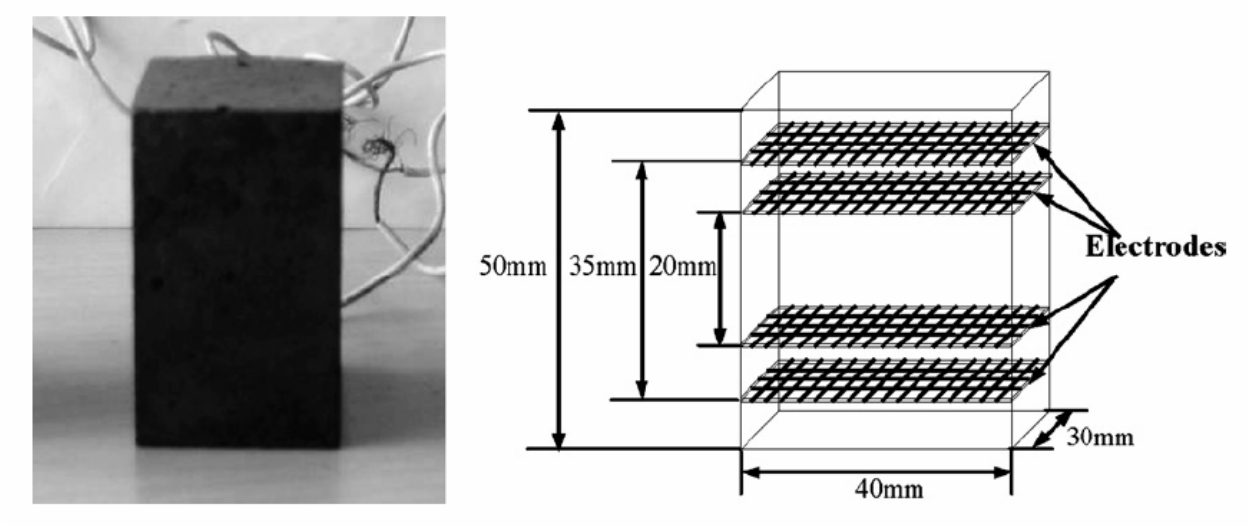


Figure 3- 11: Cement-based sensor with carbon fibre and carbon black (Han and Ou 2007)

Upon single compressive loading, the fractional change in electrical resistivity of the sensors decreased (by up to 27%) as the compressive stress/strain increased. Compressive stress, in turn, increased approximately linearly with the compressive strain until the specimens crushed. At the ultimate stress, which was about 40 MPa, the electrical resistivity started to increase (Han and Ou 2007).

The results from specimens tested under repeated compressive loads found the piezoresistivity of this type of sensor to be reversible and stable within the elastic regime (Figure 3-11) with a gauge factor of 227. The relationship between the fractional change in resistivity (ρ) and the compressive stress/strain was expressed as (Han and Ou 2007):

$$\rho = -1.35\sigma \qquad (3\text{-}1)$$

*or*

$$\rho = -0.0227\varepsilon$$

Where ρ is electrical resistivity, σ is the compressive stress (MPa) and ε is the compressive strain (με).

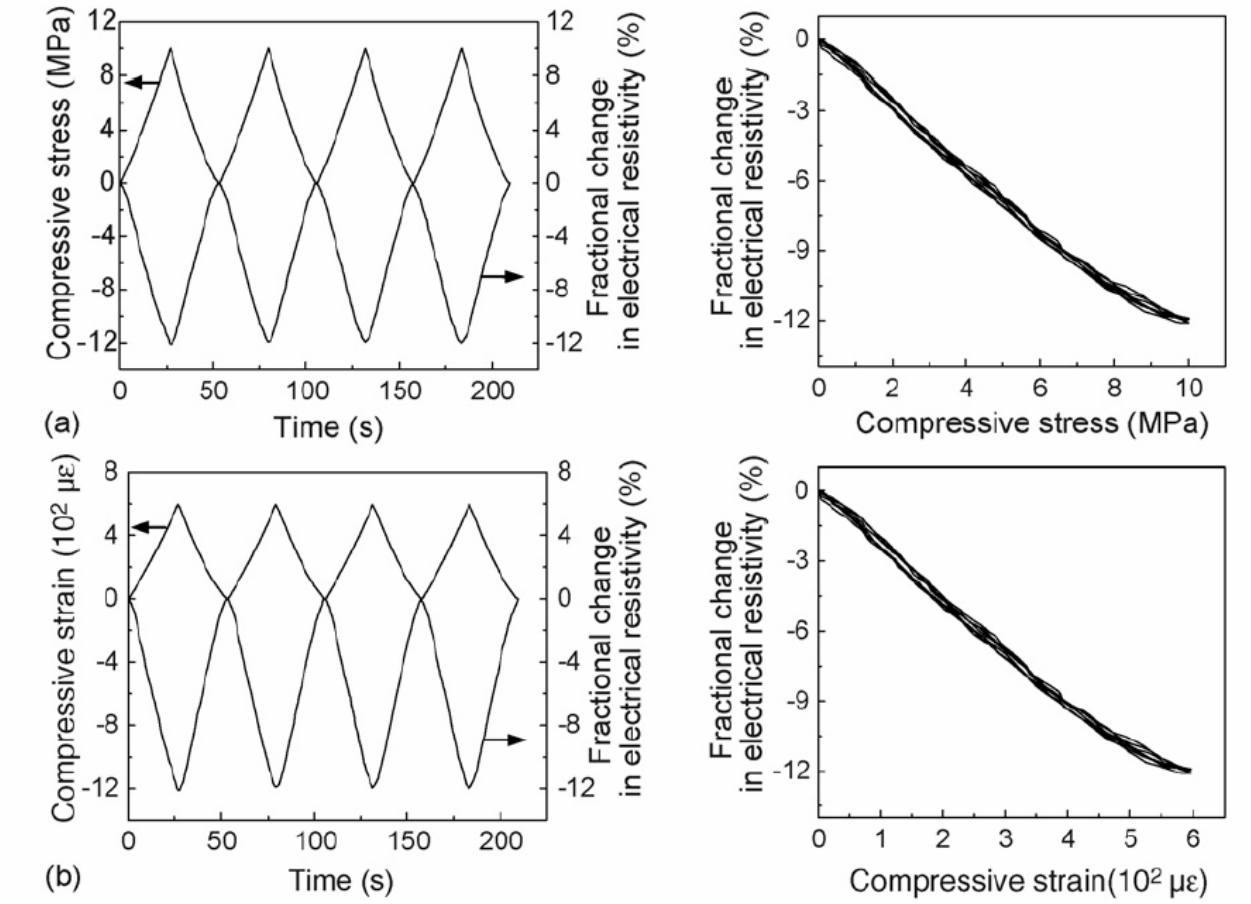


Figure 3- 12: Fractional change in electrical resistivity of cement-based sensors with carbon fibre and carbon black at different (a) compressive stress values and (b) compressive strain values, in the elastic regime (Han and Ou 2007)

It was confirmed, however, that when the compressive loading amplitude was increased to more than 30% of the ultimate strength, the deformation went beyond the elastic regime and as a result, response of the contact resistance to plastic deformation was irreversible (Han and Ou 2007).

The performance of the carbon fibre – carbon black hybrid cement-based sensors in monitoring the strain of structures was examined in China (Ou 2006), through a number of tests on concrete members with embedded sensors. It was concluded that the sensors can monitor the strain of concrete columns and beams. In fact, these sensors have recently been embedded into the girders of the Chongqing Guangyang Island Bridge, as shown in Figure 3-12, and the results

indicate that the strain measured by these cement-based sensors agree well with the strains measured by Fibre Bragg Gratings (Ou 2006).

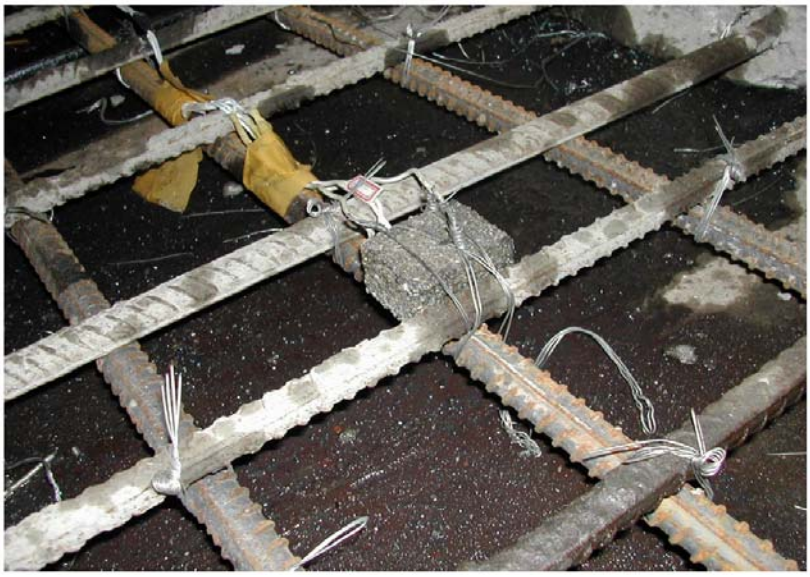

Figure 3- 13: Carbon fibre – carbon black cement-based sensors embedded in the Chongqing Guangyang Island Bridge in China (Ou 2006)

# 3.6 Carbon NanoTube Cement-Based Sensors

## 3.6.1 Nanotechnology

A nanometre (nm) is one billionth of a meter. The devices and materials dealt with in nanotechnology are typically in a size range of 0.1 nm to 100 nm. Nanotechnology is referred to the science and technology of developing materials at the atomic and molecular level and generating techniques in order to measure and utilize their unique and special electrical, mechanical and chemical features. The application of Nanotechnology in almost every field, from microelectronics, mechanical devices, semiconductors and computer technology to biotechnology, chemistry and medicine to materials science, manufacturing and energy, is increasingly growing. Nanotechnology is expected to make a significant contribution to future scientific and hi-tech developments.

### 3.6.2 Carbon NanoTubes

Discovered almost 30 years ago Iijima (Iijima 1991), carbon nanotubes (CNT) are one of the most important materials employed in nanotechnology.

Graphite consists of numerous layers of carbon atoms bonded in a hexagonal pattern in flat sheets, with weak bonds between the sheets and strong bonds within them. A CNT can be visualized as a modified form of graphite, where a single sheet or several sheets of graphite are seamlessly rolled up into a tube structure (Makar and Beaudoin 2003). Single sheets rolled up are referred to as single-walled carbon nanotubes (SWCNT) and multiple sheets rolled up are termed multi-walled carbon nanotubes (MWCNT). Figure 3-13 schematically shows the two different types of CNT.

Depending on the type, growth process and treatment, CNT may have different diameters and lengths. The diameter of CNT is generally in the range of a few nanometers (more than 10,000 times thinner than a single strand of human hair) to 100 nm, while their length is generally in the order of 1 to 30 micrometers (offering aspect ratios of up to 1000). However, CNT with lengths of up to several millimeters have recently been produced which significantly enhance their aspect ratio.

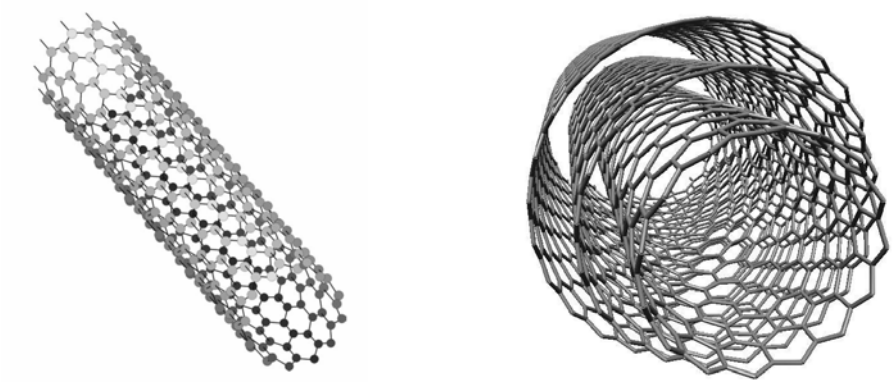

**(a) SWCNT** **(b) MWCNT**

Figure 3- 14: Schematic of a (a) Single-Walled Carbon Nanotube (Makar and Beaudoin 2003)and a (b) Multi-Walled Carbon Nanotube (Ahwahnee Technology 2007)

### 3.6.3 Carbon NanoTubes in the Construction Industry

The application of nanotechnology and in particular carbon nanotubes in civil engineering materials and structures has recently intrigued the interest of many researchers.

The properties of CNT depend on their type, chirality (the orientation of the hexagons formed by the carbon atoms with respect to the tube axis) and diameter but in general carbon nanotubes present outstanding mechanical properties such as elastic moduli in the TPa range, ultimate strength as high as 60 GPa and ultimate strain of up to 10% (Wansom et al. 2006; Makar et al. 2005).

It is suggested by researchers (Makar and Beaudoin 2003) that longer CNT, formed into ropes, would possibly be utilized in the future in applications such as longer-span suspension bridges, improved pre- or post- tensioned concrete structures and the construction of very large, space based structures, including space elevators.

In addition to their extraordinary mechanical properties, CNTs have extremely high aspect ratios (generally greater than 1,000,000:1). The combination of these properties has established CNT as ideal reinforcing fibres for stronger and tougher cement and concrete materials. CNT is known to have diameters similar in scale to the layers in calcium-silicate-hydrate (C-S-H) in hydrated cementitious composites (Makar and Beaudoin 2003).

The results of a comparative study on the microstructure and mechanical properties of carbon fibre cement mortar (CFCM) and carbon nanotubes-cement mortar (CNTCM) (Gengying and Peiming 2005), reveal that CNTCM has superior compressive and flexural strengths than CFCM. The authors (Gengying and Peiming 2005) also state that carbon nanotubes are enwrapped

by C-S-H and that the pore size distribution in matrix is significantly refined when incorporating CNT, decreasing the porosity of the cement mortar.

In another study at the National Research Council Canada (Makar et al. 2005), SWCNT (at 0.02 by weight of composite) were dispersed by sonication in isoproponal to produce SWCNT-cement composites. Scanning electron microscopy (SEM) of these composites confirms observable crack bridging and fibre pullout (see Figure 3-14) as well as bonding between SWCNT and the cement matrix. As a result of these reinforcing mechanisms, higher micro-hardness measurements were obtained at early stages of composite hydration as compared to cement control samples without SWCNT (Makar et al. 2005).

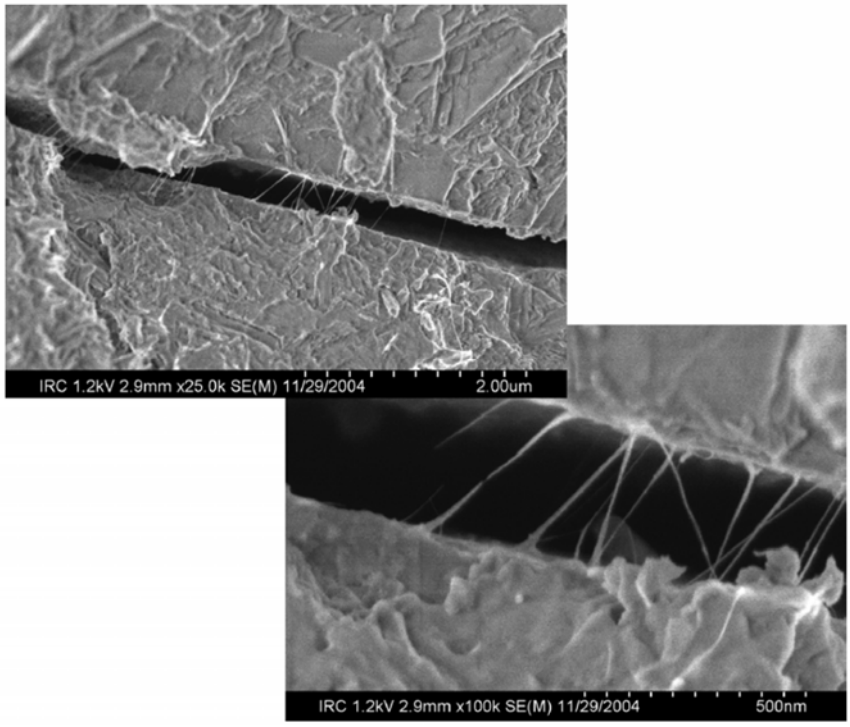


Figure 3- 15: SEM of crack bridging and reinforcing behaviour in SWCNT-cement composites at 3 days hydration (Makar et al. 2005)

Comparing the mechanical properties of CNT reinforced cement composites to control Portland cement composites and the widely used carbon fibre reinforced cement composites, have proven that given their efficient reinforcing mechanism,

CNTs improve the flexural and compressive strengths as well as the failure strain of cement composites (Li et al. 2007).

The use of carbon nanotubes as reinforcement for production of foam non-autoclave concrete produced on the basis of Portland cement has also been investigated (Yakovlev et al. 2006) and the results showed that the use of carbon nanotubes (0.05 % by mass) in production of these concretes decreases their heat conductivity up to 12 – 20 % and increases its compressive strength up to 70 %.

### 3.6.4 Sensing Application of Carbon Nanotubes

With regards to their electrical properties, SWCNT can be either semi-conducting or metallic, depending upon their chirality, while MWCNT are metallic in character with electrical conductivities in the order of $10^5$–$10^6$ $S.m^{-1}$ (Wansom et al. 2006).

The electrical resistance and pressure-sensitive properties as well as mechanical properties and microstructure of CNT-cement paste were investigated by Li et al. (Li et al. 2007). In this study, cement paste containing untreated CNT (PCNT), and cement paste containing treated CNT (which are known to improve the flexural and compressive behaviour of the composite), using a mixed solution of $H_2SO_4$ and $HNO_3$, (SPCNT) were tested. Electrical resistivity and pressure-sensitive properties under cyclic compressive loading were analyzed and compared for both sample types. Results indicated that the addition of CNT, treated or untreated, to cement paste leads to a notable decrease in volume electrical resistivity and a distinct enhancement in the pressure-sensitive properties for cement composites. SEM observations revealed that both treated and untreated CNT were dispersed homogenously in the cement matrix. As shown in Figure 3-15, illustrating the variation of the electrical resistivity for SPCNT and PCNT composites under repeated compressive loading, the resistivity of both SPCNT and PCNT specimens remarkably change under cyclic compressive loading. However, according to this figure, the fractional change in

resistivity for SPCNT goes up to 14%, whereas that of PCNT reaches 10%, which means that the treated CNT have a stronger effect on enhancing pressure-sensitive properties. The untreated CNT, on the other hand, have a greater effect on reducing the electrical resistivity of the composite. These effects are explained through microscopic observations. SEM images reveal a well-formed three-dimensional meshwork in the PCNT samples responsible for higher conductivities. However, due to the fact that this meshwork was already well developed, the number of contact points of PCNT showed relatively fewer changes with the variation of compressive load. Conversely, the SPCNT were covered by C–S–H (leading to a higher mechanical strength) and no meshwork was formed; thus, both the contact points and the distances among SPCNT noticeably vary with the variation of applied compressive force (Li et al. 2007).

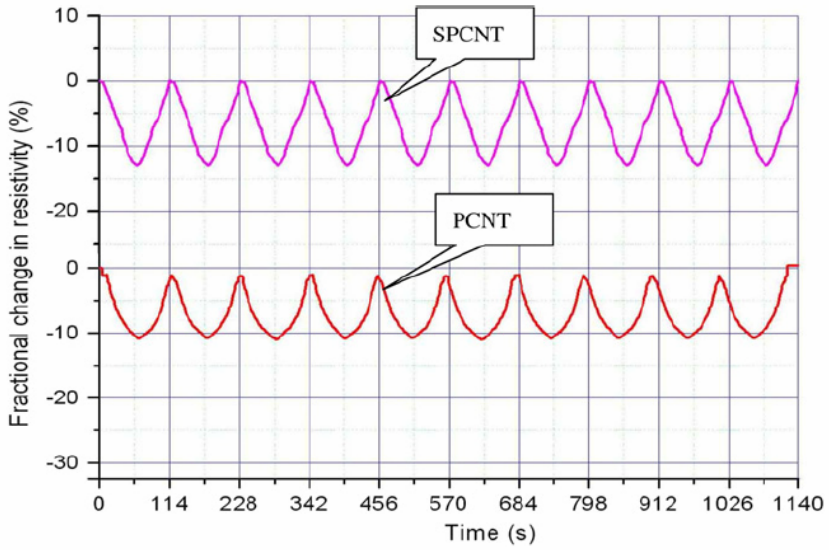


Figure 3- 16: Fractional change in resistivity of PCNT and SPCNT under repeated compressive loading (Li et al. 2007)

Apart from a few recent studies, mostly in China, very little work has been done on developing cement-based sensors using carbon nanotubes. Nevertheless, CNT has been integrated into other matrices to develop novel strain gauges with high gauge factors for SHM. The piezoresistive nature of CNT and their composites are utilized along with nanotechnology to develop a new class of sensing

transducers at the molecular length-scale. One of these sensors, known as conformable SWNT-PE thin film strain sensor, is based on a layer-by-layer chemical film deposition technique to produce a nano-composite consisting of SWCNT and polyelectrolytes (PE), capable of sensing strains through linear changes in resistivity with applied strain (Loh et al. 2005; Loh et al. 2006). Another example of these strain sensors are the ones constructed by incorporating CNT in silicon substrates using the fabrication tools offered by microelectromechanical systems (MEMS) (Loh et al. 2005).

These nanotechnology and MEMS-based systems have matured in the recent years to provide wireless, inexpensive, durable, compact, and high-density information sensors and hence can be used to wirelessly monitor the health and safety of concrete structures through detecting various damage mechanisms (Robinson and Saafi 2006). MEMS devices can be embedded or surface mounted to detect key parameters affecting the integrity and durability of civil infrastructure such as cracks and other types of damage, temperature, moisture, $Cl^-$, pH and $CO_2$. These devices are therefore able to monitor the stability of critical structures during floods and barge impact (Robinson and Saafi 2006).

# CHAPTER 4

# Preliminary Experiments

## 4.1 Material

### 4.1.1 Cement

GU (formerly Type 10) Portland cement was used in these experiments. The specific gravity reported for this type of cement is 3.15.

### 4.1.2 Silica Fume

Densified silica fume with a specific gravity of 2.27 from Norchem, Inc. was used as a densifier as well as a dispersant.

### 4.1.3 Water

Normal tap water was used for these experiments.

### 4.1.4 Carbon Fibre

Petroleum pitch-based carbon fibre (PPCF) from Kureha Corporation with specifications presented in Table 4-1 was used. Figure 4-1 displays an image of these fibres.

Table 4- 1: Properties of petroleum pitch-based carbon fibres

| Length (mm) | Diameter (μm) | Specific Gravity | Tensile Strength (MPa) | Modulus of Elasticity (GPa) | Volume Resistivity (Ω-m) |
|---|---|---|---|---|---|
| 6 | 18 | 1.65 | 590 | 35 | $150 \times 10^{-6}$ |

Figure 4- 1: 6mm petroleum pitch-based carbon fibres

### 4.1.5 Methycellulose

METHOCEL* A15 LV Methylcellulose from Dow Chemical Canada Inc. was used to help disperse carbon fibres. Methylcellulose, when used, should be added at a preferred amount of 0.4% of the cement weight.

### 4.1.6 Superplasticizer

The high-range water-reducing admixture used in these experiments was Glenium 3000 NS from Master Builders which is a polycarboxylate-based superplasticizer with a specific gravity of 1.08.

### 4.1.7 Copper Plates

Thin copper plates with excellent electrical conductivity, cut into 25mm x 7mm pieces, were used as electrodes.

## 4.2 Mix Proportions

Five sets of twelve specimens were made; the control specimens containing no fibre (0N), specimens with 2% and 5% of carbon fibre by volume (0N and 5N) and samples containing 2% and 5% carbon fibre as well as methylcellulose (2M and

5M), in order to investigate the effects of methylcellulose. The mix proportions for these preliminary experiments are presented in Table 4-2.

Table 4- 2: Mix proportions for preliminary tests

| **Batch Name** | **0N** | **2N** | **5N** | **2M** | **5M** |
|---|---|---|---|---|---|
| **Fibre (volume %)** | 0 | 2 | 5 | 2 | 5 |
| **Methylcellulose (g)** | 0 | 0 | 0 | 4 | 10 |
| **W/CM** | 0.3 | 0.3 | 0.3 | 0.3 | 0.3 |
| **Silica Fume/ Cement (by weight)** | 0.2 | 0.2 | 0.4 | 0.2 | 0.4 |
| **Superplasticizer (g)** | 0 | 5 | 12 | 5 | 12 |

# 4.3 Mixing Procedure

A Hobart mixer (4.5 L) was used for mixing. However, a high shear mixer would have been a more preferable device for the purpose of mixing cement based materials containing fibres. The following procedure was used:

- The fibres were dispersed manually as much as possible.
- For the batches with methylcellulose, a solution of methylcellulose with three quarters of the required water was prepared according to the directions on the product container. The fibres were then introduced into this solution and manually mixed.
- Cement and silica fume were mixed thoroughly in the mixer.
- Fibre (dry for the normal batches and mixed with methylcellulose solution for 2M and 5M batches) was gradually added to the cement and silica fume.
- Superplasticizer was added to the remaining water and the solution was gradually added to the mix.

- Mixing continued for 3 more minutes until the mixture formed a paste. In the case of high fibre volume fractions, this was very difficult to achieve.

## 4.4 Specimen Preparation

The mix was poured into oiled 150 mm x 25 mm x 15 mm plexiglass moulds. The moulds were then placed on a mechanical shake table, gently vibrating the specimens while inserting the copper electrodes. Two electrodes spaced at 70mm were inserted into the cement paste specimens. Specimens were air cured in the curing room for twenty four hours before carefully stripping the moulds. Figure 4-2 displays a few prepared specimens.


Figure 4- 2: Preliminary Specimens (0%, 2% and 5% $V_f$)

## 4.5 Test Setup

### 4.5.1 Equipment

The equipment used in the preliminary set of tests is as follows (Figure 4-3):

- A hand-made circuit board prepared by the technicians
- A function generator
- Two alligator clip leads
- A laptop with DASY Lab 8.0 software

- Instron FastTrack 8802 Servo-hydraulic Mechanical Testing System

Figure 4- 3: Preliminary Test Setup

### 4.5.2 Resistivity Measurement Technique

A schematic view of the test setup is shown in Figure 4-4. The two-probe technique was employed for the electrical resistivity measurements. A known AC voltage of ±10V was applied across the electrodes using a function generator. The current frequency for these tests was approximately 1.46 Hz.

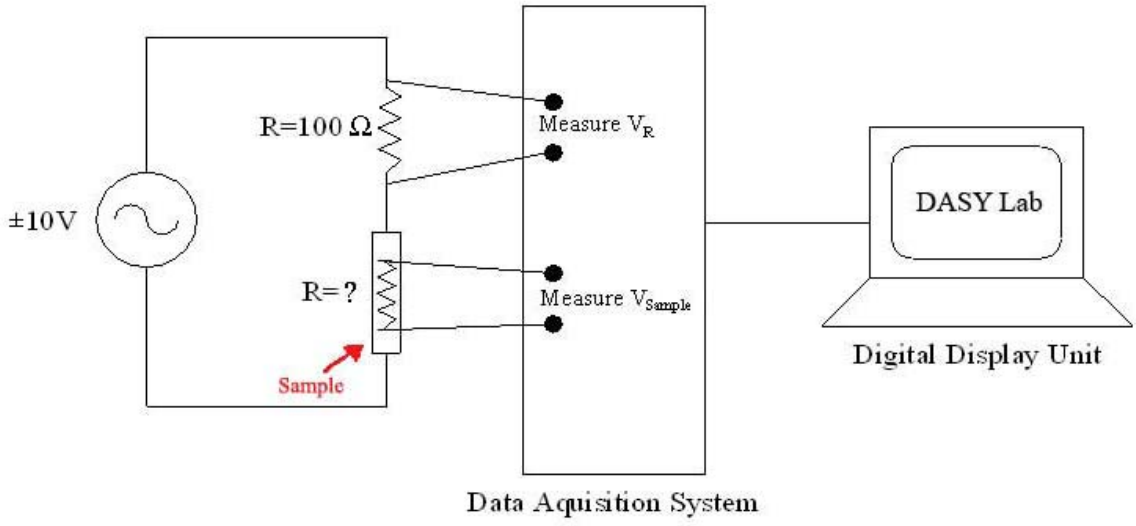


Figure 4- 4: Schematic Display of the Preliminary Test Setup

As shown in Figure 4-4, a known resistance of 100 ohms and the specimen are connected in series on the circuit board. The voltages across the known resistor and the sample are acquired and sent to DASY Lab. The current flowing through both the resistor and the sample is constant, hence according to Ohm's law:

$$I = \frac{V_R}{R} = \frac{V_{Sample}}{R_{Sample}} \qquad (4\text{-}1)$$

Where,

$V_R$: voltage across the known resistor R

R: resistance of the known resistor =100 Ω

$V_{Sample}$: voltage across the sample which is the unknown resistor, and

$R_{Sample}$: resistance pf the sample

The resistance of the sample is easily computed in DASY Lab using the above equation. The resistivity values of the specimens are then calculated using Equation 2-3 and plotted against various parameters.

# CHAPTER 5

# Main Experiments

## 5.1 Material

### 5.1.1 Cement

GU (formerly Type 10) Portland cement was used in the main set of experiments. The specific gravity reported for this type of cement is 3.15.

### 5.1.2 Silica Fume

Densified silica fume with a specific gravity of 2.27 from Norchem, Inc. was used as a densifier as well as a dispersant.

### 5.1.3 Water

Normal tap water was used for these experiments with the exception of specimens with carbon nanotubes, where distilled water was used.

### 5.1.4 Carbon Fibre

K6371T Carbon Fibre DIALEAD from Mitsubishi Chemical FP America, Inc. was used in these experiments. These coal tar pitch-based carbon fibres (CPCF) have specifications indicated in Table 5-1. An image of these fibres is shown in Figure 5-1.

Table 5- 1: Properties of K6371T coal tar pitch-based carbon fibres

| Length (mm) | Diameter (μm) | Specific Gravity | Tensile Strength (MPa) | Modulus of Elasticity (GPa) | Volume Resistivity (Ω-m) |
|---|---|---|---|---|---|
| 6 | 11 | 2.12 | 2620 | 634 | $2.3 \times 10^{-6}$ |

Figure 5- 1: K6371T coal tar pitch-based carbon fibres

### 5.1.5 Carbon Nanotubes

Both Multi-Walled Carbon NanoTubes (MWCNT) and Single-Walled Carbon NanoTubes (SWCNT) were obtained from Cheaptubes.com for these experiments. Purified MWCNT with specifications listed in Table 5-2 were used. Figure 5-2 is an image of these MWCNTs. Schematics of both SWCNT and MWCNT are presented in Figure 3-12 of Chapter 3.

Table 5- 2: Properties of MWCNT

| Outer Diameter (nm) | Inside Diameter (nm) | Purity | Length (μm) | Specific Surface Area ($m^2/g$) | Specific Gravity | Electrical Conductivity (s/cm)* |
|---|---|---|---|---|---|---|
| 10-20 | 3-5 | > 95 wt% | 10-30 | 233 | ≈1.5 | $> 10^{-2}$ |

* SI unit for electrical conductivity (siemens per centimeter).

Figure 5- 2: Multi-Walled Carbon NanoTubes

SWCNT used have specifications listed in Table 5-3.

Table 5- 3: Properties of SWCNT

| Outer Diameter (nm) | Inside Diameter (nm) | Purity | Length (µm) | Specific Surface Area ($m^2/g$) | Specific Gravity | Electrical Conductivity (s/cm) |
|---|---|---|---|---|---|---|
| 1-2 | 0.8-1.6 | > 60 wt% | 5-30 | 407 | ≈1.5 | $> 10^{-2}$ |

### 5.1.6 Methycellulose

METHOCEL* A15 LV Methylcellulose from Dow Chemical Canada Inc. was used to help disperse carbon fibres. Methylcellulose, if used, must be added at a preferred quantity of 0.4% of the cement weight.

### 5.1.7 Defoamer

A defoamer should be used whenever methylcellulose is used in the amount of 0.13 vol. %. RHODOLINE 1010 which is a water base defoamer was obtained from Rhodia Group and used in these experiments.

### 5.1.8 Superplasticizer

The high-range water-reducing admixture used in these experiments was Glenium 3400 NV from Master Builders which is a polycarboxylate-based superplasticizer with a specific gravity of 1.1.

### 5.1.9 Copper Plates, Mesh and Wire

Thin copper plates and copper mesh cut into 25mm x 7mm pieces and uncoated copper wire were used as electrodes.

### 5.1.10 Silver Paste

To attach the copper wire to the surface of the specimens, SPI conductive silver paste plus which is a high purity, uniform, viscous silver paste was used.

## 5.2 Mix Proportions

Fourteen sets of specimens were made with varying carbon fibre and carbon nanotube volume fractions. Mix proportions for these experiments are presented in Table 5-4. The amount of carbon fibre was increased gradually until it reached a point were mixing became very difficult. Silica fume was used in all specimens as a supplementary cementing material and to assist in fibre dispersion. For specimens with very high fibre contents and specimens containing carbon nanotubes, the water to cement ratio was increased from 0.3 to 0.4. Methylcellulose and defoamer were also used in these batches to improve the dispersion of carbon fibres and nanotubes.

Table 5- 4: Mix proportions for the main set of tests

| Type (Vol. % of Carbon Fibre or CNT) | SF/Cement (by weight) | (W/CM) | SP (% of CM) | MC (% of CM) | Defoamer (% of CM) |
|---|---|---|---|---|---|
| 0 % | 0.2 | 0.3 | 0.2 | 0 | 0 |
| 0.5 % | 0.2 | 0.3 | 0.3 | 0 | 0 |

| | | | | | |
|---|---|---|---|---|---|
| 1% | 0.2 | 0.3 | 0.3 | 0 | 0 |
| 2% | 0.2 | 0.3 | 0.4 | 0 | 0 |
| 7% | 0.2 | 0.3 | 0.8 | 0 | 0 |
| 3.5% | 0.2 | 0.3 | 0.4 | 0 | 0 |
| 5% | 0.2 | 0.3 | 0.5 | 0 | 0 |
| 15% | 0.2 | 0.3 | 1.2 | 0 | 0 |
| 15%MD | 0.2 | 0.3 | 1.2 | 0.4 | 0.2 |
| 20%MD | 0.2 | 0.4 | 2.5 | 0.4 | 0.2 |
| MWCNT (1%) | 0.2 | 0.4 | 0.8 | 0.4 | 0.2 |
| SWCNT (1%) | 0.2 | 0.4 | 0.8 | 0.4 | 0.2 |
| MWCNT (3%) | 0.2 | 0.4 | 0.8 | 0.4 | 0.2 |
| Hybrid (15%CF +1% MWCNT) | 0.2 | 0.4 | 2 | 0.4 | 0.2 |
| Hybrid (15%CF +3% MWCNT) | 0.2 | 0.4 | 2 | 0.4 | 0.2 |

SF/cement: silica fume to cement ratio

W/CM: water to cementitious material (cement and silica fume) ratio

SP (% of CM): superplasticizer as a percentage of cementitious material

MC (% of CM): methylcellulose as a percentage of cementitious material

Defoamer (% of CM): defoamer as a percentage of cementitious material

# 5.3 Mixing Procedure

## 5.3.1 Mixing Procedure for Batches with Carbon Fibre

A Hobart mixer (4.5 L) was used for mixing. However, in hindsight, a high shear mixer would have been a more preferable device for the purpose of mixing cement based materials containing fibres. The following procedure was used:

- For the batches with methylcellulose, a solution of methylcellulose with the required water was prepared according to the directions on the product container.
- Cement and silica fume were mixed thoroughly in the mixer.

- Fibre was gradually added to the cement and silica fume.
- Superplasticizer was added to the water (or the water + methylcellulose solution) and the solution was gradually added to the mix.
- The defoamer was added to the mix at this stage.
- Mixing continued for 3 more minutes until the mixture formed a paste. In the case of high fibre volume fractions, this was more difficult to achieve.

### 5.3.2 Mixing Procedure for Batches with Carbon NanoTubes

For the batches containing carbon nanotubes, the following procedure was conducted:

- A solution of methylcellulose with the required water was prepared according to the directions on the product container. Superplasticizer was also added to this solution.
- MWCNT or SWCNT was carefully weighed and the correct amount was added to the water in a jar.
- The CNT and water mixture were sonicated for at least an hour (Figure 5-3) in order to help disperse the CNT.
- Cement and silica fume were mixed thoroughly by hand.
- The CNT and water solution was gradually added to the cement and silica fume and were mixed or a few minutes under a fume hood, until the mix became a paste.
- The defoamer was added to the mix at this stage and the paste was mixed for another minute by hand.
- In the case of the hybrid batch, a cooking hand mixer was used and the cement, nanotubes and silica fume were mixed thoroughly under a fume hood (see Appendix C on health and safety issues associated with carbon nanotubes). The carbon fibre first and then the water were added gradually to the mix until a paste was formed.


(a) (b)

Figure 5- 3: Preparing CNT for the mix; (a) CNT in water and (b) Sonication of the mixture

# 5.4 Specimen Preparation

The specimens were prepared in a variety of shapes and sizes (150 x 25 x 15mm, 150 x 25 x 10mm, 300 x 25 x 15mm and 50 x 10 x 10mm rectangular prisms, as well as 50.8 x 100mm cylinders) suitable for different loading and environmental experiments.

The mix was poured into previously oiled moulds. The moulds were then placed on a mechanical shake table, gently vibrating the specimens while inserting the copper electrodes. Either two or four electrodes were inserted into the rectangular cement paste specimens. Specimens were air cured in the curing room for twenty four hours before carefully stripping the moulds. The cylinder specimens were ground and tile sawed after 28 days and copper wire was tightly wound around the specimens and a thin line of conductive silver paste was applied over them. Four pieces of wire were attached in this manner to create four electrodes.

# 5.5 Test Setup

## 5.5.1 Equipment

The equipment used in the main set of tests is as follows (Figure 5-4):

- Agilent 4263B LCR Meter

- HP 16089B Kelvin Clip Leads
- HP 16089D Alligator Clip Leads
- Laptop with NI LabVIEW 8.2 platform
- Agilent 82357B USB/GPIB Interface
- Hitachi S-3000N Scanning Electron Microscope (SEM)
- Solartron 1260 Impedance/Gain-Phase Analyzer
- Autoclave
- USB-502 RH/Temperature Data Logger
- Environmental Chamber
- Freezer
- Desiccator
- Instron FastTrack 8802 Servo-hydraulic Mechanical Testing System
- Signal Conditioning Device
- NI USB-6251 Multifunctional Data Acquisition System

Figure 5- 4: Main Resistivity Test Setup

### 5.5.2 Resistivity Measurement Technique

A schematic view of the test setup is shown in Figure 5-5. The LCR meter provided the resistance values of the specimen subjected to an alternating current (AC) at specific frequencies. For the majority of the experiments, the frequency was set to 100 kHz and the voltage to 100 mV. These resistance data was then transferred to LabVIEW through the GPIB (general purpose interface bus), where it was converted to resistivity values (Equation 2-3) and plotted against time and various loading and environmental parameters. Moreover, in addition to resistance values, the LCR meter was at times set to provide other impedance parameters, such as the reactance, the phase angle and the impedance itself.

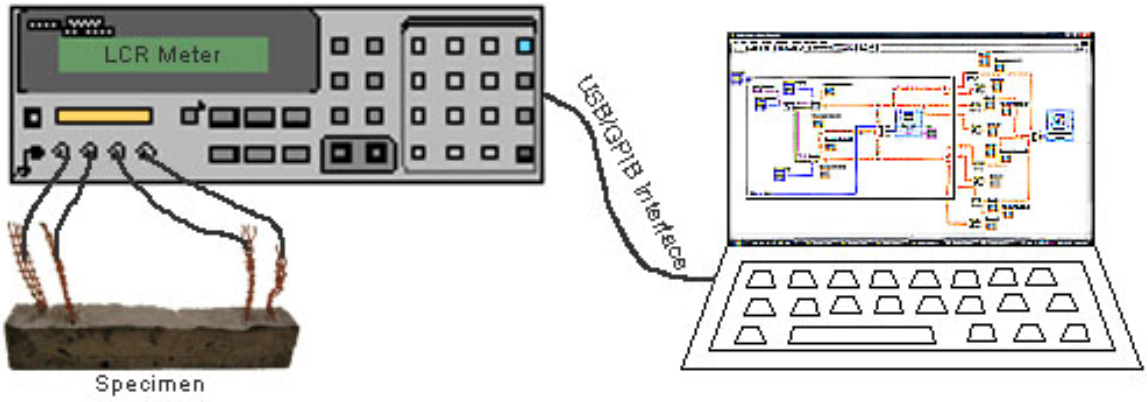


Figure 5- 5: Schematic Display of the Main series of Resistivity Test

## CHAPTER 6

# Effect of Fibre Content

In a cementitious material, electrical current results from the flow of free ions such as $Ca^{2+}$, $Na^{+}$, $K^{+}$ or $OH^{-}$ in the porous matrix and not from the flow of electrons. In conductive fibres, on the other hand, the motion of free electrons leads to electrical current. Thus, if the cementitious material contains conductive fibre, the electrical conduction will be through a combination of ion and electron flow. Depending on the fibre content and various other internal parameters, this combination may include three possible conduction pathways in carbon fibre reinforced cement paste (McCarter et al. 2007):

a. Via the capillary pore water within the cementitious composite;
b. Through a continuous network of carbon fibres; and,
c. Through the cement paste and the conductive carbon fibres in series.

Within the percolation zone, where a network of carbon fibres has formed, the two latter paths dominate the conduction route and hence overall electrical conductivity is increased.

The distribution of conductivity between these two paths (b and c), however, depends on the fibre volume fraction. Path b brings about ohmic conduction, strictly through the flow of free electrons. While in path c, an electron tunnelling conduction mechanism occurs which is due to the fact that the cementitious matrix interrupts the formation of a continuous path of fibres, causing the electrons to tunnel from one fibre to another (McCarter et al. 2007).

Results from the preliminary tests, shown in Figure 6-1, reveal an 85% reduction in the electrical resistivity of samples with 2% PPCF from the plain samples. Yet again, the resistivity values decreased significantly (99%) when the fibre content increased from 2% volume fraction ($V_f$) to 5% $V_f$.

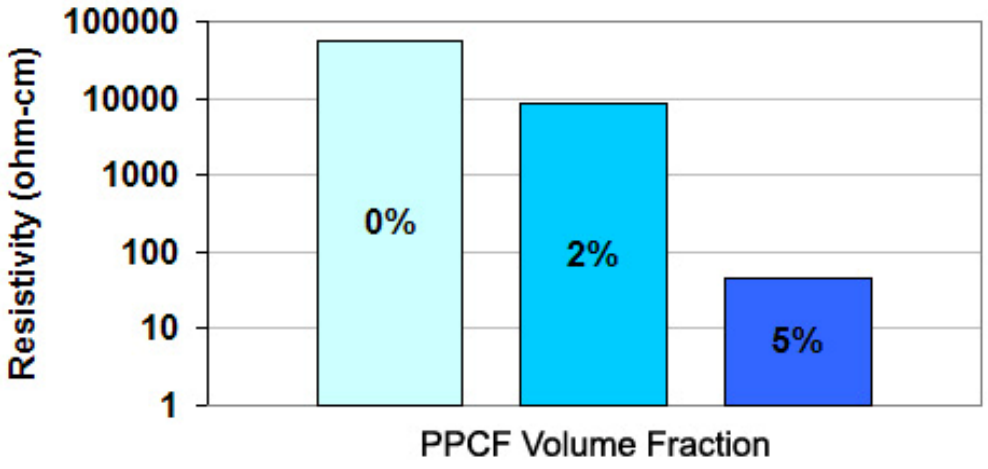


Figure 6- 1: Effect of petroleum pitch-based carbon fibre content on electrical resistivity at 28 days

This outcome was confirmed by the results from the main series of tests, illustrated in Figure 6-2. These results indicate that the resistivity values of samples with even just 0.5% $V_f$ of CPCF dropped considerably (97%) compared to plain samples. As shown in Figure 6-2, the resistivity of the specimens with 0.5% $V_f$ to about 15% $V_f$ remained almost constant, which validates the existence of a percolation threshold. However, identical to what happened in the preliminary experiments, the resistivity values could yet be significantly decreased (up to a thousand times smaller than the values at percolation threshold) by adding more fibre to the mix; samples with 20% $V_f$ of fibre exhibited electrical resistivity values as low as 5 ohm-cm. It should be noted, however, that in the case of CPCF, this point was reached at a much higher $V_f$. This may be explained by the fact that form of CPCF made them easer to disperse and that they seemed to be more brittle.

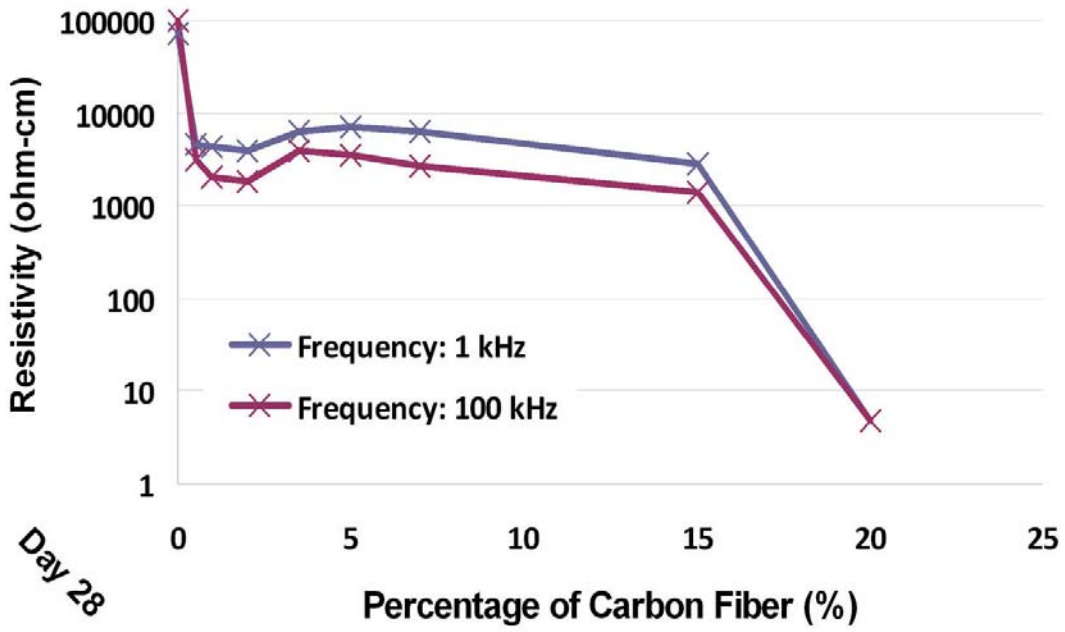


Figure 6- 2: Effect of fibre (CPCF) content on electrical resistivity at 28 days

Another parameter affecting the electrical resistivity of these samples is frequency. As seen in Figure 6-2, the resistivity values differ with changing the current frequency from 1 kHz to 100 kHz. It is suggested that the reason for this effect lies in the role of the interface between the carbon fibres and the cement paste matrix (Tsung-Chin Hou and Lynch 2005). Chapter 7 will thoroughly discuss the effect of frequency.

Plots from experiments comparing different fibre contents after 1, 7 and 14 days of curing may be found in Appendix A. Comparing these plots to Figure 6-2 (at 28 days), implies that the gap between the resistivity values at 1 kHz and 100 kHz current frequencies becomes smaller and smaller as the curing time increases.

Experiments were also conducted to investigate the effect of different amounts of MWCNT and SWCNT (Figure 6-3). It was found that the addition of CNT at 1% or 3% $V_f$ slightly decreases the resistivity of the cement paste. Due to the extremely high conductivity values reported for CNT ($10^5$-$10^6$ S.m$^{-1}$), this

reduction was expected to be much greater, but the dispersion of CNT is very difficult to achieve. Moreover, even if the dispersion was perfect, the extremely small size of CNT prevents any contact or network among them in such low volume fractions. This triggered the idea of a hybrid specimen, containing 3% MWCNT and 15% CPCF. This combination, as shown in Figure 6-3, yielded a very low electrical resistivity (3.2 ohm-cm), similar to what we had for 20% carbon fibre.

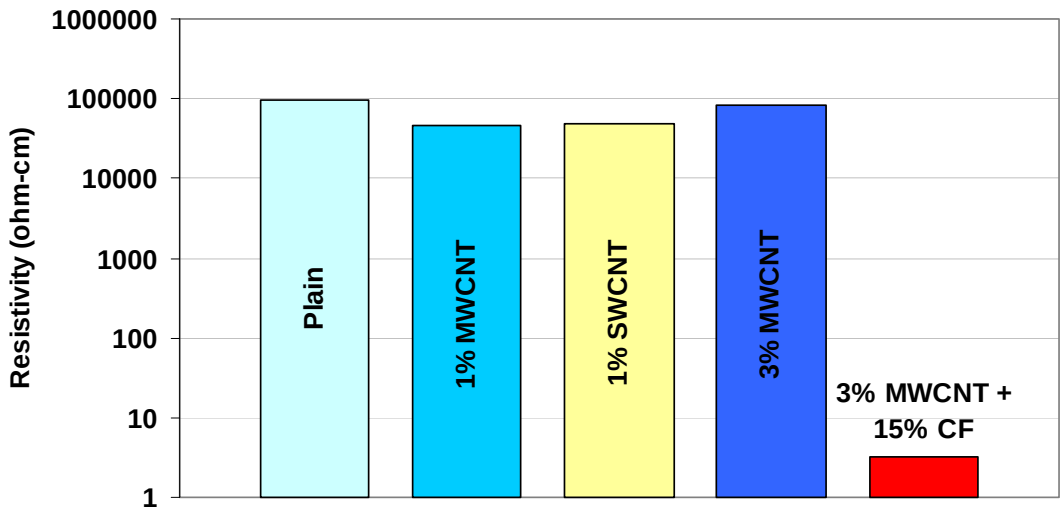


Figure 6- 3: Resistivity values (at 100 kHz) of CNT and hybrid samples at 28 days

Although the "3% MWCNT + 15% CF" hybrid and the 20% CF samples had preferable resistivity values more suitable for the sensing application, they each had their downfalls; the former being very soft and brittle (most of the specimens failed while stripping the moulds) and the latter extremely hard to prepare. Therefore samples with 15% CF were mostly used as sensors. Another hybrid set of samples with 1% MWCNT + 15% CF (which were not soft or brittle) was also prepared and used as sensors.

In order to observe the interaction between fibres and their dispersion, a series of images were obtained using a scanning electron microscope (SEM). These images, shown in Figure 6-4, visualize how the increase in fibre content affects their dispersion and in turn the electrical properties of the specimens.

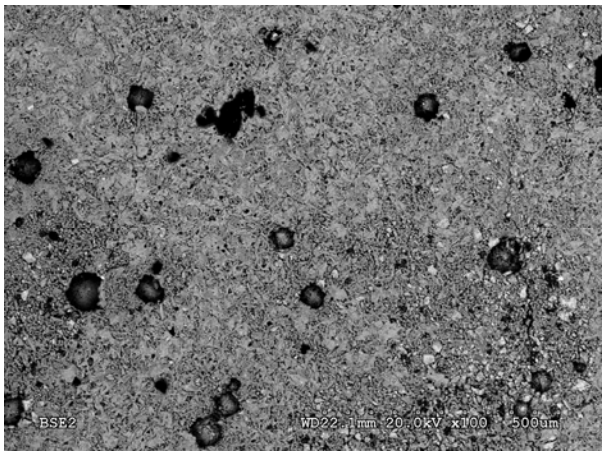


Plain cement paste at x100 magnification

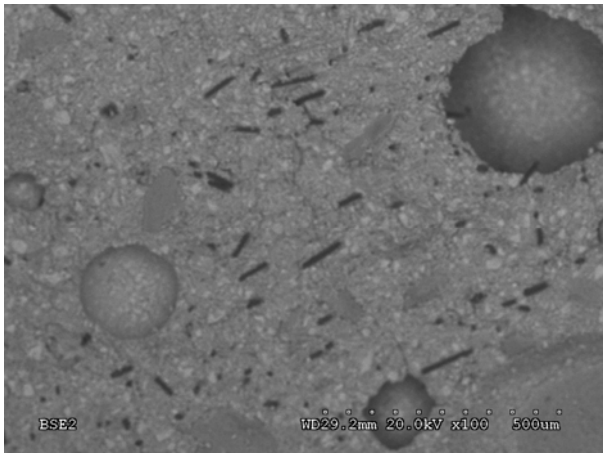


1% CPCF at x100 magnification

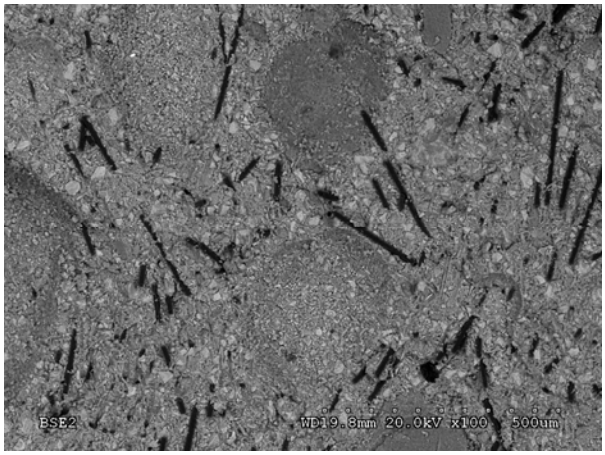


3.5% CPCF at x100 magnification

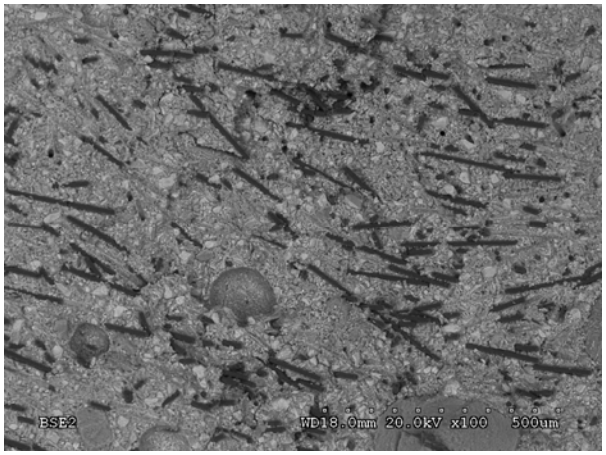


5% CPCF at x100 magnification

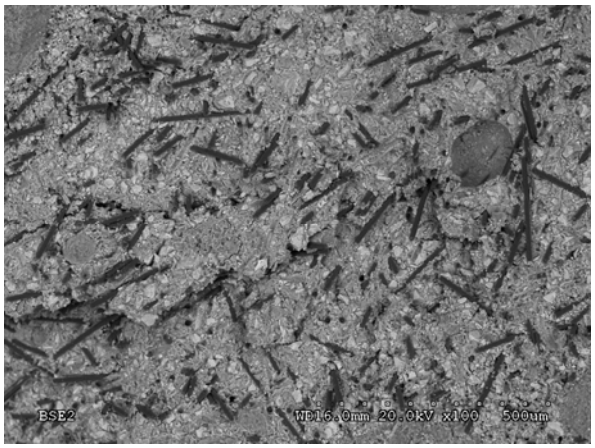


7% CPCF at x100 magnification

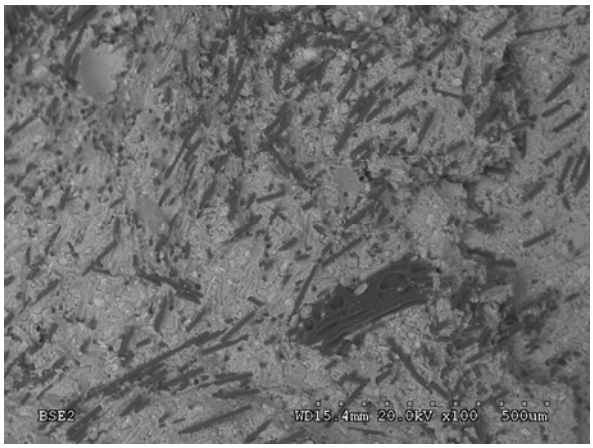


15% CPCF at x100 magnification

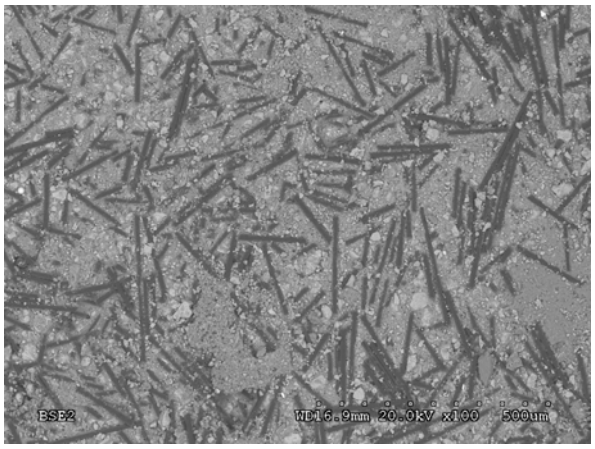


20% CPCF at x100 magnification

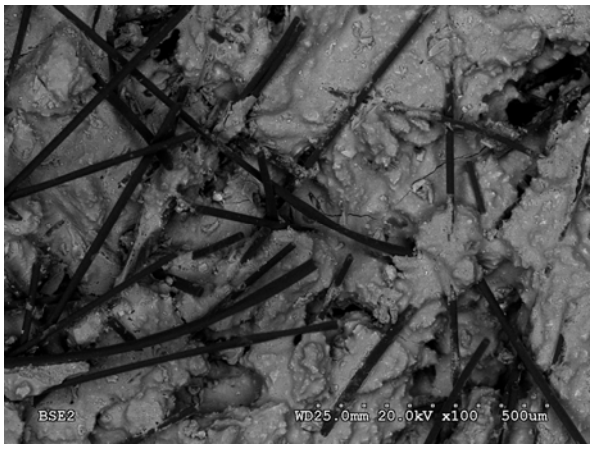


5% PPCF at x100 magnification

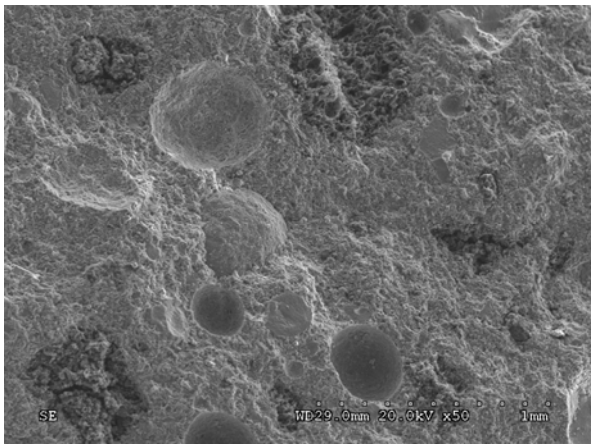


3% MWCNT at x50 magnification

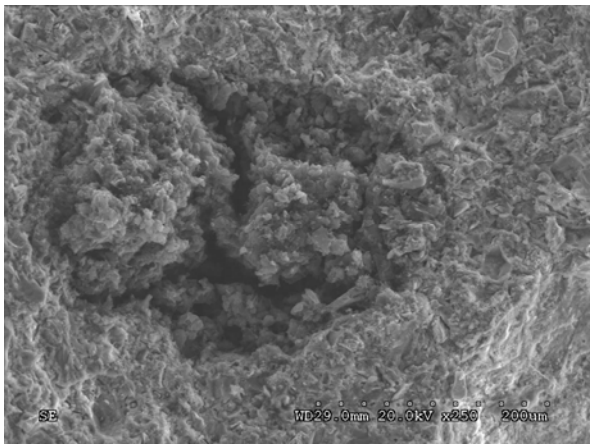


3% MWCNT at x250 magnification

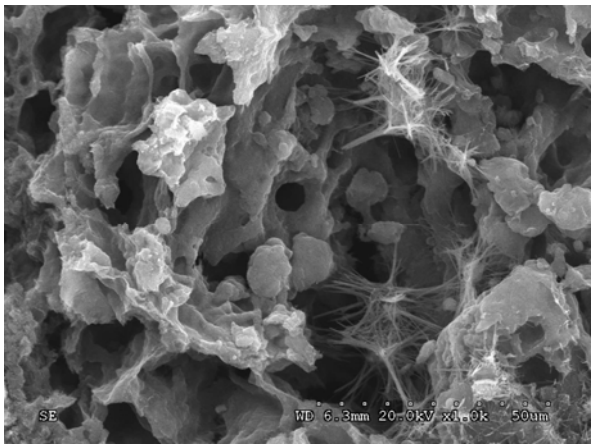


3% MWCNT at x1.0k magnification

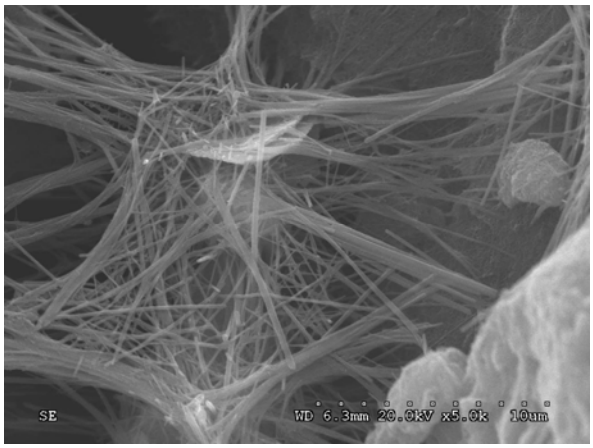


3% MWCNT at x5.0k magnification

Figure 6- 4: SEM images of specimens with different fibre and CNT contents

# CHAPTER 7

# Effect of Current Frequency

Since we are using AC, the current frequency becomes a crucial element to be considered. As mentioned in Chapter 2 (electrical concepts), for a capacitive mechanism, higher frequency leads to lower capacitive reactance and for an inductive mechanism, the lower the frequency, the lower the inductive reactance.

Cement based composites are capacitive in nature. Introducing a capacitor in parallel with the resistance (Figure 7-1), the impedance is expressed as follows:

$$Z = \frac{R_s}{\sqrt{(1+\omega^2 C_s{}^2 R_s{}^2)}} \qquad (7\text{-}1)$$

Where,

Z: impedance in ohms (Ω)

$R_s$ : resistance in ohms (Ω

$\omega = 2\pi f$ : angular frequency in radians per second (rad/s)

$C_s$ : capacitance in farads

$f$ : signal frequency in hertz (Hz)

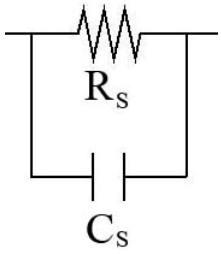


Figure 7- 1: Parallel C-R arrangement of cement-based sensor resistance ($R_s$) and capacitance ($C_s$)

According to Equation 7-1, in order to reduce the reactance part of impedance, higher frequencies should be used. This is the theoretical approach for obtaining more pure resistance values, efficient for the sensing purpose.

Many factors may have a role in the effect of current frequency; internal factors such as fibre content and specimen geometry and external factors such as moisture and temperature. When the electrical current is conducted through both the conductive fibres and the matrix, the interface between the fibres and the cement paste affects the conductivity. It has been found that in tests where DC or low frequency AC is used, the cement matrix plays a dominant role in the electrical conductivity, but as the AC frequency is increased, the interface impedance decreases and thus the electrical conductivity of the composite is strongly governed by the conductive fibres (Reza et al. 2003a). This also leads us to use higher frequencies for this type of sensors.

In order to investigate the effect of current frequency on the cement-based sensor specimens, a series of frequency tests were conducted. According to Equation 2-7, purely resistive impedance occurs when the phase angle is zero. Therefore, phase angles at different current frequencies were compared to find the best frequency.

The LCR meter, used for the main experiments, only has four frequency options to choose from: 100 Hz, 1 kHz, 10 kHz and 100 kHz. A snapshot of the impedance-frequency and phase angle-frequency of a sample test using the LCR meter is presented in Figure 7-2.

Since the frequency options of the LCR meter were very few, the frequency tests were conducted using Solartron 1260 Impedance/Gain-Phase Analyzer (Figure 7-3). A frequency sweep between 1Hz and 1MHz ($1x10^6$Hz) was completed for every specimen. The results are plotted in Figure 7-4.

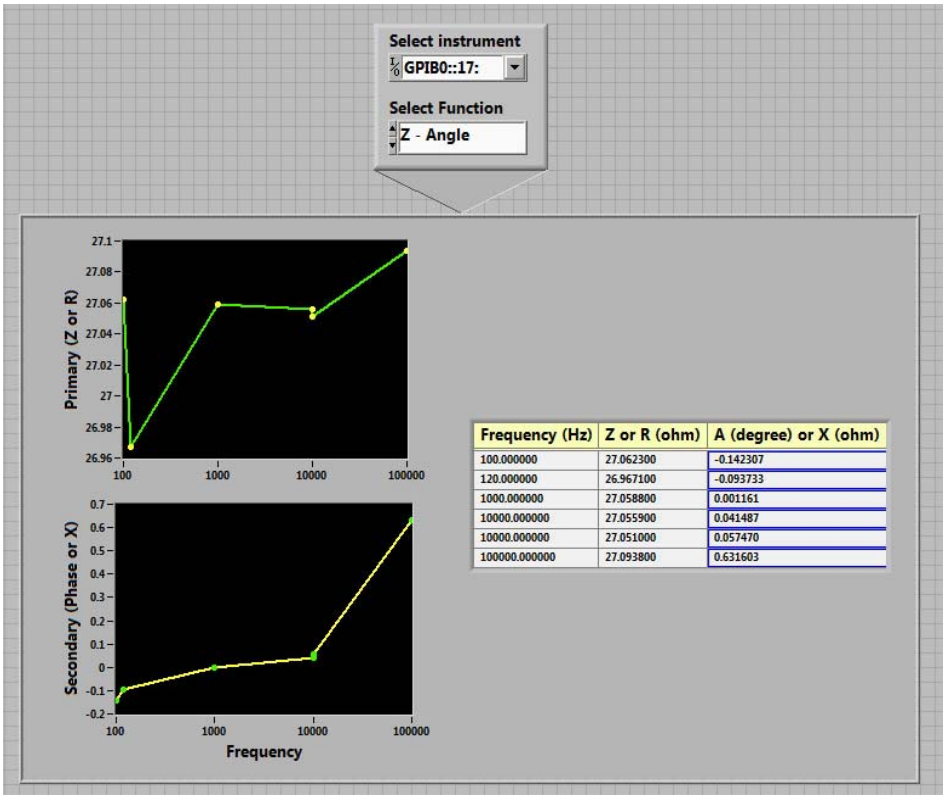


Figure 7- 2: Frequency test using the LCR meter

Figure 7- 3: Frequency test setup using Solartron 1260 Impedance/Gain-Phase Analyzer

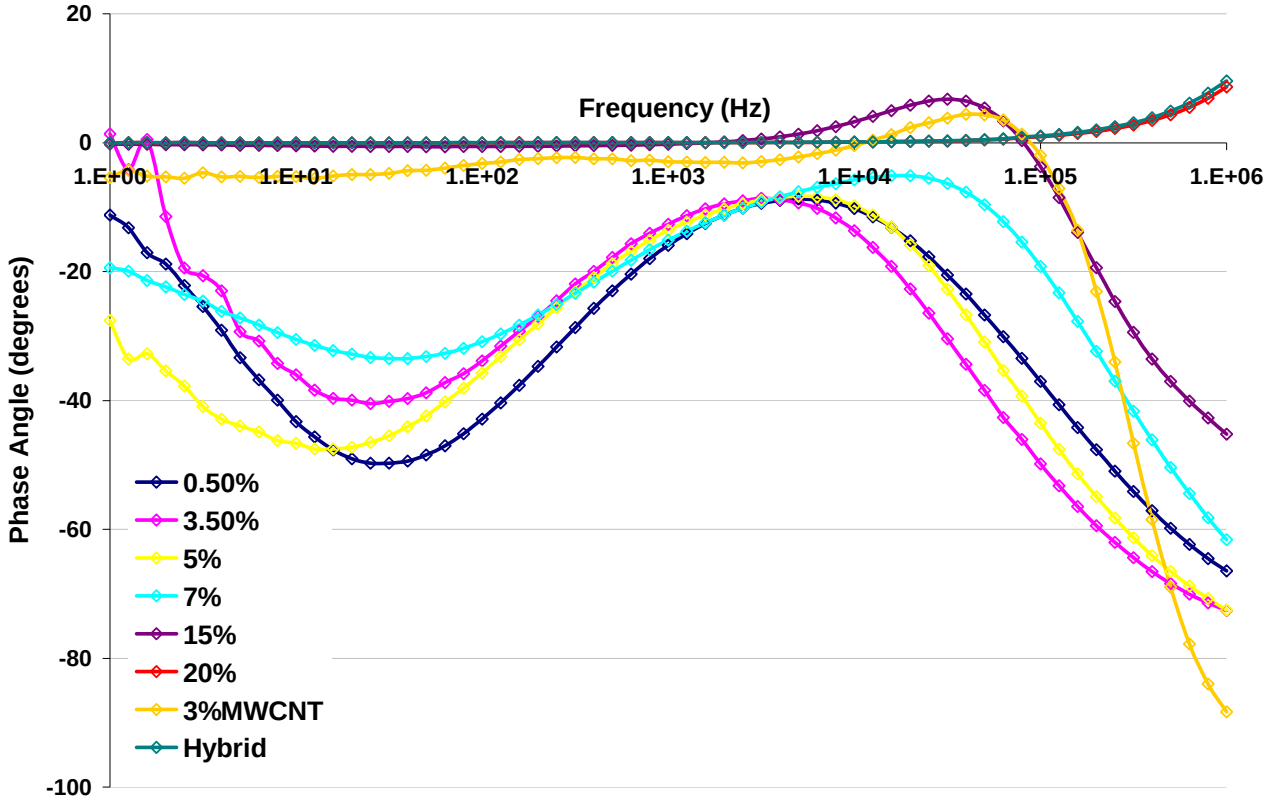


Figure 7- 4: Phase angle (θ) at current frequencies between 1Hz and 1MHz for different specimens

It is observed in Figure 7-4 that phase angle for the specimens are for the most part negative, which confirms the fact that these cement-based composites are capacitive rather than inductive. For samples with fibre contents in the moderate range (0.5%-7% $V_f$), phase angle values fluctuated, lowering at 1 Hz and about 10 kHz. Samples with high volume fractions of fibre (15% and 20% $V_f$), the 3% MWCNT specimens as well as the hybrid samples, exhibit much lower phase angle values especially at frequencies of 100 kHz and below. These samples seem to show inductive characteristics at some frequencies (where $\theta>0$). Judging from these results and considering the theoretical reasoning, the highest current frequency available on the LCR meter, 100 kHz, was chosen to be used as the applied current frequency in all of the experiments.

The geometry of the specimens also plays a role in how frequency affects conductivity. Figure 7-5 compares phase angle values at frequencies of 1Hz to

1MHz for different specimen geometries. At a constant volume fraction of fibres, specimens with smaller cross sections were proven to be less dependent on frequency, showing lower phase angle values at most frequencies.

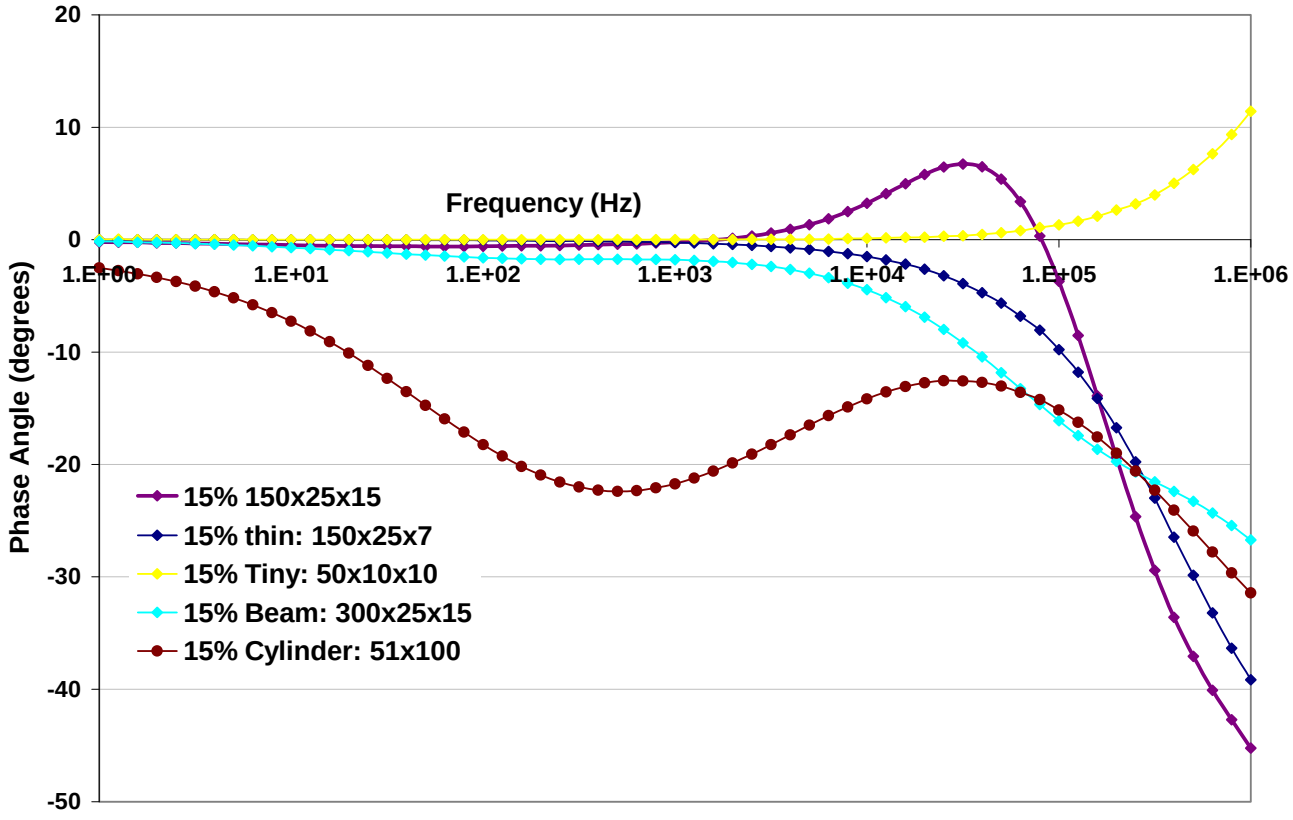


Figure 7- 5: Phase angle (θ) at current frequencies of 1Hz to 1MHz for different specimen geometries

A set of supplementary experiments were also performed to compare the effect of current frequency on resistivity measurements of specimens with MWCNT and SWCNT. Results from resistivity tests conducted on samples with 1% MWCNT and 1% SWCNT, at two different frequencies of 1 kHz and 100 kHz, shown in Figure 7-6, revealed that the SWCNT specimens seem to be independent of current frequency as their resistivity values are identical at both frequencies. This, however, did not hold true or the MWCNT sample.

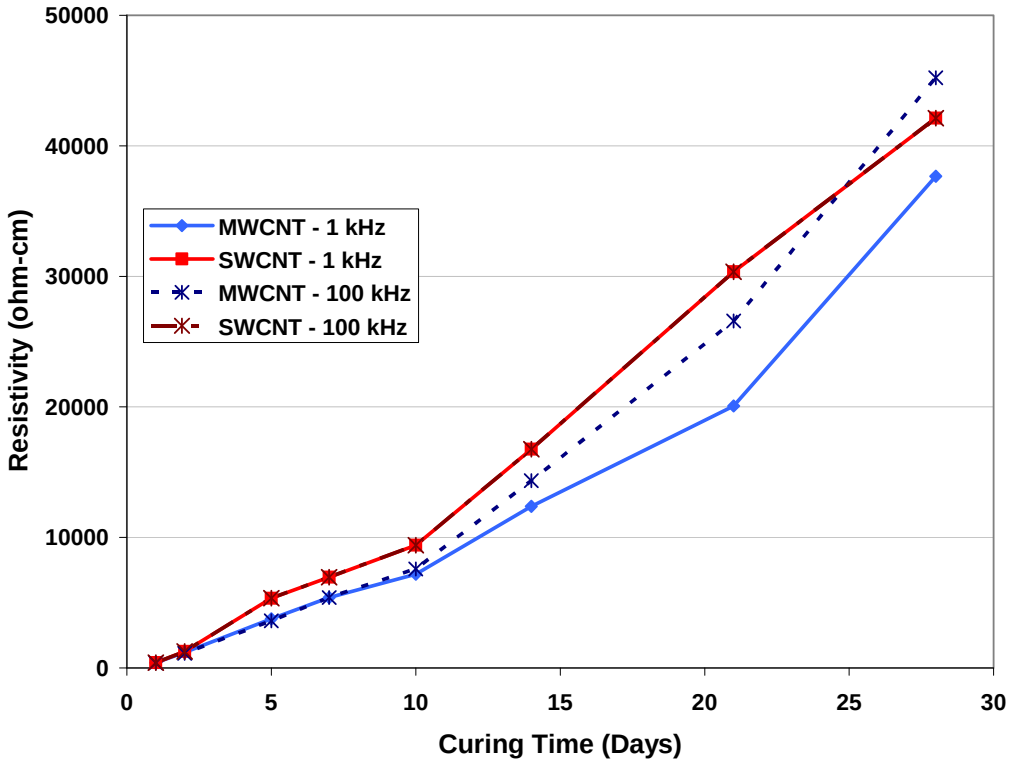


Figure 7- 6: Effect of current frequency on resistivity values of MWCNT and SWCNT specimens

# CHAPTER 8

# Electrodes

The resistance values obtained from a specimen is basically more than the actual resistance of the cement composite itself, because it also comprises the resistance of the electrodes as well as the contact resistance between the electrodes and the cementitious material. The resistance of the electrode, however, is comparatively negligible, since the electrode material is a highly conductive metal. Consequently, it is the contact resistance that is responsible for the disparity between the measured and real resistance values of the cement-based sensors. Therefore it is important to achieve the least possible amount of contact resistance. Some factors that affect the contact resistance include the type (shape and attachment) of the electrodes, the measurement configuration and the test fixtures.

## 8.1 Electrode Type

A series of tests were conducted on specimens containing 3.5% $V_f$ of carbon fibres (this volume fraction was randomly chosen at the beginning of the project as a reasonable amount of fibre). These specimens were prepared using five different electrode types and configurations:

- Four-probe copper plate
- Four-probe copper mesh
- Four-probe copper wire with silver paste
- Four-probe copper wire with silver paste, attached so that they measure diagonal resistance of the specimen.
- Two-probe copper plate

The resistivities of the samples were measured during a 28-day curing period. Comparing the results, demonstrated in Figure 8-1, it was found that the contact resistance of the samples with copper plate and mesh were slightly less than that of the specimens with copper wire and silver paste. What is more, the silver paste would splinter in the long term, which would cause more contact resistance and scattered measurements. Although copper mesh and wire produced pretty much the same resistivity values throughout the testing period, at 28 days, the copper electrodes showed signs of higher contact resistance. Moreover, owing to its small openings, copper mesh had a better interaction with the cement composite, creating a better interface.

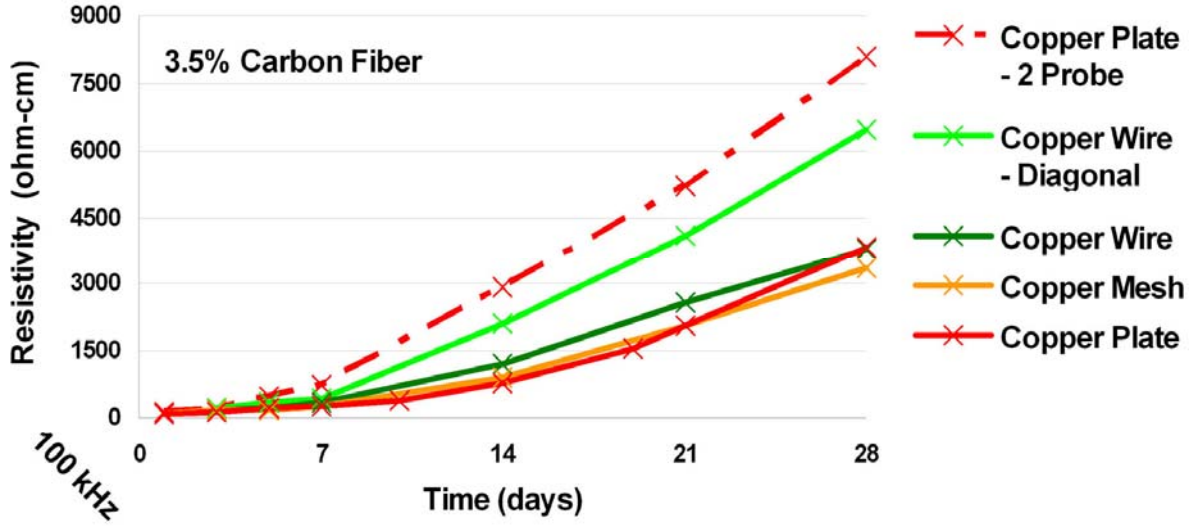


Figure 8- 1: Effect of electrodes on the resistivity values during 4 weeks of curing (Unless noted, the 4 probe technique was used)

Consequently, copper mesh was, for the most part, used as electrode material for the cement-based sensors. For the cylindrical compression test specimens, though, copper wire and silver paste were the only fitting electrode materials. The contact resistance can be further reduced by having clean and corrosion-free electrodes.

Also, comparing the two wire-electrode specimens, it is clear that the diagonal measurement provides higher resistivity values. This was expected because in

the diagonal case, the actual distance between the electrodes was greater than the 7 cm electrode distance considered in the resistivity calculation.

## 8.2 Electrode Configuration

As mentioned in Chapter 2, there are two commonly used methods for resistance measurements; two-probe and four-probe. While the two-probe technique is much simpler, error sources such as lead inductance, lead resistance, and stray capacitance between the two electrodes affect the measured resistance. In the four-probe method, on the other hand, the effect of lead impedances is reduced due to the fact that the current and voltage paths are separate.

Using the two-probe technique, the measured voltage comprises of voltages from the electrodes ($V_E$; which is almost negligible), cement-based sensor ($V_S$) and contact resistance ($V_C$). Through the four-probe method, on the other hand, $V_E$ and $V_C$ are eliminated and the voltage measurement consists of only the sensor voltage; $V_S$. Figure 8-2 schematically displays the equivalent circuits for two-probe and four-probe measurement techniques.

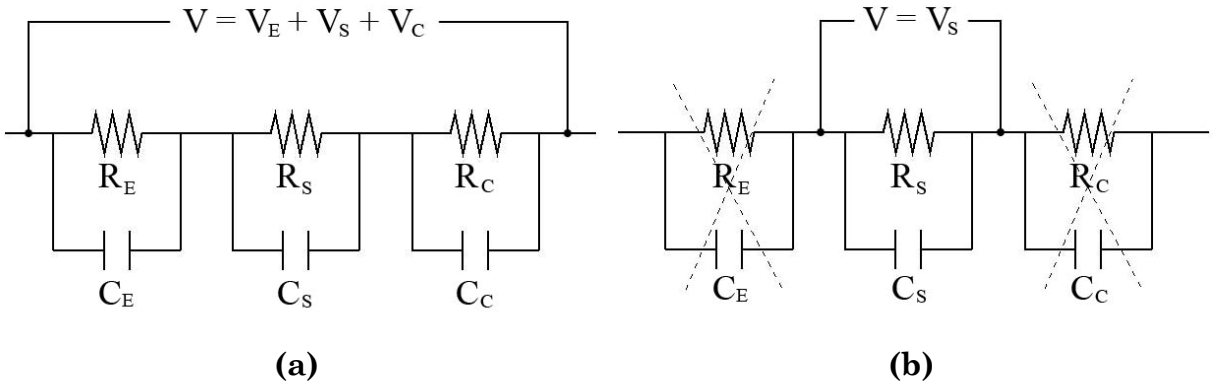


Figure 8- 2: Equivalent circuits for (a) two-probe and (b) four-probe resistivity measurement techniques
$V_E$, $R_E$ and $C_E$: voltage, resistance and capacitance from the electrodes, respectively;
$V_S$, $R_S$ and $C_S$: voltage, resistance and capacitance from the sensor, respectively;
$V_C$, $R_C$ and $C_C$: voltage, resistance and capacitance from the contact, respectively.

In order to confirm this theory, resistivity values of specimens with two-probe and four-probe electrode configurations were compared (Figure 8-1). It became

clear from the results that the resistivity values of the sample with two-probe copper plate electrodes was up to 75% more than that of the samples with four-probe copper plate electrodes. It was concluded that the two-probe configuration produces very high contact resistance and hence is not suitable for resistivity measurements of cement-based sensors. The four-probe technique was used for the main set of experiments.

Another important issue in the resistance measurement procedure is the role of test fixtures and their quality. Open/short compensation was used during the experiments in order to lessen the effect of test fixture residuals.

# CHAPTER 9

# Effect of Curing

As a result of hydration, the microstructure of the cement paste in cement-based sensors changes, and in consequence, its resistivity increases over time. The effect of curing time was investigated on specimens with different amounts of carbon fibre or CNT for a 28-day curing period. In addition, the effects of methylcellulose (MC) and defoamers on the curing process were examined.

## 9.1 Petroleum Pitch-based Carbon Fibres

In the preliminary set of experiments, petroleum pitch-based carbon fibres (PPCF) were used as the conductive phase for cement-based sensors. The results from resistivity measurements during the curing period are illustrated in Figure 9-1.

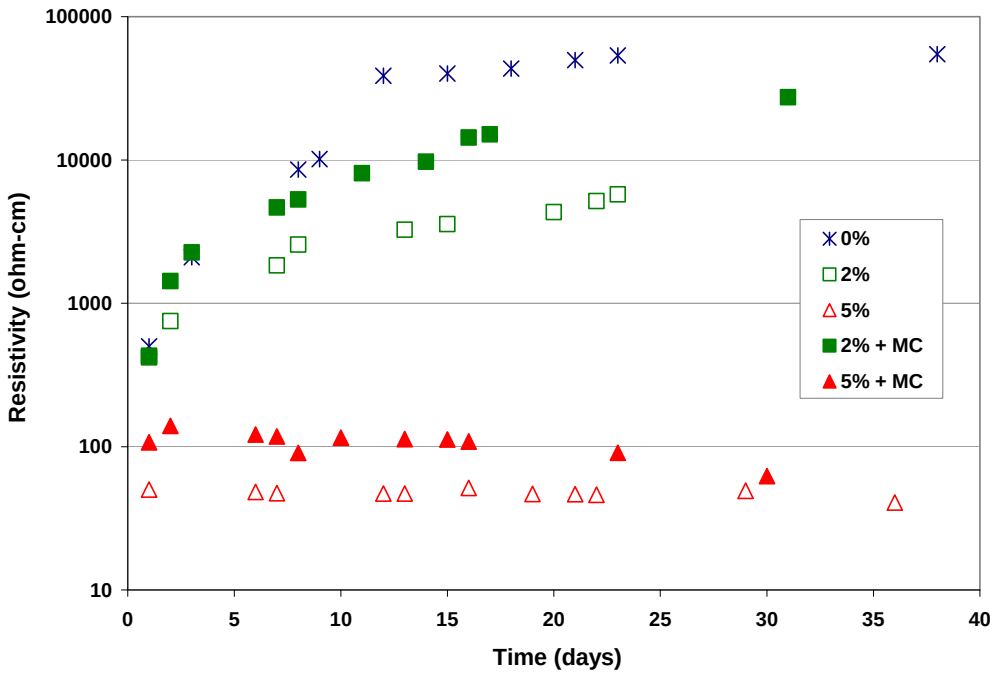


Figure 9- 1: Resistivity values of PPCF cement paste specimens while curing

It is clear from the plot in Figure 9-2 that the plain and 2% $V_f$ specimens gained resistivity as time went. The rate of resistivity increase in these samples was very high during the first ten days, but slowed down after that, almost stabilizing after 30 days. This attests that in these specimens, where the cementitious matrix plays an important role in the resistance, the resistivity values increase as the specimen hydrates and loses moisture and that the loss of moisture and hydration process are more significant at the early ages.

Conversely, the resistivity values of the specimens with high volume fraction of fibre (5%) actually decreased with curing time, although gradually and at very slow rate. This explains that in these specimens, where the fibres are the main route of conduction, as hydration progresses and loss of moisture increases, the role of cement matrix becomes less and less and the fibres become even more dominant in the conductivity of the specimen.

Specimens with methylcellulose, used in order to obtain better fibre dispersion, exhibited higher resistivity values than their corresponding samples with the same fibre content and no methylcellulose. This may suggest that although it is helpful in the dispersion process of fibres, methylcellulose acted as a paste, creating small clumps of carbon fibre. These clumps of fibre (see Figure 9-2) apparently led to less fibre-to-fibre contact and thus an increase in the resistivity values.

Figure 9- 2: From left to right: Sample without and with methylcellulose

It is worth noting that the resistivities of the 5% $V_f$ specimens both with and without methylcellulose ultimately reached comparable values, which once again confirms that in the high $V_f$ samples, the fibres are the chief contributors to the electrical conductivity.

## 9.2 Coal Tar Pitch-based Carbon Fibres and CNT

In the main series of experiments, coal tar pitch based carbon fibres (CPCF) were used as the conductive phase for cement-based sensors because these fibres were much easier to mix and dispersed more uniformly than the petroleum pitch-based carbon fibres. Impedance, phase angle, resistance and reactance values of all the specimens were measured at least every seven days during the 28 days of curing. At each round, the average of 10 measurements was recorded for each specimen. Figure 9-3 shows the interface for these measurements. These values were then averaged for each type of specimen. Thus the reliability of the measurements was as high as possible.

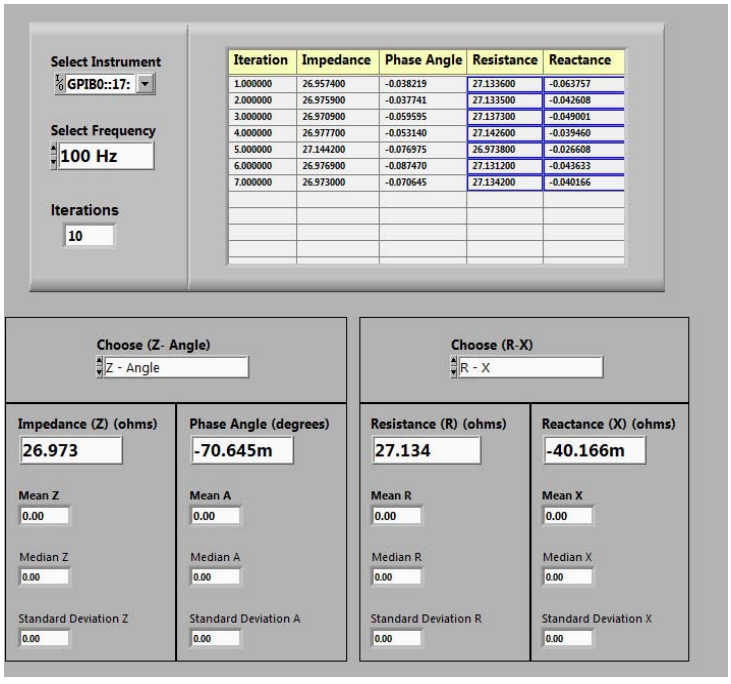


Figure 9- 3: LabVIEW interface for measuring the impedance components

The results from resistivity measurements during the curing period of a number of these samples are illustrated in Figure 9-4. The resistivity trends were very similar to the results from the preliminary tests presented in section 9.1.

The electrical resistivity of plain, 1%SWCNT and 1%MWCNT samples increased as the curing time increased (at a higher rate during the first week) and ultimately reached values of up to 100,000 ohm-cm at 28 days. The same trend was observed for the samples with fibre contents between 0.5% and 15% $V_f$, with resistivities reaching values in the range of 1500 to 5000 ohm-cm at 28 days of curing. The resistivity of the 20% $V_f$ samples increased very gradually (almost negligible) from 3.3 ohm-cm to a stable value of 4.7 ohm-cm at 28 days of curing. Finally, the resistivity values for the hybrid (15%CF + 3%MWCNT) samples decreased from about 10 ohm-cm to almost 5 ohm-cm during the first week (due to hydration and loss of moisture), but remained constant thereafter.

These results confirm once more that in specimens with a large amount of conductive phase, where the fibres (and CNT) are the dominant route of conduction, curing time has a much smaller effect on the resistivity values.

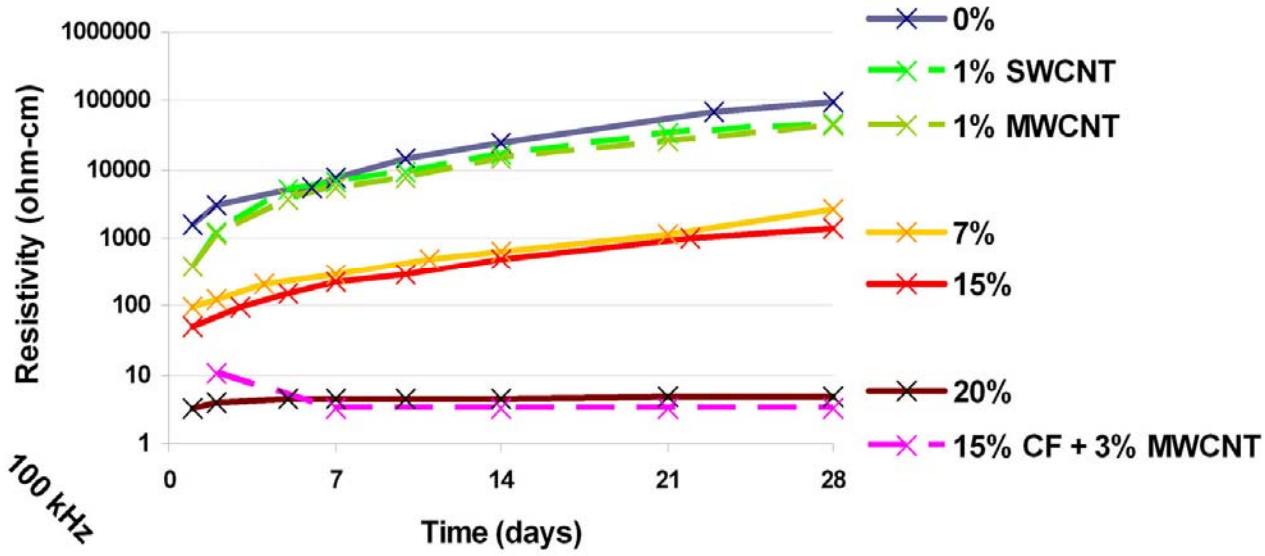


Figure 9- 4: Resistivity values of CPCF cement paste specimens while curing

In order to inspect the effect of autoclaving on the curing process, three specimens from each fibre $V_f$ were autoclaved for 30 minutes on the first day of curing. Figure 9-5 shows the results from the 0% and 7% $V_f$ specimens. The autoclaved specimens had higher resistivity values than the non-autoclaved samples throughout the curing time, but the values merged at the end of the 28 day curing period. It appears that autoclaving reduced the rate of resistivity in crease by speeding the curing process at the beginning. Higher resistivity is clearly due to the higher strength in the autoclaved specimens at early ages, which eventually approaches non-autoclaved specimens.

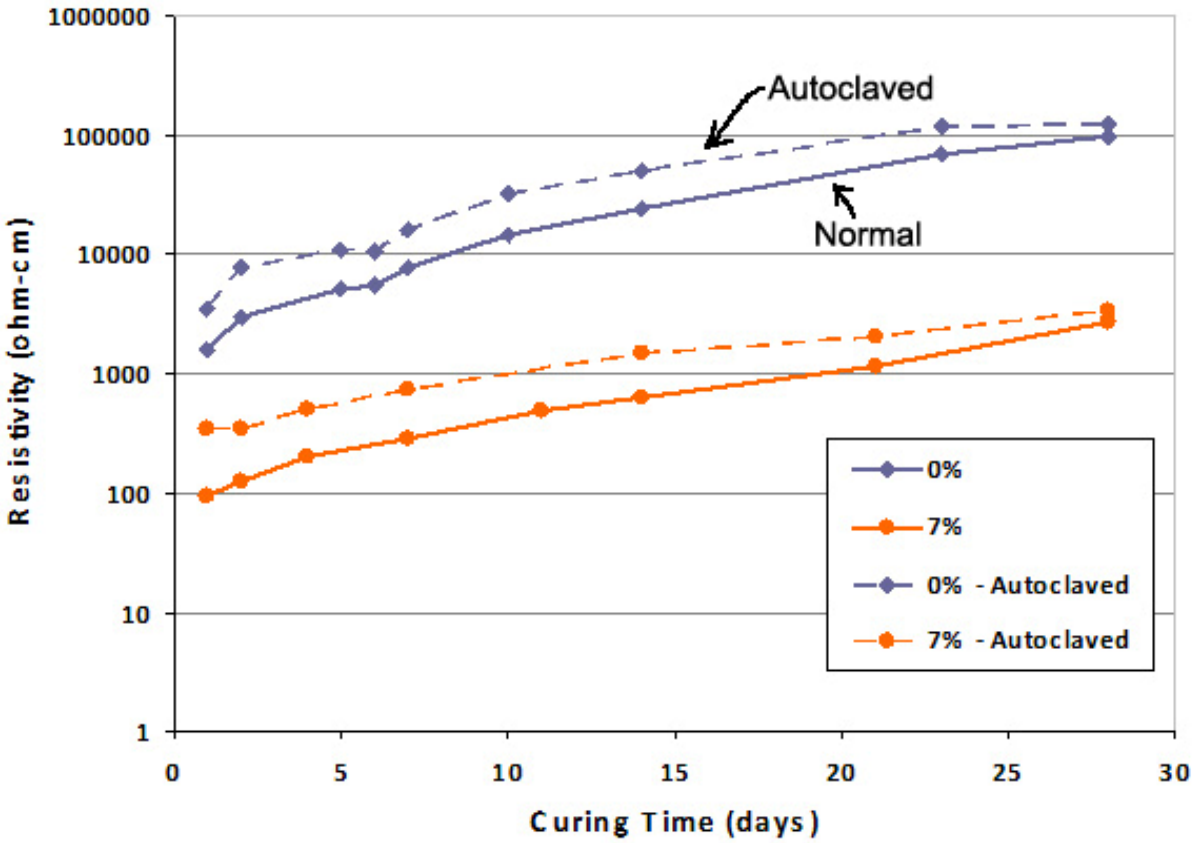


Figure 9- 5: the effect of autoclaving on the curing process

Figure 9-6 compares the resistivity values of 15% fibre $V_f$ specimens without any dispersing agent, with methylcellulose and with both methylcellulose and a defoamer at 1 kHz and 100 kHz frequencies. The results indicate that at both

frequencies, the addition of methylcellulose and defoamer increases the resistivity values. This is apparently due to the increase in strength due to reduction in air (defoamer) and pore-refinement (methylcellulose). This rise in resistivity becomes more pronounced as the curing time increases.

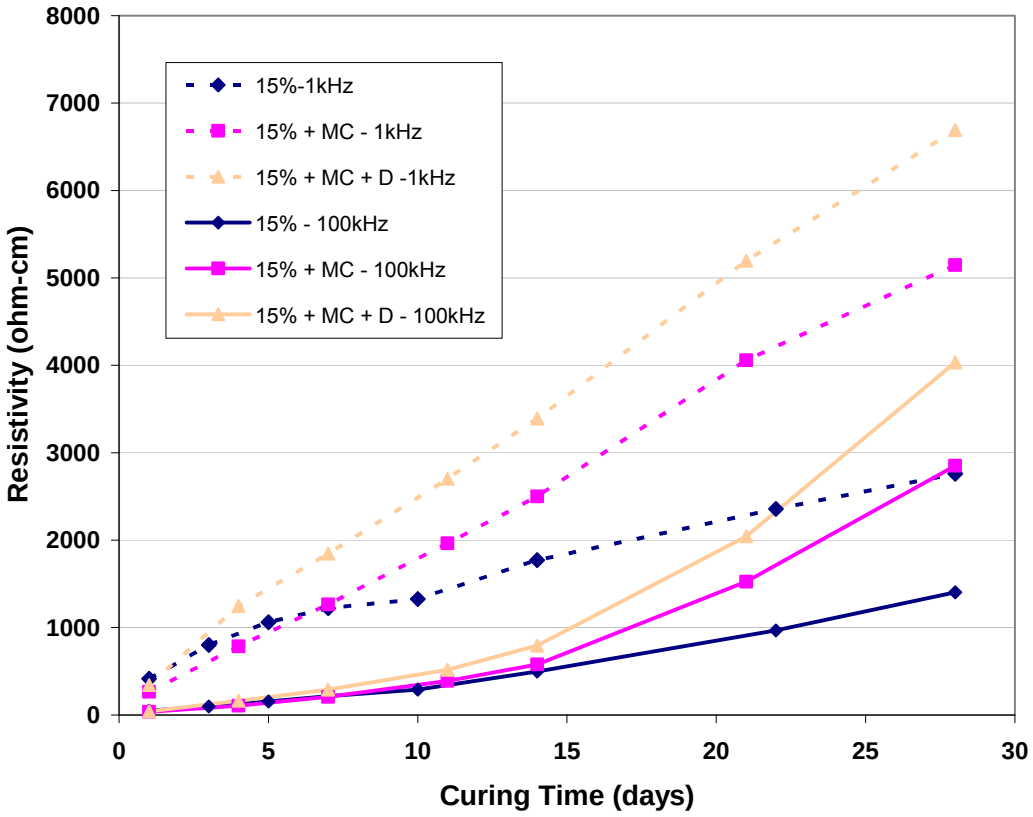


Figure 9- 6: Effect of methylcellulose (MC) and defoamer (D) on the resistivity values

# CHAPTER 10

# Effect of Temperature Variation

It has become apparent that temperature variation during SHM influences the resistivity values acquired from cement-based sensors. Therefore, appropriate measures should be taken to reduce the effect of temperature on the sensing ability of these sensors.

In this chapter, the influence of both high and low temperatures on the electrical resistivity and the sensing feature of CFRC are investigated. The rate and reversibility of these effects are also examined and correction factors are suggested.

## 10.1 High Temperatures

To simulate high temperatures, CFRC specimens with 15% fibre $V_f$ were placed in an environmental chamber along with a temperature data logger. The temperature inside the chamber varied from 20°C to about 60°C, fluctuating at some points in order to completely verify the effect of temperature variation on resistivity values. The electrical resistivity of the specimen inside the chamber was measured at the same rate (every minute) that the data logger recorded the temperature. The setup for this experiment and the results are shown in Figures 10-1 and 10-2, respectively.

According to the results, resistivity is related inversely to high temperatures, decreasing with an increase in the temperature and increasing with a decrease in the temperature. This effect may be explained by the fact that at higher temperatures, the viscosity of the pore solution decreases, hence enabling easier

movement of ions (Chacko et al. 2007). The resistivity plot clearly mirrors the temperature plot in Figure 10-2.

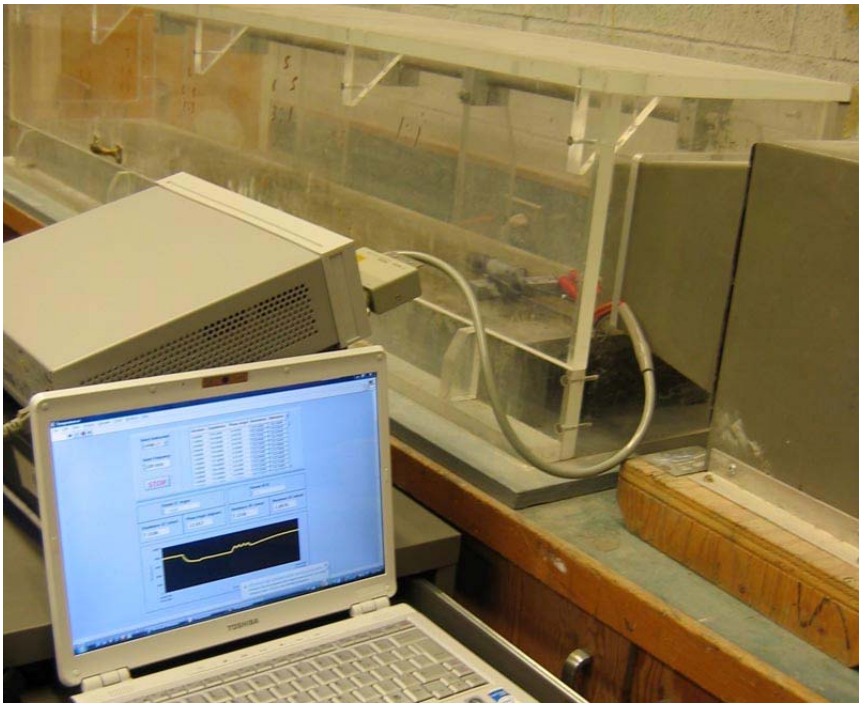

Figure 10- 1: High temperature variation experimental setup

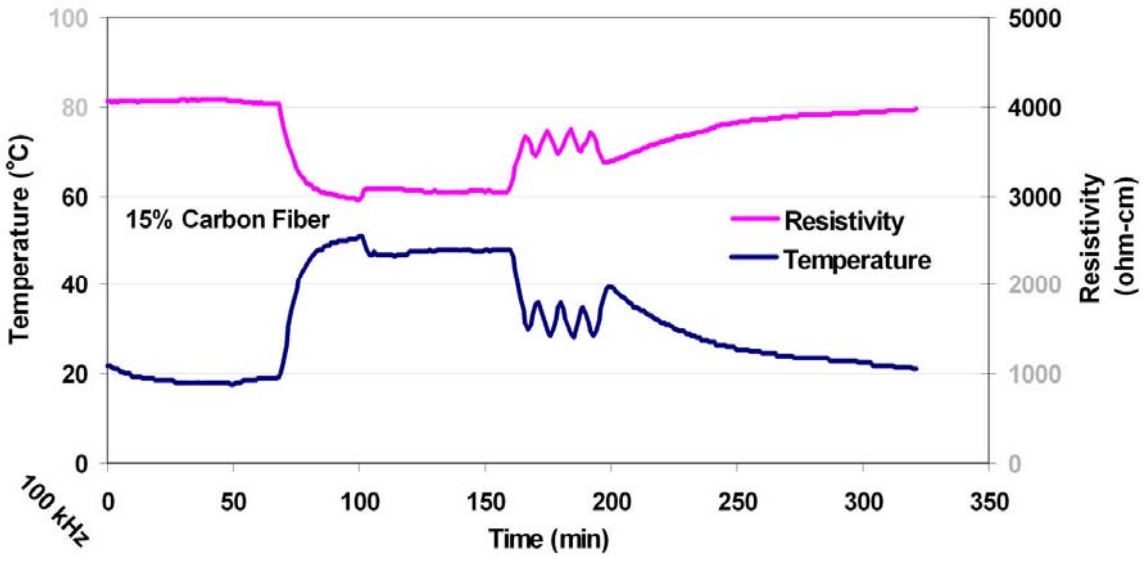


Figure 10- 2: Effect of high temperature variation on the electrical resistivity of CFRC

## 10.2 Low Temperatures

Similarly, in order to simulate low temperatures, CFRC specimens with 15% fibre $V_f$ along with a temperature data logger were placed in a freezer. The low temperature recorded by the data logger ranged between 30°C and around -15°C. The higher temperatures in this range were from before the sample was put into the freezer and after it was taken out. The electrical resistivity of the specimen was measured at the same rate (every minute) that the data logger recorded the temperature. The setup for the low temperature range experiment and the results are shown in Figures 10-3 and 10-4, respectively.

The results show that resistivity is related inversely to low temperatures as well, once again demonstrating decreasing resistivity values with the increase in temperature and increasing resistivity values with the decrease in temperature. Again, the shape of the resistivity plot is a mirror of the temperature plot in Figure 10-4.

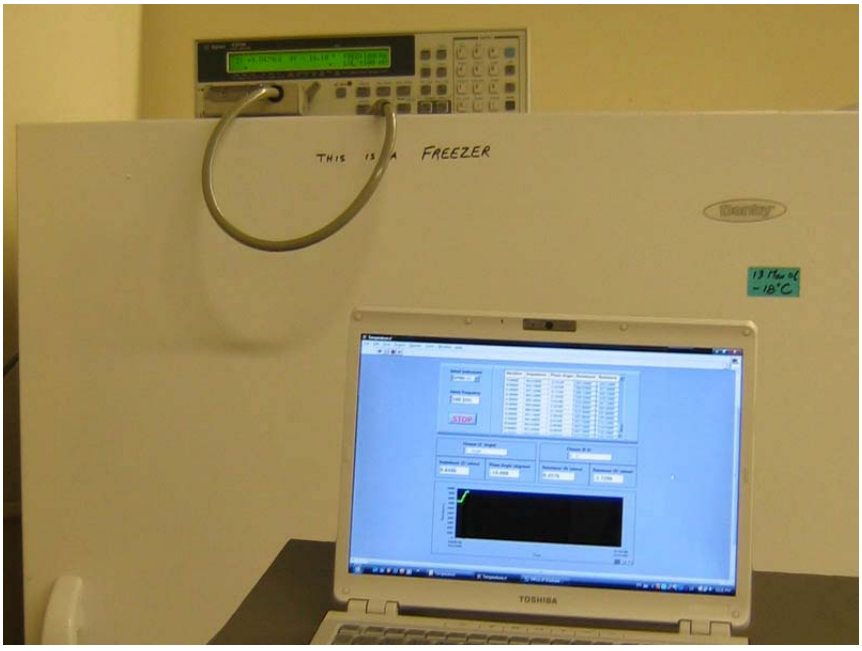


Figure 10- 3: Low temperature variation experimental setup

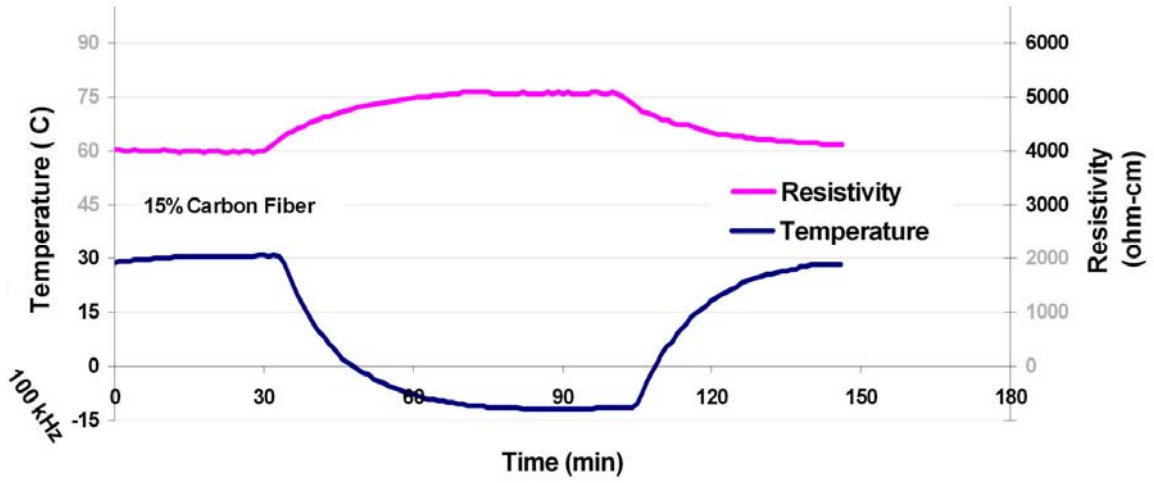


Figure 10- 4: Effect of low temperature variation on the electrical resistivity of CFRC

## 10.3 Reversibility

Resistivity measurements were made in a full cycle of temperature variation, returning to the initial room temperature. Resistivity and temperature values from both high and low temperature variation experiments were plotted against each other in Figure 10-5 in an attempt to inspect the reversibility as well as the rate of the temperature effect.

The results depict that the temperature variation is in fact completely reversible; the resistivity values are almost the same at equal temperature values whether it is on the increasing branch or the decreasing part of the test.

Since the same exact specimens were not used for both experiments and the experimental equipment and setup for the high and low temperature simulation were different, the resistivity values at overlapping temperature ranges did not merge (Figure 10-5). The fact that the specimens were not subjected to continuous change in temperature from low to high is another reason for this gap. It was probably for the same reasons that the rates of resistivity change at high and low temperature ranges were different. According to these results, in the high temperature range, the resistivity values decreased or increased at a

rate of 35 ohm-cm/°C, while this rate was calculated at about 22 ohm-cm/°C for the low temperature range. These rates may be considered as the correction factors in the case of temperature variation during sensing using CFRC sensors. It is anticipated that if the proper temperature variation equipment was used and experiments were conducted continuously from very low temperatures to very high temperatures, the results would provide a single and more reliable correction factor. In the case of temperature variation during SHM, this correction factor could then be applied to the data recorded from the cement-based sensors in charge of sensing stress/strain. Of course the temperature should be recorded through an unloaded sensor.

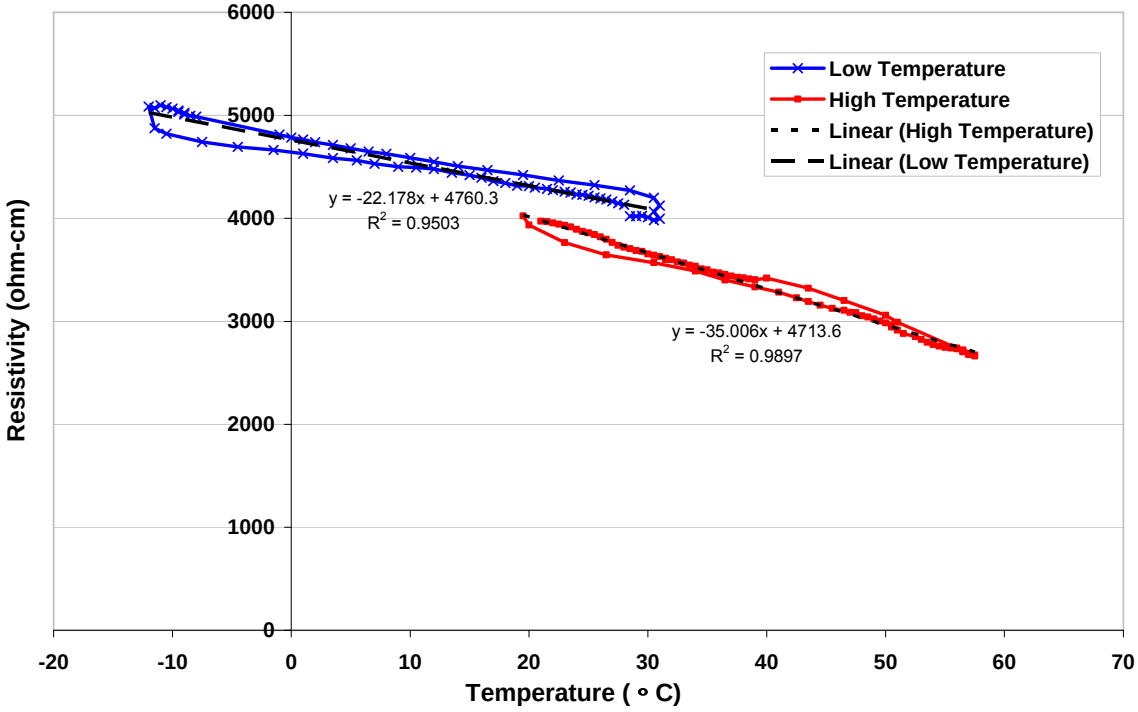


Figure 10- 5: Reversibility of the temperature effect on the electrical resistivity of CFRC

# CHAPTER 11

# Effect of Chloride and Moisture

The electrical conductivity of cement-based sensors is through both the conductive fibres and the cementitious matrix. Conductivity of the matrix part of the conduction path is through the pore structure and is referred to as the electrolytic conductivity. This electrolytic conduction of cement paste depends on the paste composition, curing process and the overall condition of the pore structure. The presence of moisture and chloride changes the chemical composition of the pore structure and therefore affects the electrical resistivity of cementitious composites. In order to assess the effect of these environmental conditions on the resistivity properties of cement-based sensors, experiments were conducted on specimens exposed to moisture and chloride.

## 11.1 Petroleum Pitch-based CFRC Samples

In the experiments involving PPCF cement paste, the specimens were first loaded in flexure until thin cracks started to appear on the bottom face (see section 14.1 of Chapter 14 for loading details). These samples were then removed from the loading apparatus and submerged in chloride solution. The chloride solution was prepared by adding 35 g of NaCl (salt) to 1 litre of water. After 6 days, resistivity measurements were made and the values were compared against the resistivity values from control specimens of the same type (Figure 11-1).

Since the specimens were cracked, the resistivities would normally have decreased compared to the control samples; but the cracks were filled with

chloride solution, which is conductive and therefore the resistivity values of the 2% and 2%+MC specimens decreased by 40% and 28% respectively.

For the high fibre content specimens, however, the cracks interrupted the fibre-to-fibre connection and even though chloride solution is conductive, it is not as conductive as the carbon fibres; therefore the resistivity values increased by 33% and 40% for the 5% and 5%+MC specimens, respectively.

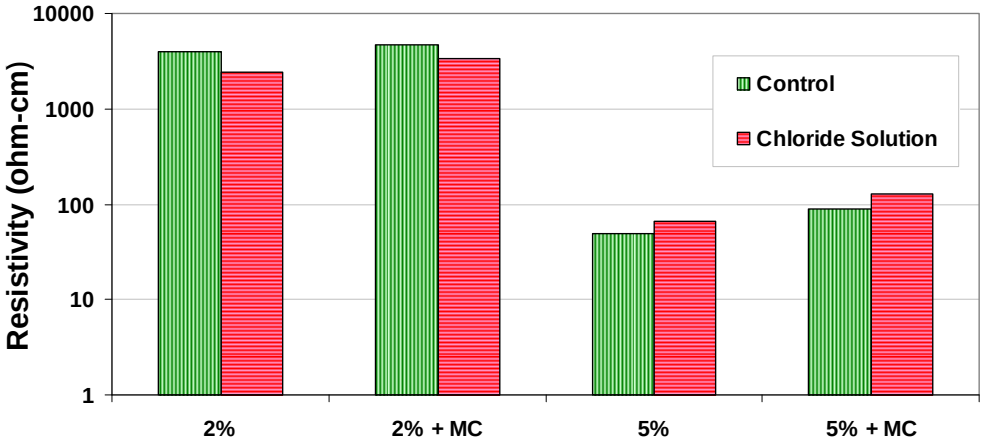


Figure 11- 1: Effect of chloride solution on the resistivity of cracked PPCF specimens

# 11.2 Coal Tar Pitch-based CFRC Samples

In the main series of experiments in which coal tar pitch based carbon fibres (CPCF) were used, the effect of chloride and moisture on the electrical resistivity of CFRC samples was investigated in a different manner than in the preliminary experiments.

Two containers were prepared, one containing water and the other 100 grams of NaCl desolved in 1 litre of water. As shown in Figure 11-2, three specimens from each of plain, 3.5% $V_f$ and 7% $V_f$ types were chosen for this experiment; one of each were kept in normal conditions at room temperature (control), and the others were kept in the moisture and chloride solution containers. One sample from the 15% $V_f$ batch was also added to the chloride solution container.

Resistivity measurements were taken from the specimens before they were put in their conditions and after one month of exposure. The specimens were then dried using a desiccator†, so that all the moisture was taken out of the specimens.


Figure 11- 2: CPCF cement paste specimens subjected to moisture and chloride solution

Figure 11-3 shows the resistivity values of the specimens inside the chloride solution container at three stages: before exposure, at one month of exposure to chloride solution and after drying the specimens in the desiccator. According to the results:

- The plain specimen experienced an 85% decrease in resistivity when exposed to chloride solution for one month, but after the drying procedure the resistivity value increased to just 17% below the original value measured before the test.

- The 3.5% and 7% $V_f$ specimens experienced a 98% decrease in resistivity when exposed to chloride solution for one month. This value changed to 95% once the specimens were dried.

† A glass jar fitted with an air-tight cover, used for drying solid material by means of a desiccant.

- In the case of the 15% $V_f$ specimen, the resistivity value decreased by 80% after the one month exposure to chloride solution. After the drying procedure, the resistivity was measured to be 78% less than the original value measured before the test.

These outcomes indicate that while the one month submersion in chloride solution caused a significant decrease the electrical resistivities of all the specimens, the plain sample was the only one to recover most of its resistivity. The CFRC samples just recovered 2 to 3% of their original resistivity after completely drying out. This may be indicating that for CFRC, the effect of chloride ingression on the electrical resistivity sustains even after the exposure even they are completely dried. Also, at very high fibre dosages (15%), the effect of chloride intrusion becomes relatively insignificant.

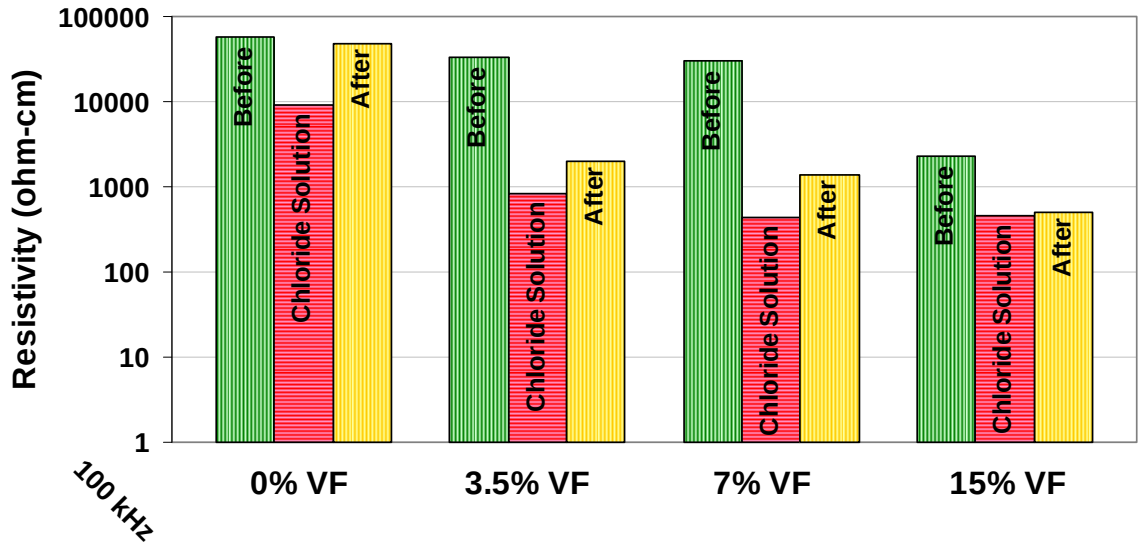


Figure 11- 3: Resistivity values of the specimens in the chloride solution at different stages

In addition, it was observed (see Figure 11-4) that the plain specimen and to some extent the 3.5% $V_f$ specimen experienced some delamination and blemishes, which proves that the addition of carbon fibres reduces the defects caused by chloride ingression.

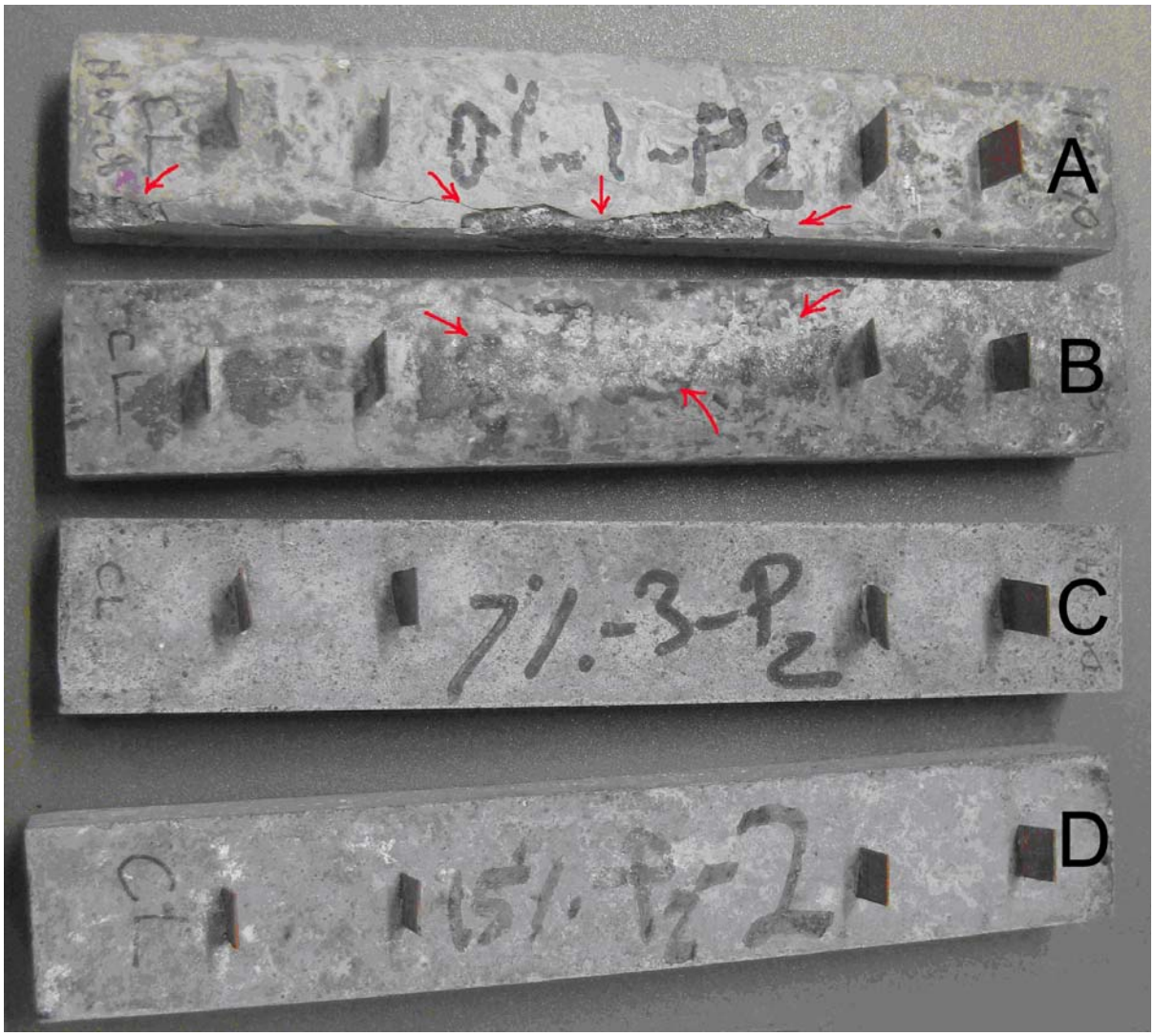


Figure 11- 4: Effect of chloride solution on the appearance of the specimens
(**A**: 0% CF; **B**: 3.5% CF; **C**: 7% CF; **D**: 15% CF)

In order to compare the effect of normal water and chloride solution on resistivity values, the results from resistivity measurements on plain, 3.5% and 7% $V_f$ specimens after one month of submersion in water and chloride solution were compared to the values from control samples. This comparison, illustrated in Figure 11-5, implies that it is in fact the moisture that is playing a significant role in reducing the resistivity values, showing a considerable and similar reduction (about 85% and 98% for the plain and CFRC samples, respectively) in

the resistivity values of specimens when subjected to both water and chloride solution.

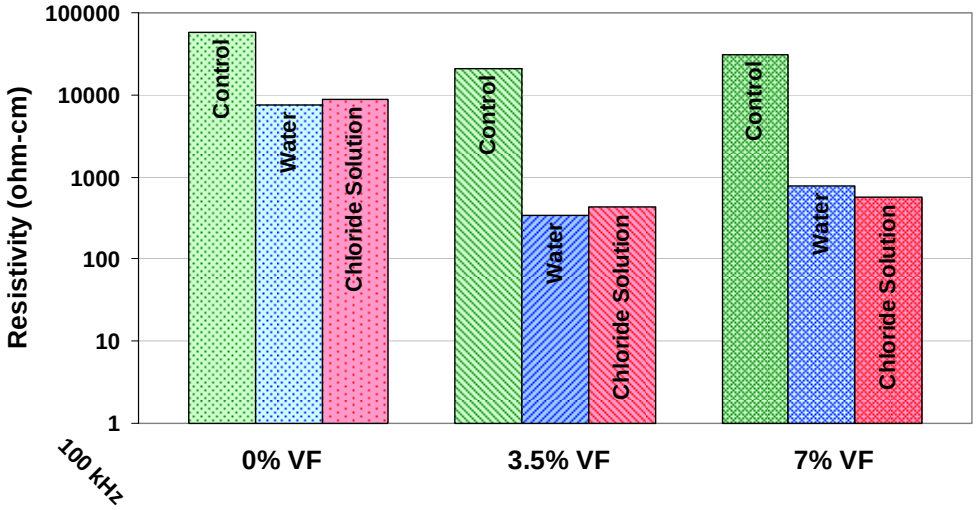


Figure 11- 5: Effect of moisture with and without chloride on the electrical resistivity of CFRC

It is suggested that more experiments be conducted in a more precise way and under different loading conditions in order to fully understand the effect of these exposure conditions. Nevertheless, it was observed from the findings in this chapter that moisture and chloride do influence the resistivity values obtained from CFRC sensors which may affect the accuracy of their stress/strain sensing ability. Thus it is important to take this effect into consideration if and when the sensors are employed in environments subjected to moisture and chloride. This may be done by installing a sensor merely to detect the effect of moisture and chloride on resistivity measurements. Coating the sensors with moisture resistant material may also be a solution to this issue.

# CHAPTER 12

# Compressive Loading

Upon loading, the carbon fibres and nanotubes inside the cement-based sensors bridge the internal micro-cracks, which in addition to strengthening the composite, is the basis of its sensing ability. Under tensile loading, these fibres pull out a little, slightly increasing the electrical resistivity whereas under compressive loading, a slight decrease in resistivity occurs.

A series of tests were conducted in order to investigate the sensing ability of the cement-based sensors under compressive loading. The reversibility and repeatability of resistivity measurements upon cyclic stress and strain was also evaluated and the sensors were compared to conventional strain gauges.

## 12.1 Specimens

Three kinds of cement-based sensor specimens were used in these experiments:

- 15% CF cylindrical specimens with 50.8 mm diameter and 100 mm length and 60 mm inner-electrode spacing (Figure 12-1-a)
- 15%CF +1% MWCNT hybrid cylindrical specimens with 50.8 mm diameter and 100 mm length and 60 mm inner-electrode spacing (Figure 12-1-a)
- 15%CF +3% MWCNT hybrid cubic specimens with 50 mm dimensions and 20 mm inner-electrode spacing (Figure 12-1-b)

Note that cylindrical specimens were the initial choice of shape for compressive loading since stress concentration at corners is eliminated. However, the 15%CF +3% MWCNT hybrid samples were very soft and brittle causing breakage and

health problems while grinding cylinders (see Appendix C for an overview on the health issues associated with using carbon nanotubes). Therefore, for this type of sensor samples, the cube shaped specimens were used.

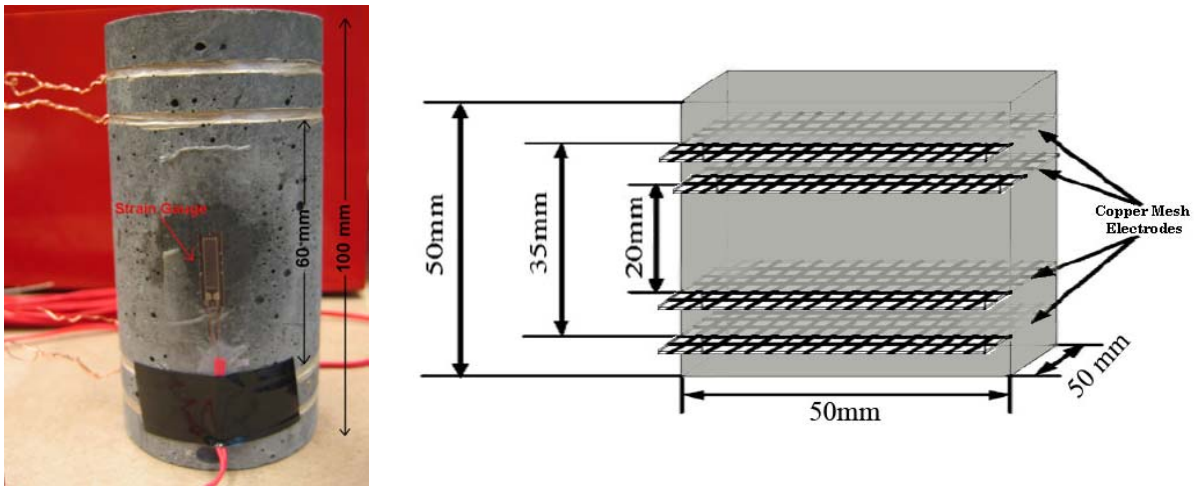


**(a)** **(b)**

Figure 12- 1: Specimens used for compressive loading tests: (a) 15% CF and 15%CF +1% MWCNT cylindrical specimens; (b) 15%CF +3% MWCNT cubic specimen

## 12.2 Setup and Procedure

Instron FastTrack 8802 Servo-hydraulic Mechanical Testing System was the loading device used for these experiments. As shown in Figure 12-2-a, the Agilent 4263B LCR Meter was employed for resistivity measurements.

10mm strain gauges were attached to either side of the samples to compare the results obtained from these sensors and conventional strain gauges. In addition to that two LVDTs, one on either side, were used to measure the displacement. The experimental setup is displayed in Figure 12-2.

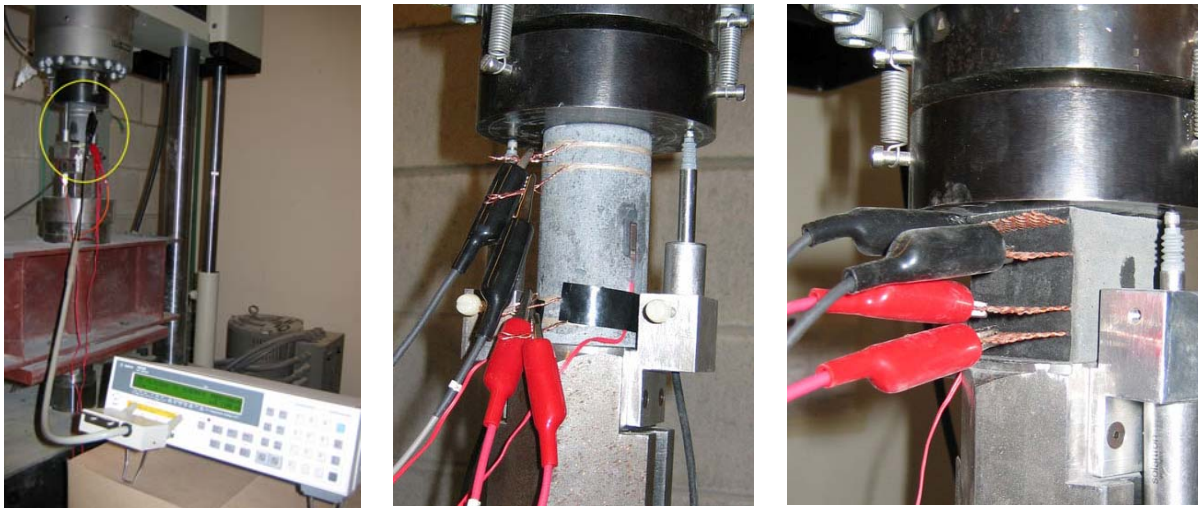

**(a)** **(b)** **(c)**

Figure 12- 2: (a) Experimental setup for the compressive loading tests; (b) Cylindrical specimens' setup; (c) Cubic specimens' setup

Each specimen was cyclically loaded to different load values at a rate of 0.002 cycles per second. The load and LVDT data was transferred through a signal conditioning device and a data acquisition system to a laptop equipped with NI LabVIEW platform. The impedance data (resistance and reactance) was simultaneously collected from the LCR meter and transferred to the laptop via a general purpose interface bus (GPIB). The AC frequency used was 100 kHz.

The LabVIEW interface, shown in Figure 12-3, was designed to monitor and display the variation of resistivity, load and strain over time. All the data including time, resistance, reactance, resistivity, load, displacement, stress and strain were recorded as the test was conducted.

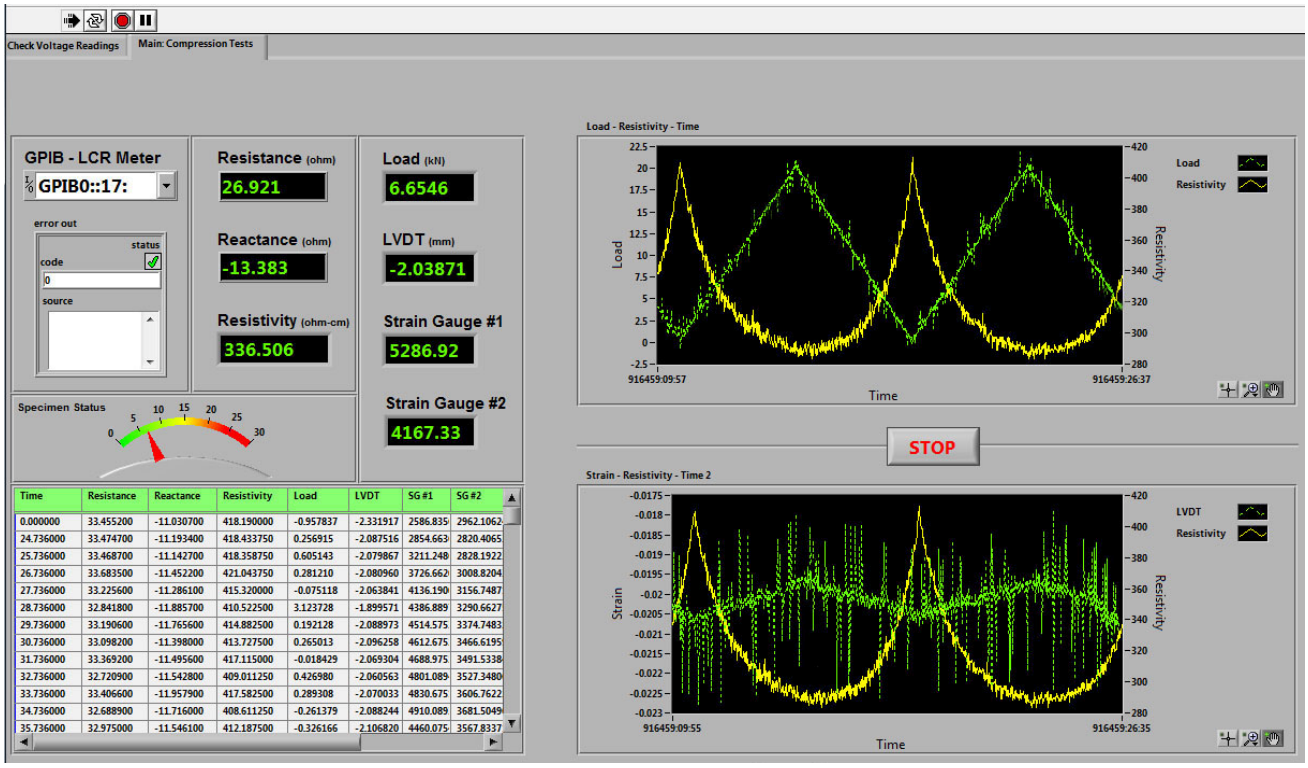


Figure 12- 3: LabVIEW interface for the compressive loading tests

# 12.3 Results and Discussion

In order to evaluate the sensing ability of cement-based sensors, the load, stress and strain values were plotted against the fractional change in resistivity.

Fractional change in resistivity (FCR) is given by:

$$FCR = \frac{\rho_t - \rho_0}{\rho_0} \qquad (12\text{-}1)$$

Where,

$\rho_t$ : Electrical resistivity at time t during the tests;

$\rho_0$ : Electrical resistivity at the beginning of the test (prior to loading)

FCR was used because it is a dimensionless quantity and thus easy to compare across different specimens.

The results for the three types of specimens are plotted and discussed in the following sections.

### 12.3.1 Cement-based sensors with 15% CF

Some specimens were loaded until failure and the ultimate load capacity was estimated at 100±10kN. The resistivity values for these specimens at first decreased during the compressive loading, but dramatically increased at the time of failure (see Figure 12-4). This confirmed that the sensors actually had a response to loading, showing decreasing resistivity values when compressed but very high resistivity values when substantial micro-cracks followed by macro-cracks and failure occurred.

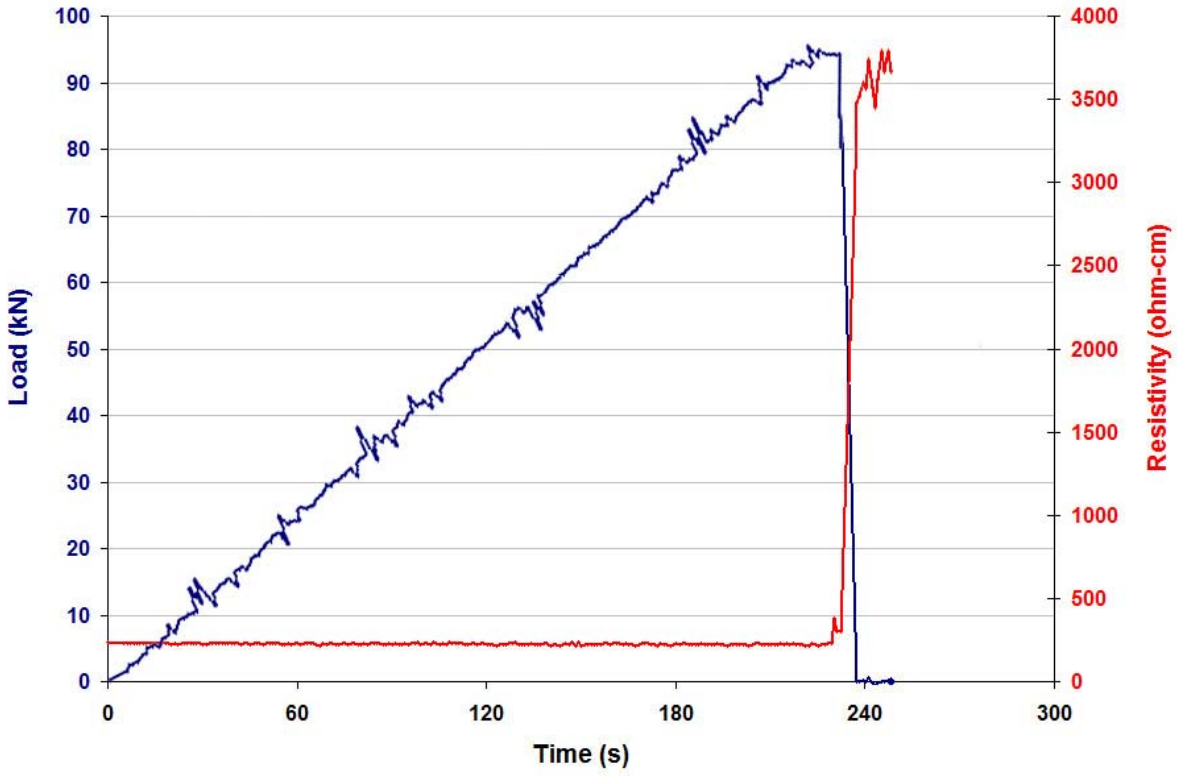


Figure 12- 4: Response of 15% CF cement-based sensors to failure at ultimate compressive load

Remaining specimens were then cyclically loaded to 5kN, 10kN, 20kN, 30kN and 60kN for several cycles to represent approximately 5%, 10%, 20%, 30% and 60% of the ultimate load respectively. Figure 12-5 displays the variation in load and FCR during these loading periods.

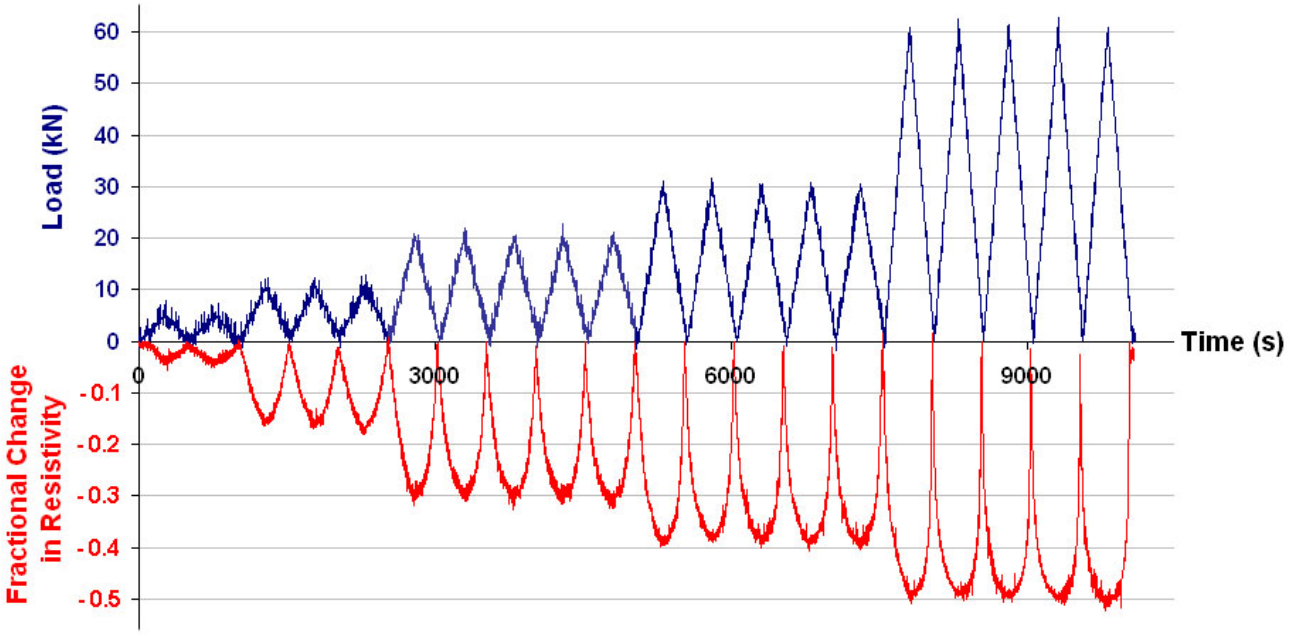


Figure 12- 5: Load and FCR variation of 15% CF sensors at different levels of cyclic loading

It is clearly observable from Figure 12-5 that the electrical resistivity of this sensor varies distinctly in response to the cyclic compressive loading, following a similar pattern. Thus the piezoresistive quality of the sensors is confirmed.

During each loading cycle, the resistivity values decrease with the increase in compressive load, resulting in negative FCR values, and then increase to the initial value when the unloading branch of the cycle takes place. The higher the load, the larger the fractional change in resistivity. The fact that the sensors regain their initial resistivity at the end of each cycle indicates reversibility and is highly encouraging.

The reason for the decrease in resistivity is that when the specimen is compressed, the conduction length between the electrodes decreases, and

potentially leading to more contact among the conductive fibres. Note that this only holds true while the sensor is in the elastic regime and the fibre volume fraction is more than a certain amount. In fact the same test was performed on plain and low fibre content specimens and the results showed a slight increase in the resistivity with the increase in compressive loads (Figure 12-6).

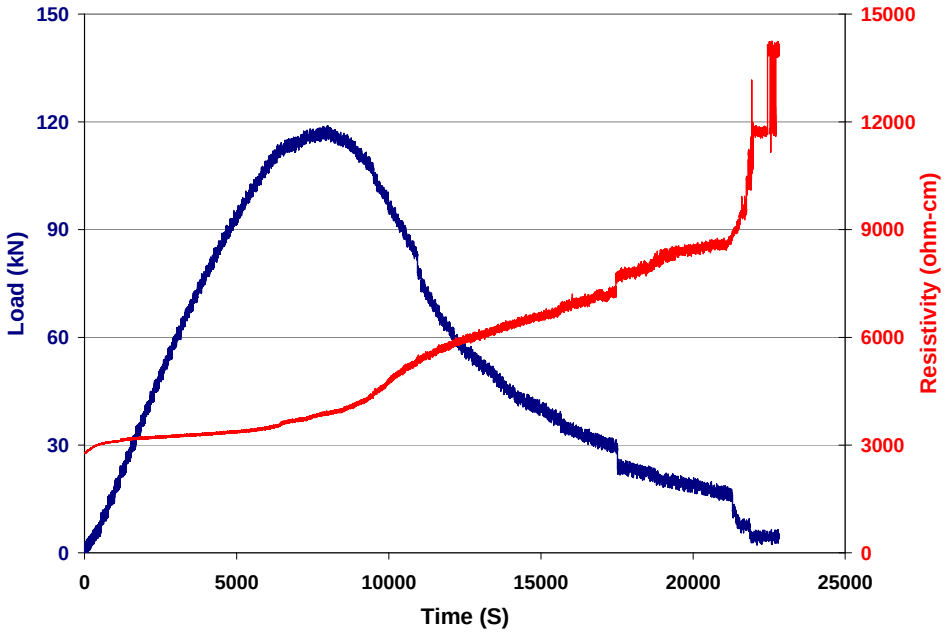


Figure 12- 6: Low fibre content (5% CF) specimen loaded in compression until failure

The reason being that firstly the fibres are farther apart and there is no chance of fibre to fibre contact even when compressed, and secondly, according to Equation 2-3, resistivity should increase with the slight decrease in $\ell$ and increase in A due to the elastic volume compression. Having higher volume fractions of fibre, the increase in resistivity due to barrelling and increase in A becomes less prominent and eventually negligible in comparison to the reduction in electrical resistivity due to more fibre-to-fibre contact as a result of elastic compression.

Figure 12-7 demonstrates an attempt to cycle the load between 60kN and 90kN. The resistivity values decrease as expected with the increase in compressive load but as the load reaches values close to about 90kN, the sensor material becomes

inelastic due to the abundance of micro-cracks causing a slight increase in resistivity. As the load inches a little above 90kN (the ultimate load capacity), and macro-cracks start to appear, the increase in resistivity becomes considerable and eventually when the specimen fails, rises drastically by almost 10 fold. These sensors can thus not only act as crack detectors but also alert against imminent failure.

For 15% CF sensors, $\rho_0$ was measured to be around 400 ohm-cm. During the elastic range, the electrical resistivity changes reversibly between 400 and 200 ohm-cm leading to FCR values of 0.5 and less, depending on the cyclic loading amplitude. With the appearance and propagation of macro-cracks, the resistivity increased irreversibly from about 200 ohm-cm to almost 400 ohm-cm. Finally, at failure the resistivity values increase from about 400 ohm-cm to almost 3500 ohm-cm.

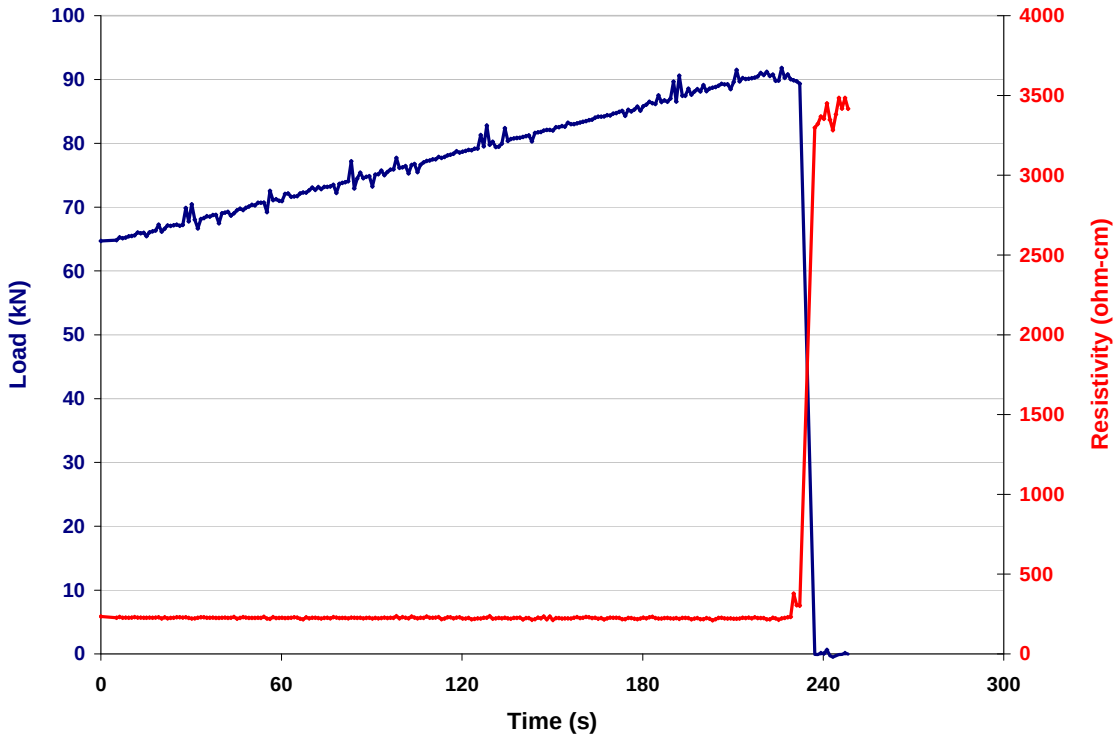


Figure 12- 7: Response of 15% CF cement-based sensors to failure at ultimate compressive load

In order to further discuss the behaviour of the sensors, the results from the 30kN cyclic loading segment of the compression tests are displayed in Figures 12-8 through 12-11.

Figures 12-8-a and b illustrate the cycling of compressive load and FCR with time and the variation of FCR with compressive stress during the four cycles, respectively (see Appendix B for the load versus resistivity plot).

As shown in part (a) of this figure, the electrical resistivity of the cement-based sensor decreases reversibly with the increasing branch of each compressive loading cycle and increases reversibly with the decreasing or unloading branch of each cycle. The relationship between the fractional change in resistivity and compressive stress, shown in part (b), yields the following correlation for stress sensitivity:

$$FCR = 0.0012\sigma^2 - 0.036\sigma + 0.0068$$

Where $\sigma$ is presented in MPa units.

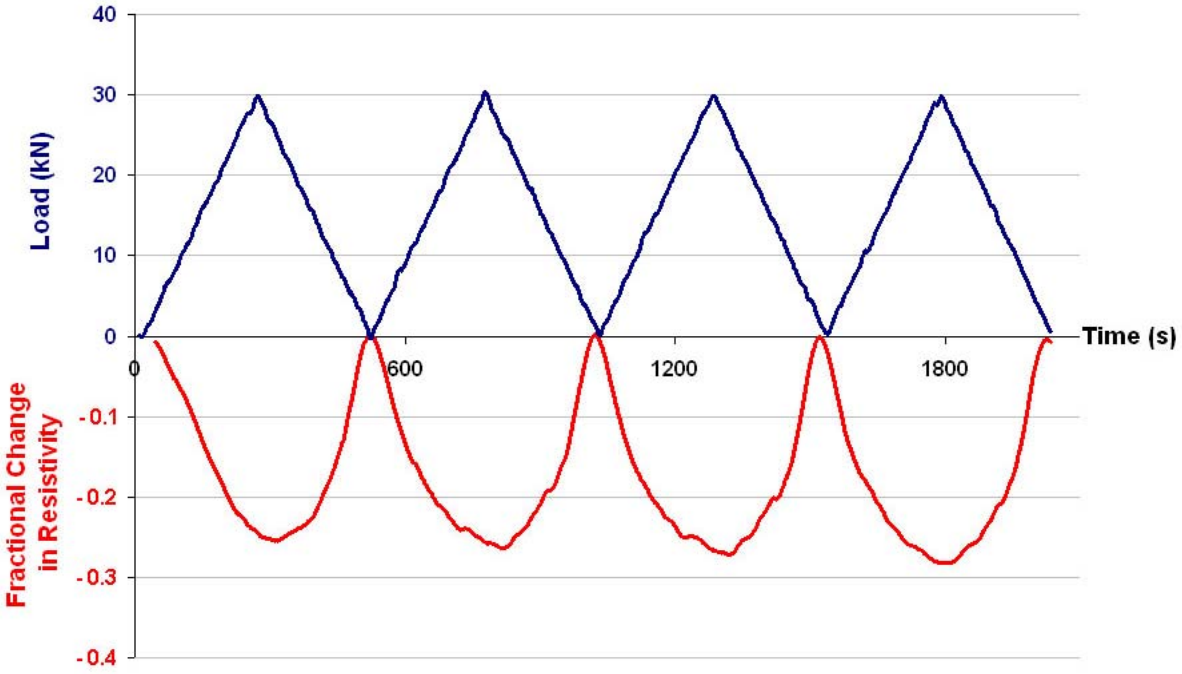


**(a)**

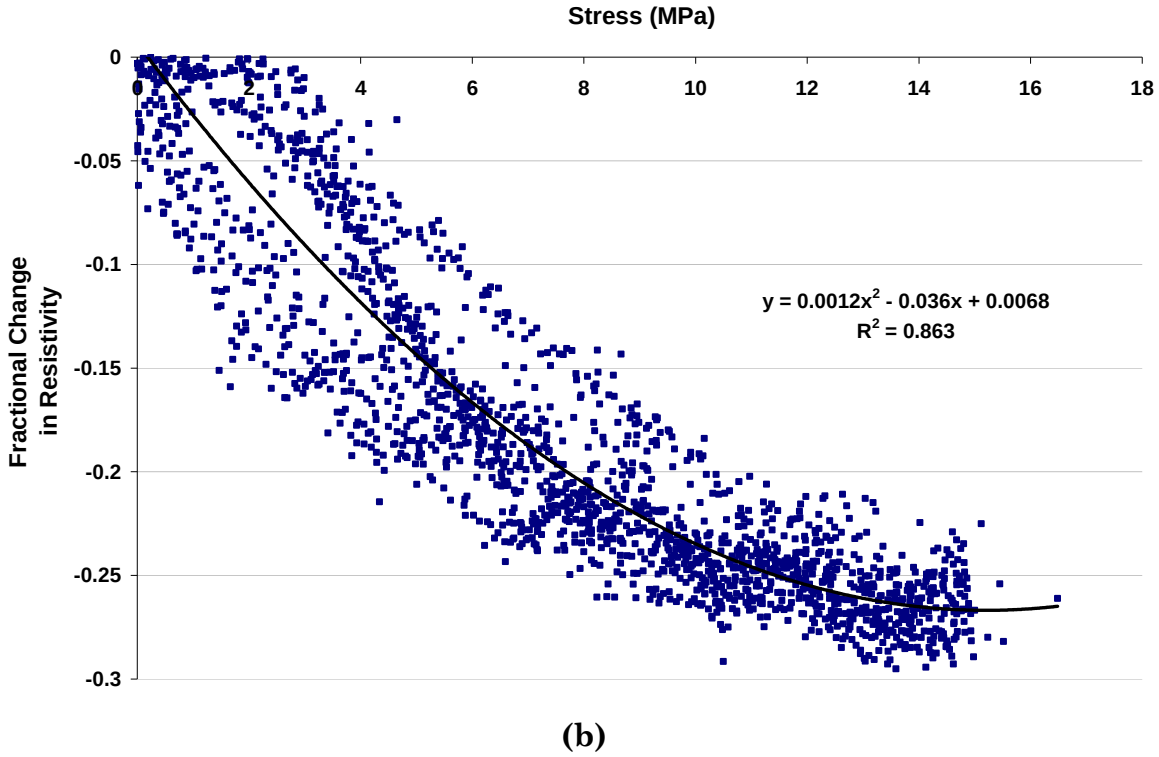


**(b)**

Figure 12- 8: Load, FCR and stress variation of 15% CF sensors under cyclic compressive loading with 30kN amplitude: (a) FCR response to compressive cyclic loading; (b) FCR/Stress correlation.

Figures 12-9-a; b and c illustrate the cyclic variation of strain obtained from LVDTs and FCR with time, the cyclic variation of strain obtained from strain gauges and FCR with time and the correlation of FCR with compressive strain during the four cycles, respectively.

It is noticeable from this figure that the strain values obtained from LVDTs are not as accurate and reversible as those obtained from strain gauges and cement-based sensors, although they respond reasonably to the cyclic loading and confirm the measured strain values.

The similar variation trends of the conventionally measured strain (in με) and FCR displayed in part (b) of Figure 12-9 indicates that the cement-based sensor can be a comparable means of strain measurement to conventional strain gauges. According to this plot, both strain and FCR values seem to have a small

amount of hysteresis‡ (see dotted lines). This may be explained with the slight change in temperature. Back-tracking this minor hysteresis with temperature/resistivity variation correlation from Chapter 10, it corresponds to a temperature increase of less than 0.3°C (see below) after four cycles of compressive loading, which is quite reasonable:

Shift in resistivity ≈ -10 ohm-cm

Rate of resistivity reduction with increasing temperature = 35 ohm-cm/°C

=> Corresponding temperature raise ≈ 0.2857 °C

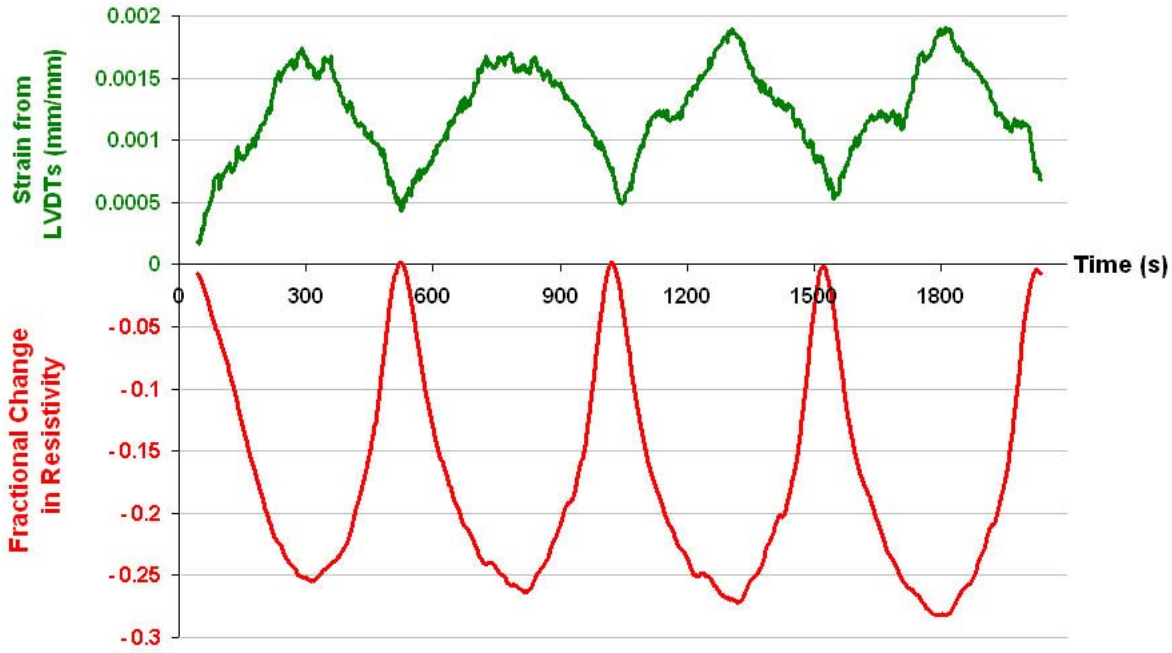


**(a)**

‡ Hysteresis occurs when sensor outputs do not return to the same value during cyclic changes of input, presented in % units (ScienceProg 2006).

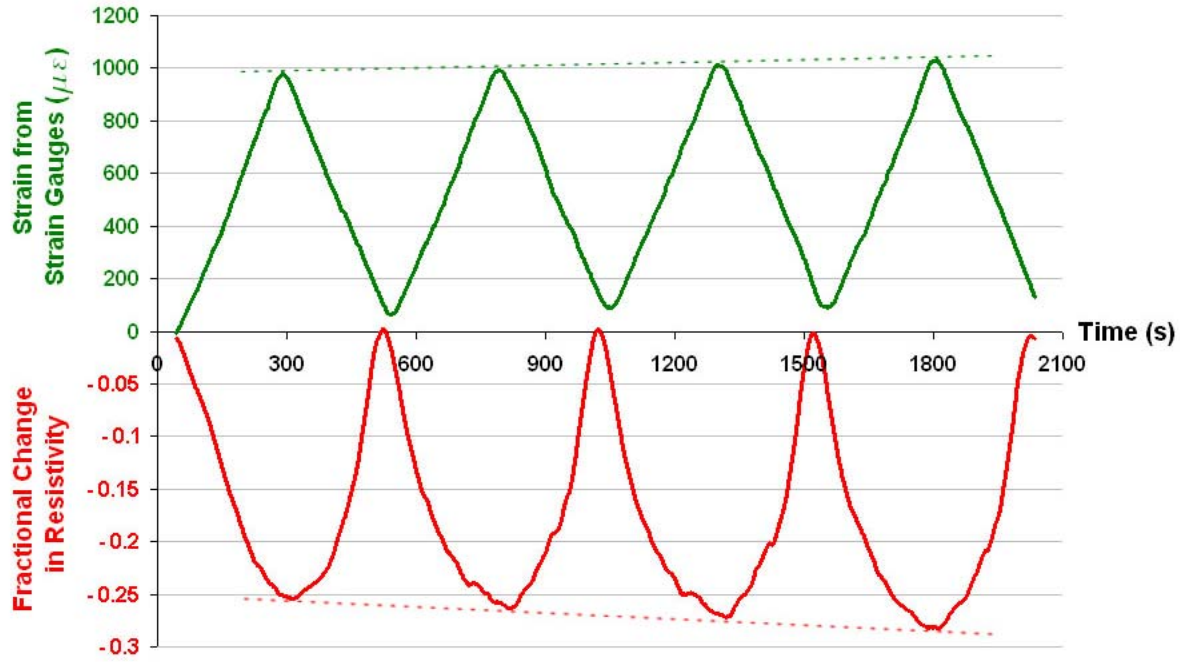


**(b)**

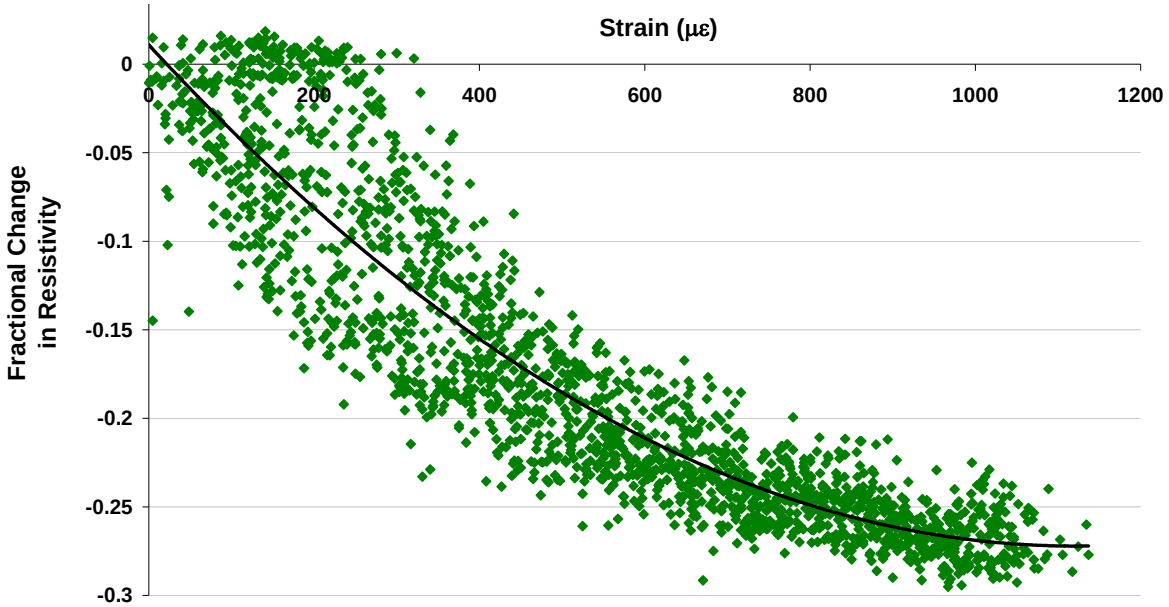


**(c)**

Figure 12- 9: Strain from LVDTs and strain gauges and FCR and stress variation of 15% CF sensors under cyclic compressive loading with 30kN amplitude: (a) LVDT strain and FCR reaction to compressive cyclic loading; (b) Conventional strain measurement and FCR response to compressive cyclic loading; (c) FCR/Strain correlation.

The stress/strain and stress/FCR correlations for four cycles of compressive loading are compared in Figure 12-10. Although, the relationship between stress/FCR is not as linear as that of the stress/strain, it is demonstrating a sensible correspondence.

One of the main characteristics of a strain gauge is its gauge factor:

$$\text{Gauge Factor} = \frac{\Delta R / R_0}{\varepsilon} = \frac{\Delta \rho / \rho_0}{\varepsilon} = \frac{FCR}{\varepsilon} \qquad (12\text{-}2)$$

Where,

$\Delta R$ (or $\Delta \rho$): Change in strain gauge resistance (or resistivity);

$R_0$ (or $\rho_0$): Unstrained resistance (or resistivity) of strain gauge;

$FCR$: Fractional Change in Resistivity;

$\varepsilon$: Strain

The gauge factor of conventional metal strain gauges is known to be 2 to 3.


Figure 12- 10: Stress/strain and stress/FCR relationships of the 15% CF sensors after four cycles of compressive loading

So as to calculate the gauge factor of the cement-based sensors, FCR and strain values for a single branch of loading are plotted against each other in Figure 12-11.

The following relationship is calculated from this figure:

$$FCR = 109258\varepsilon^2 - 391.94\varepsilon + 0.0061$$

The gauge factor of the 15% CF cement-based sensors can therefore be estimated using the above formula. Using the bilinear response presented in Figure 12-11, two unique gauge factors are obtained: 290 and 145 for strain values below and above 0.0007, respectively (using Equation 12-2), which are well above that of the conventional strain gauges attached to the specimens. This means that these sensors are much more sensitive and therefore they can provide strain data with a better resolution than conventional strain gauges.

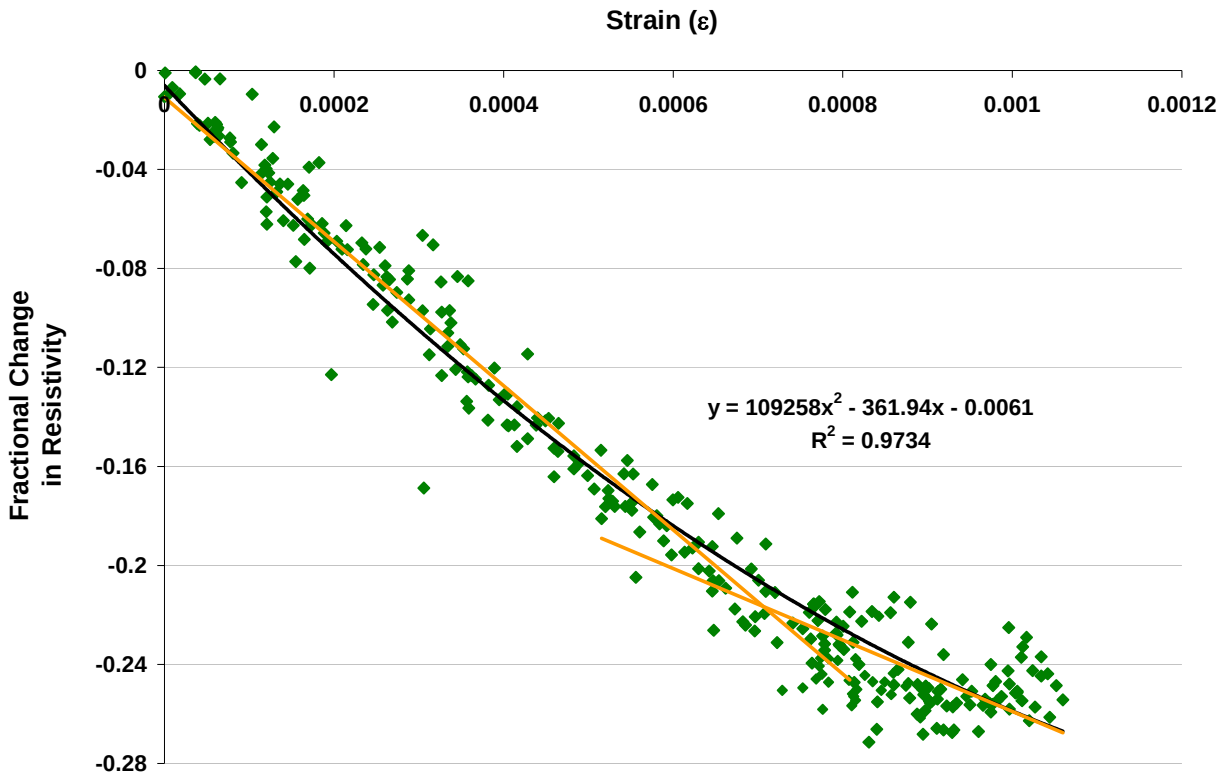


Figure 12- 11: Strain and FCR correlation pf 15% CF sensors for calculating their gauge factor

### 12.3.2 Cement-based sensors with 15% CF and 1% MWCNT

Figure 12-12-a illustrates the variation of compressive load and FCR with time during 5 cycles of compressive loading with amplitude of 30kN (see Appendix B for the load versus resistivity plot).

The results are similar to that of 15% CF sensors and it is found that this sensor is piezoresistive as well. The electrical resistivity of the cement-based sensor decreases reversibly with the increasing branch of each compressive loading cycle and increases reversibly with the decreasing or unloading branch of each cycle.

The relationship between the fractional change in resistivity and compressive stress, shown in part (b), yields a stress sensitivity of:

$$FCR = 0.0011\sigma^2 - 0.0316\sigma - 0.003$$

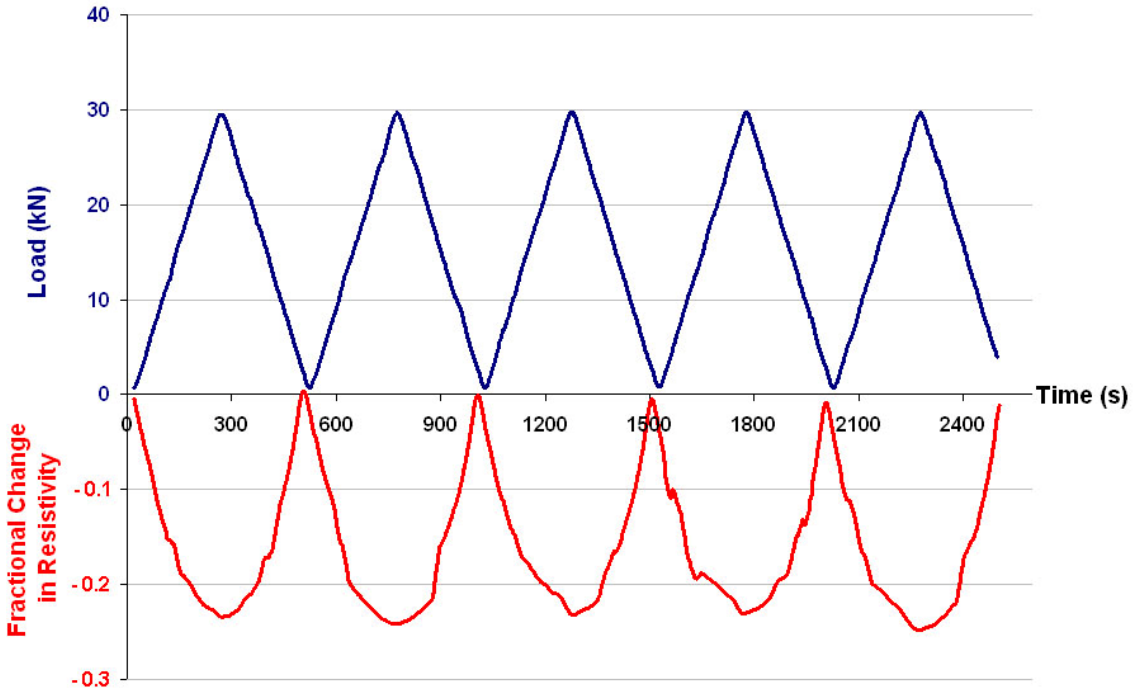


**(a)**

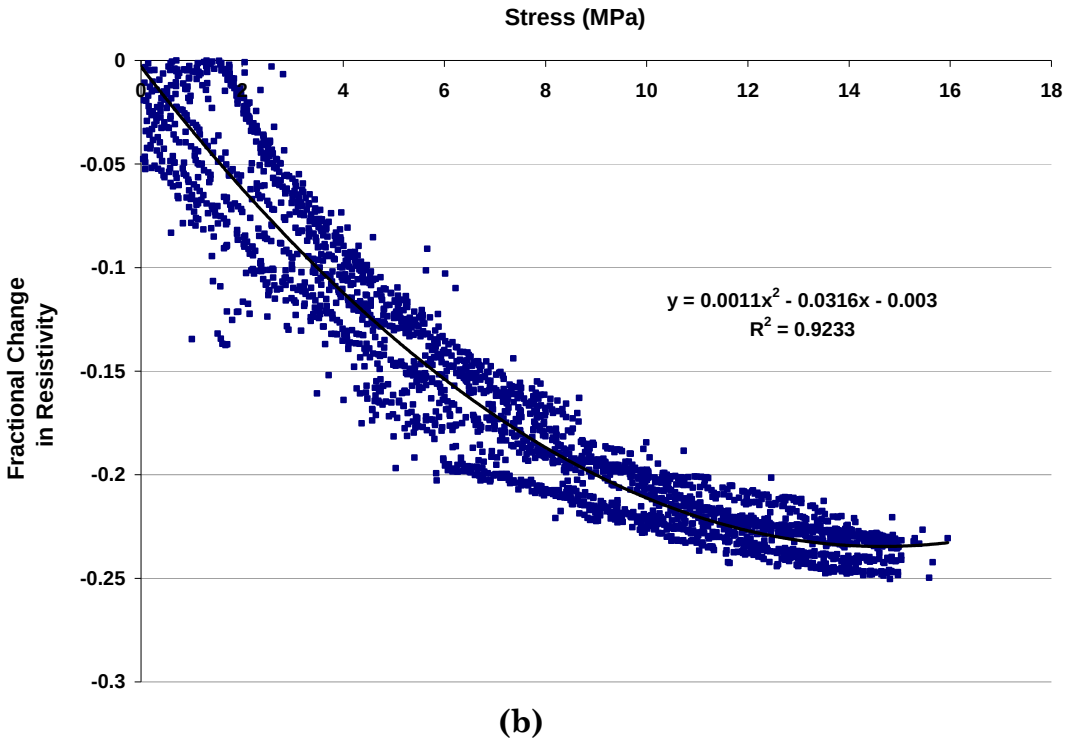


**(b)**

Figure 12- 12: Load, FCR and stress variation of 15% CF + 1% MWCNT sensors under cyclic compressive loading with 30kN amplitude: (a) FCR response to compressive cyclic loading; (b) FCR/Stress correlation

Figures 12-13-a and b illustrate the cyclic variation of strain obtained from strain gauges and FCR with time and the correlation of FCR with compressive strain during the four cycles, respectively.

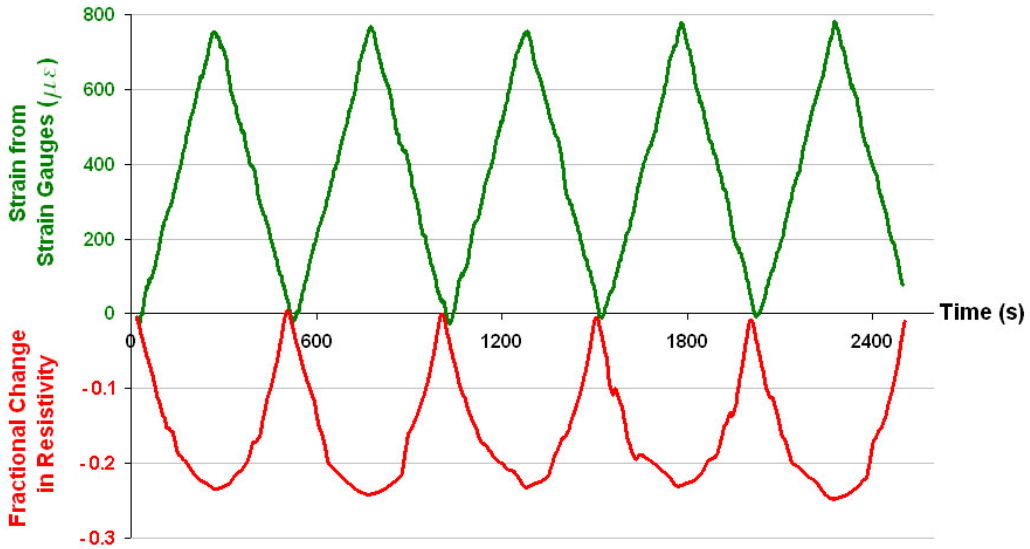


**(a)**

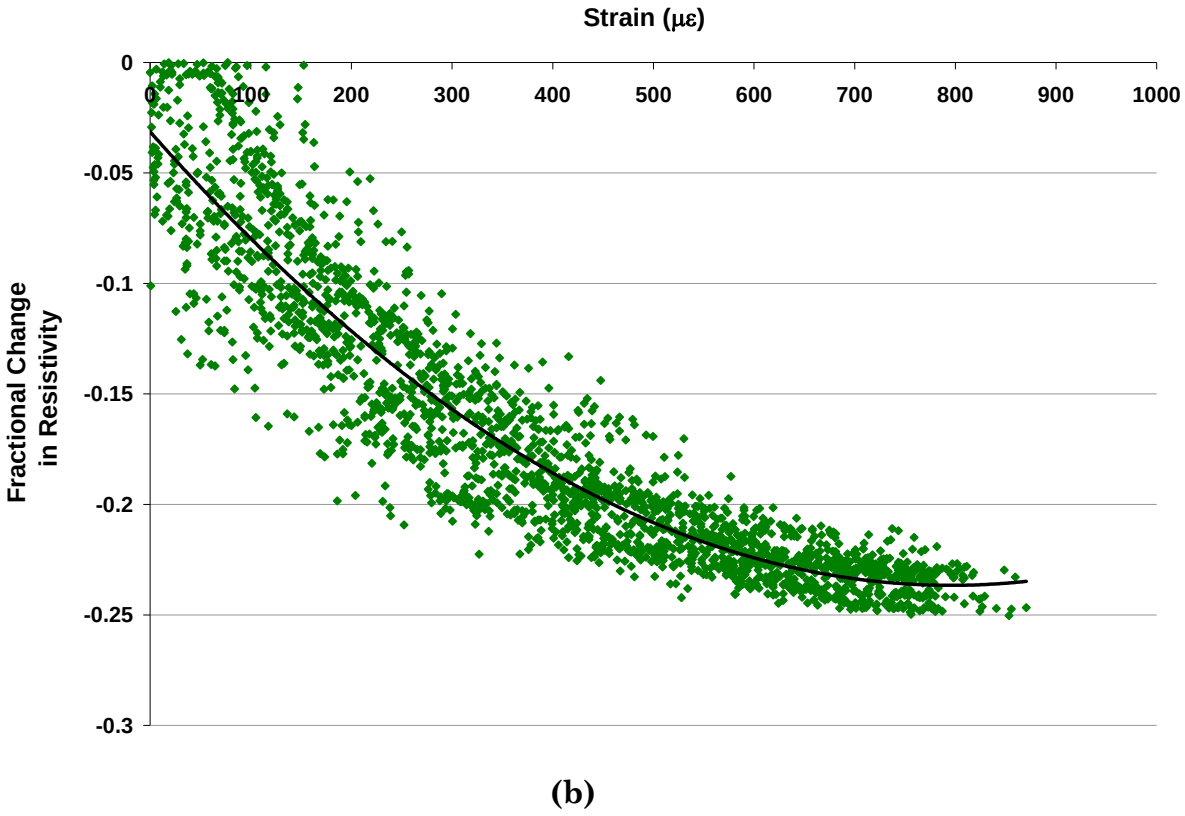


Figure 12- 13: Variation of strain gauge measurements, FCR and stress of 15% CF +1% MWCNT sensors under cyclic compressive loading with 30kN amplitude: (a) Conventional strain measurement and FCR response to compressive cyclic loading; (c) FCR/Strain correlation.

The similar variation trends of the conventionally measured strain (in με) and FCR indicates that this cement-based sensor can be a comparable means of strain measurement to conventional strain gauges.

Once again, the stress/strain and stress/FCR correlations for five cycles of compressive loading are compared in Figure 12-14 and the relationship between stress/FCR, although not as linear as that of the stress/strain, appears to have a sensible correspondence.

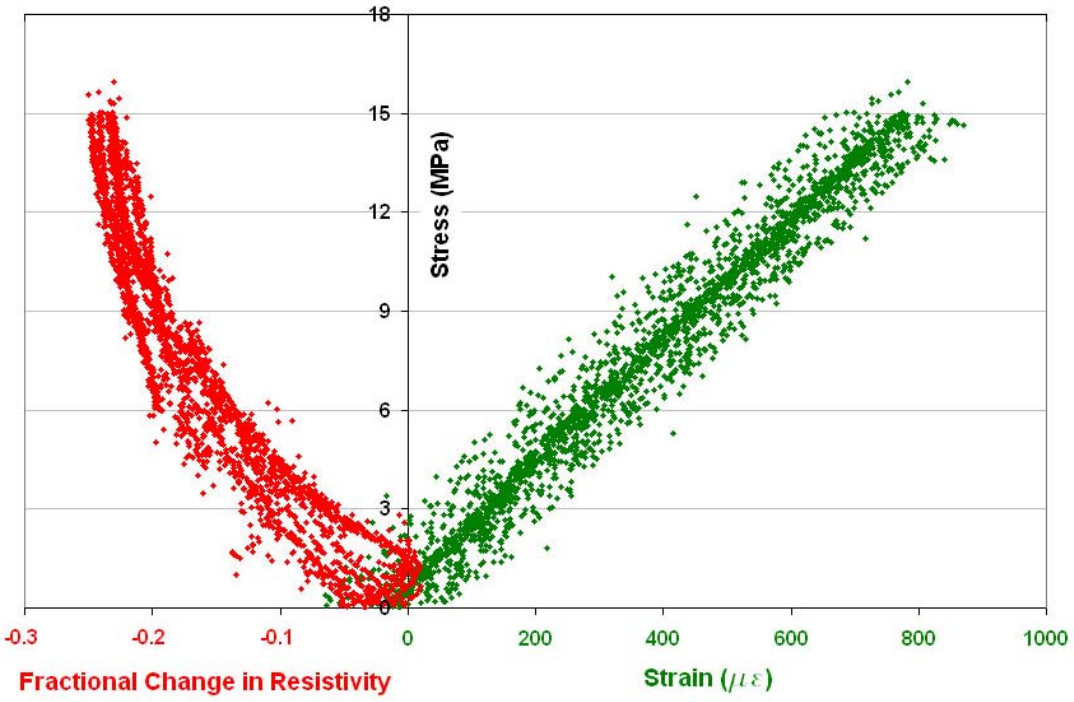


Figure 12- 14: Stress/strain and stress/FCR relationships of the 15% CF + 1% MWCNT sensors after five cycles of compressive loading

FCR and strain values for a single cycle of loading, plotted against each other in Figure 12-15, yields the following relationship between strain and FCR:

$$FCR = 327751\varepsilon^2 - 514.68\varepsilon$$

Using the bilinear response of these hybrid sensors and Equation 12-2, gauge factors of about 410 and 110 are estimated for strain values below and above 0.0004, respectively, which is not only well above that of the conventional strain gauges, but also higher than the gauge factor obtained from 15% CF sensors. This improvement is significant and justifies using CNTs in combination with carbon fibres in cement-based sensors.

It is worth mentioning that for resistivity measurements of hybrid sensors, the level of AC had to be changed from 100 volts, used for all other experiments, to 1000 volts. This was due to the fact that at 100 volts, the hybrid specimens

exhibited absurdly high resistivity values which may have been on account of their non-ohmic behaviour at lower voltages.

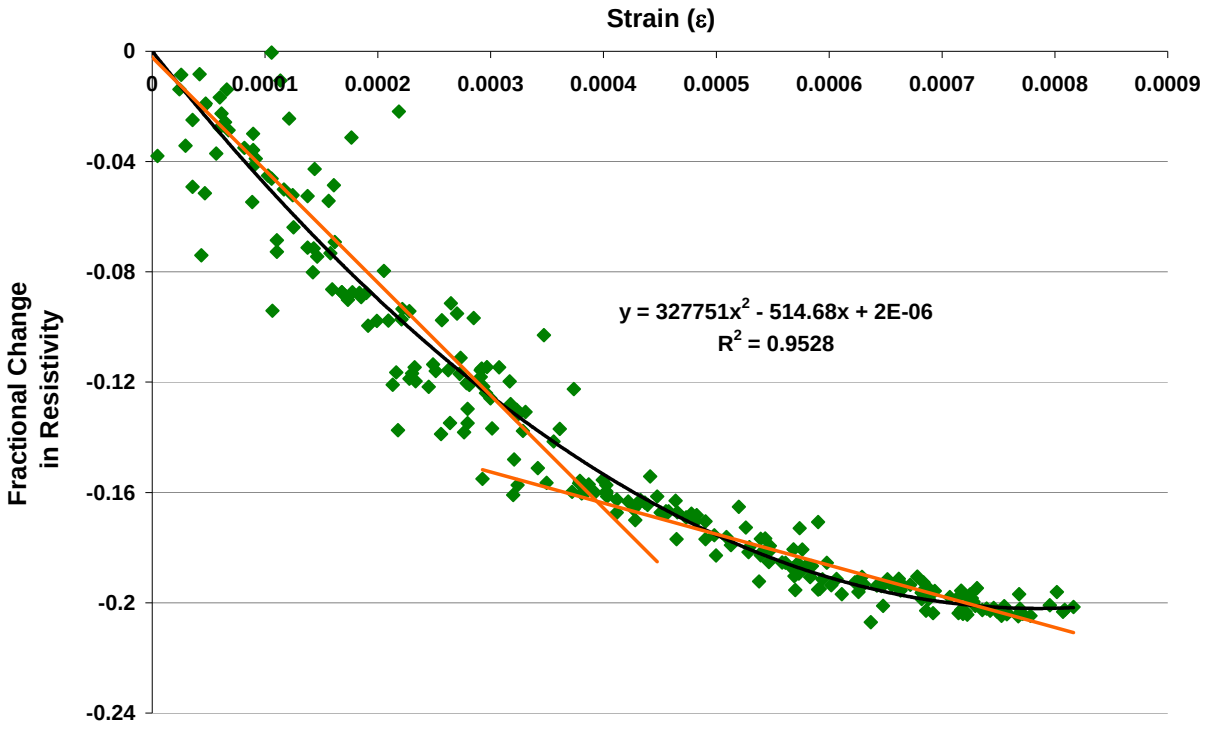


Figure 12- 15: Strain and FCR correlation of 15% CF + 1% MWCNT hybrid sensors for calculating their gauge factor

### 12.3.3 Cement-based sensors with 15% CF and 3% MWCNT

The 15% CF + 3% MWCNT hybrid sensors turned out to be very soft and brittle therefore the cylinder samples could not be ground and used.

In order to evaluate these sensors the cubic specimens with embedded copper mesh electrodes (Figure 12-2-c) were examined. These sensors were subjected to cyclic compressive loading with amplitudes of 0.5kN, 1.5kN and 5kN.

Figures 12-16 and 12-17 show the FCR response of the 15% CF + 3% MWCNT sensors to cyclic load and strain, respectively. These sensors are also found to exhibit piezoresistivity. Resistivity values decrease reversibly with compressive loading and increase reversibly with unloading. The variation in FCR follows the

same pattern as the measured strain and the gauge factor is estimated at about 50. Unfortunately the bond between the sensor material and the strain gauges was not sufficient, leading to unreliable strain measurements. Hence the strain data was only obtained from the LVDT measurements.

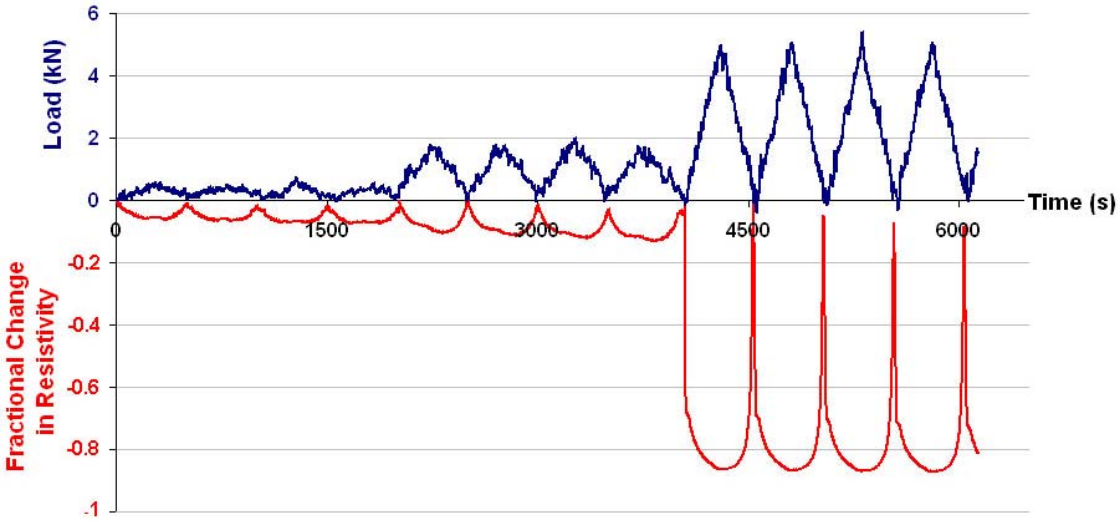


Figure 12- 16: FCR response of 15% CF + 3% MWCNT hybrid sensors to cyclic compressive loading with different amplitudes

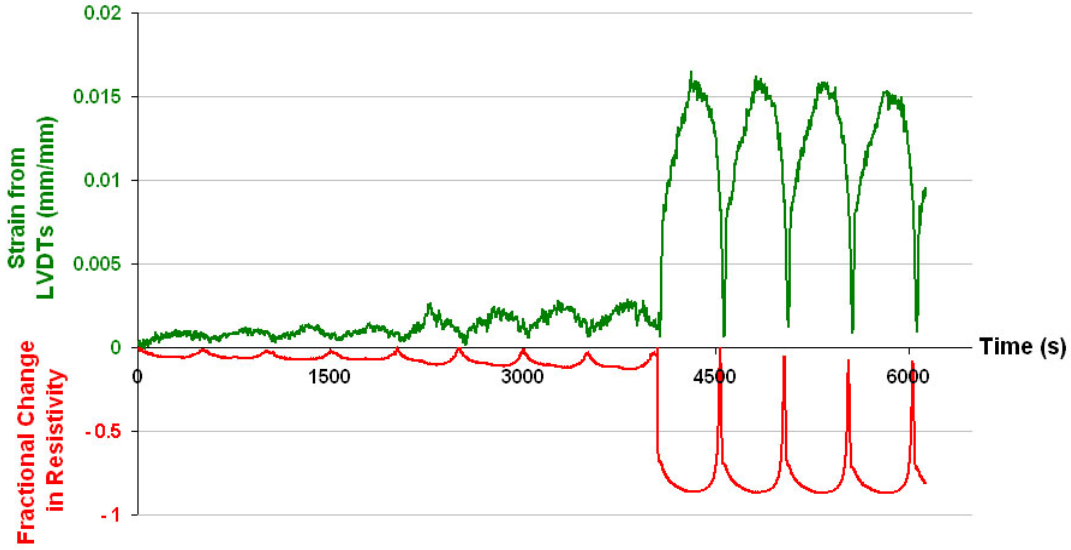


Figure 12- 17: Comparing the FCR variation of 15% CF + 3% MWCNT sensors to LVDT strain measurements in response to cyclic compressive loading with different amplitudes

# CHAPTER 13

# Tensile Loading

Upon tensile loading the fibres bridging the micro-cracks, undergo pull out, causing a small increase in the electrical resistivity of cement based sensors. These sensors are piezoresistive and measuring the change in their resistivity, provides a measure of the stress/strain experienced by the material.

A series of tests were conducted in order to investigate the sensing ability of the cement-based sensors under tensile loading, comparing them to conventional strain gauges.

## 13.1 Specimens

Two kinds of cement-based sensor specimens were used in these experiments:

- 15% CF specimens with a 25mm x 15mm cross section and 300mm length and 250 mm inner-electrode spacing
- 20% CF specimens with a 25mm x 15mm cross section and 300mm length and 250 mm inner-electrode spacing

Hybrid samples were also cast for tensile loading, but were not tested due to their brittleness and health problems.

## 13.2 Setup and Procedure

Instron FastTrack 8802 Servo-hydraulic Mechanical Testing System was the loading device used for these experiments. The Agilent 4263B LCR Meter was employed for resistivity measurements using an AC frequency of 100 kHz.

Two mechanical grips were used to grip the specimen ends in such a way the electrodes are on the outside of the grips. A more accurate set of grips, such as pneumatic grips, would have been preferred for these experiments. Two LVDTs, one on either side, were used to measure the displacement. The experimental setup is displayed in Figure 13-1.

Each specimen was cyclically loaded in tension with amplitude of about 1kN at a rate of 0.00167 cycles per second. The load and LVDT data was transferred through a signal conditioning device and a data acquisition system to a laptop equipped with NI LabVIEW platform. The impedance data (resistance and reactance) was simultaneously collected from the LCR meter and transferred to the laptop via a general purpose interface bus (GPIB).

The LabVIEW interface, shown in Figure 13-2, was developed to monitor and display the variation of resistivity, load and strain over time. All the data including time, resistance, reactance, resistivity, load, displacement, stress and strain were recorded as the test was conducted.

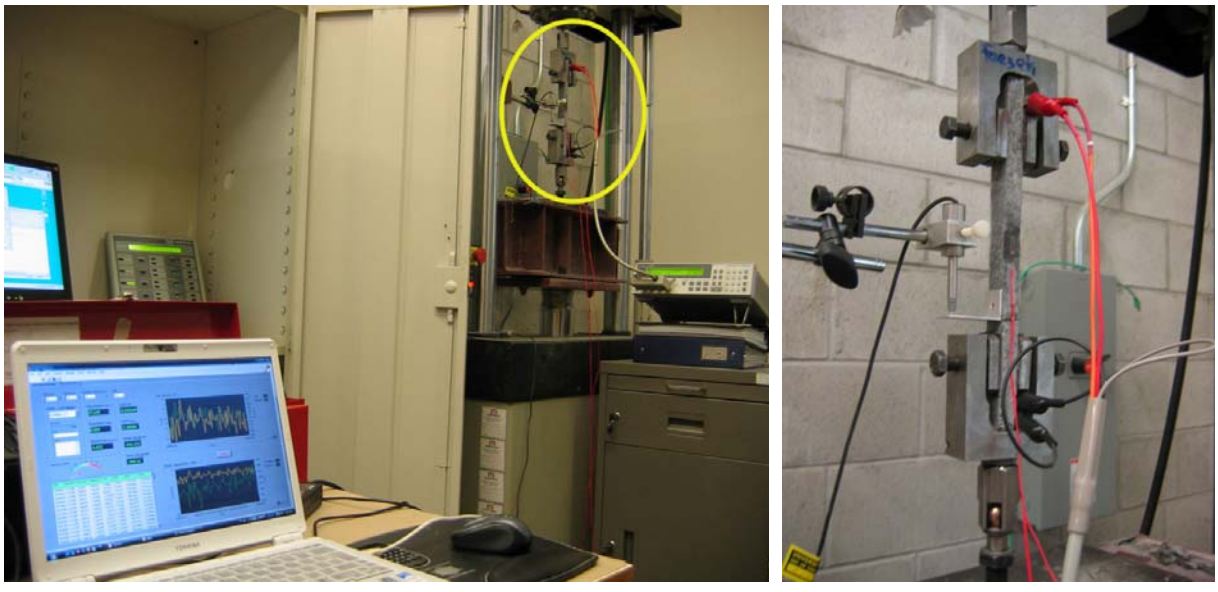

**(a)** **(b)**

**Figure 13- 1:** (a) experimental setup for the tensile loading tests; (b) Specimens setup

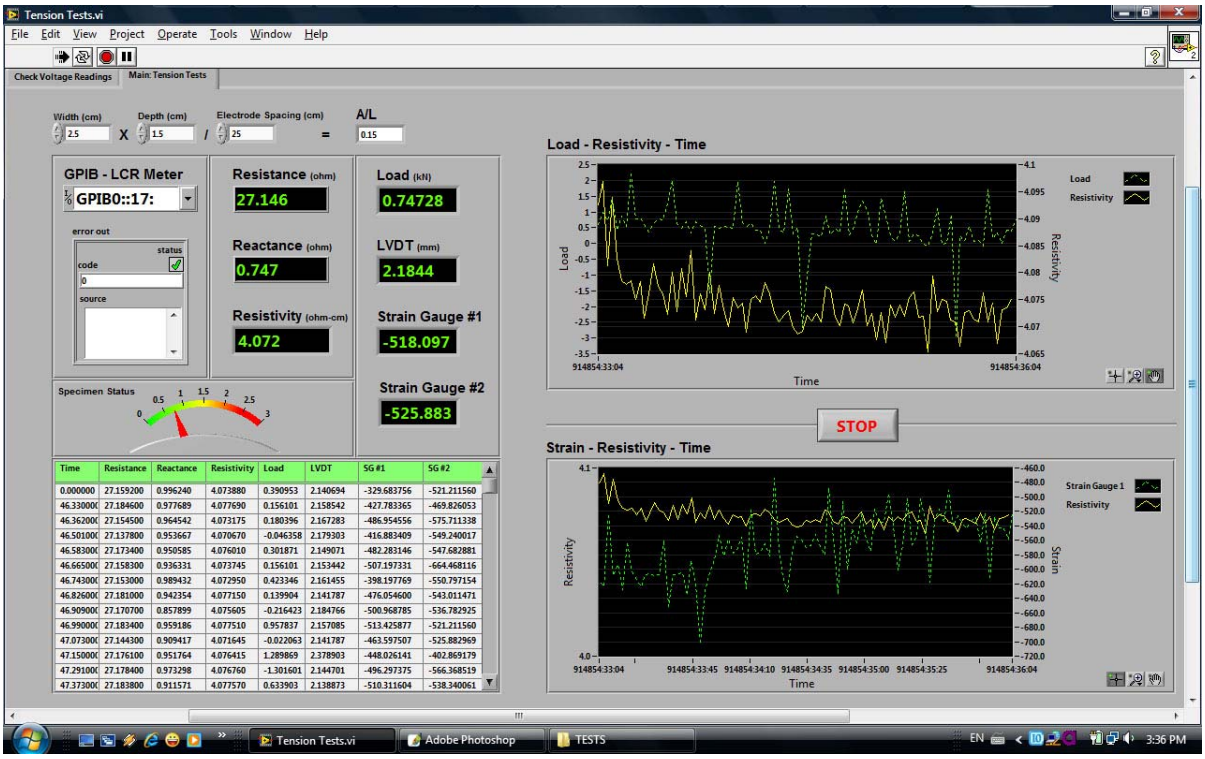


Figure 13- 2: LabVIEW interface for the tensile loading tests

# 13.3 Results and Discussion

In order to evaluate the sensing ability of cement-based sensors, the load and strain values were plotted against the fractional change in resistivity (FCR) as per Equation 12-1.

The results for the two types of specimens are plotted and discussed in the following sections.

## 13.3.1 Cement-based sensors with 15% CF

Some specimens were loaded until failure and the ultimate tensile load capacity was estimated at 2kN. As expected, the resistivity values for these specimens at first increased ever so slightly during the tensile loading, reaching FCR values of about 0.5 at the 2kN amplitude, but at the event of failure, the FCR values dramatically fluctuated in the range of ±30 (Figure 13-3). The load values

fluctuated throughout the test due to grip slippage and electrical noise (the loads were relatively small and this caused noise issues).

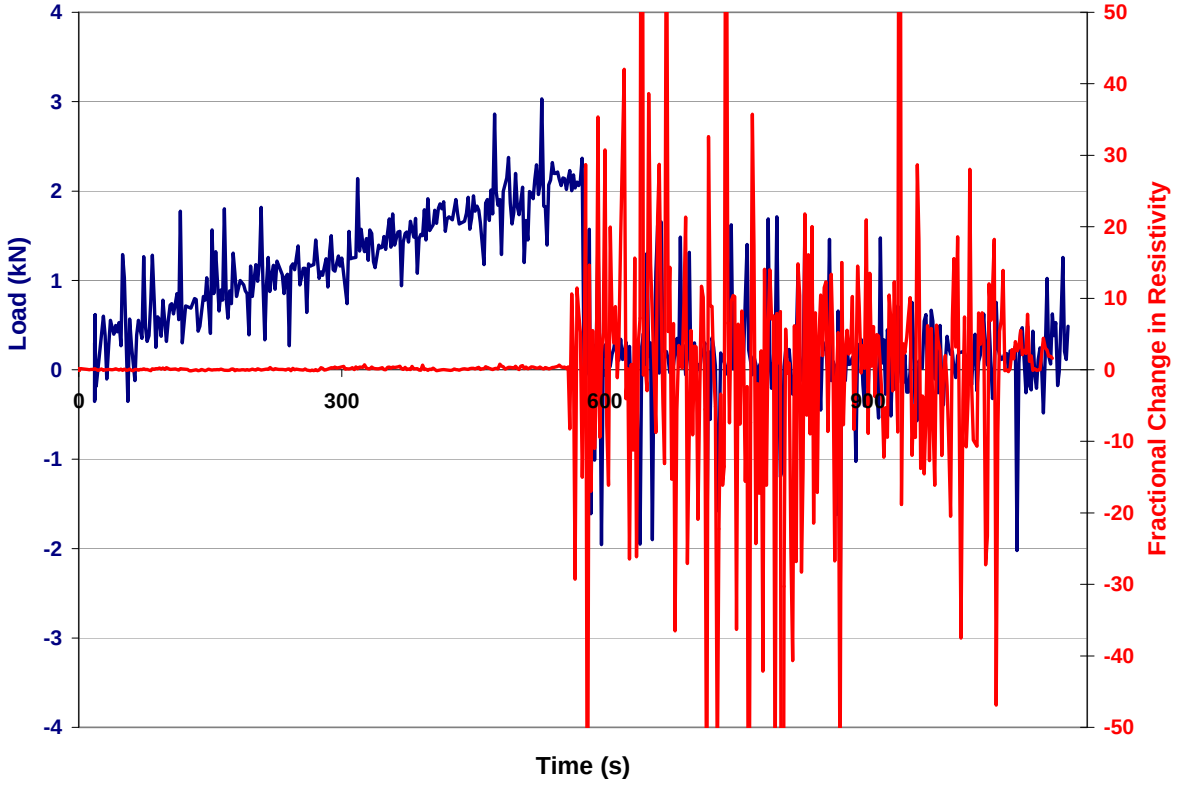


Figure 13- 3: Response of 15% CF cement-based sensors to failure at ultimate tensile load

Remaining specimens were then cyclically loaded to amplitude of 1kN, representing 50% of the ultimate tensile load. However, the mechanical grips were rather inefficient in perfectly gripping the specimens and therefore the load values fluctuated and the literal 0-1kN range of loading was not obtained.

Figure 13-4 displays the variation in load and FCR during the loading period. It is clearly observable that the electrical resistivity of these sensors varies distinctly in response to the cyclic tensile loading, following a similar pattern. Thus the piezoresistive quality of the sensors in tension is confirmed as well. The gauge factor was estimated at about 200 to 300 which is similar to the gauge factor obtained from the compressive tests.

During each loading cycle, the resistivity values increase with the increase in tensile load, resulting in positive FCR values (up to 20%), and then decrease to the initial value when the unloading branch of the cycle takes place.

The reason for the increase in resistivity is that when the specimen is subjected to tension, the conduction length between the electrodes increases respectively, potentially leading to less contact between the conductive fibres. Note that this only holds true while the sensor is in the elastic regime and the fibre volume fraction is more than a certain amount. According to Equation 2-3, resistivity should decrease with an increase in $\ell$ and decrease in A due to the elastic tension. Having higher volume fractions of fibre, this effect becomes less considerable and eventually negligible in comparison to the increase in electrical resistivity due to less fibre-to-fibre contact as a result of tensile loading.

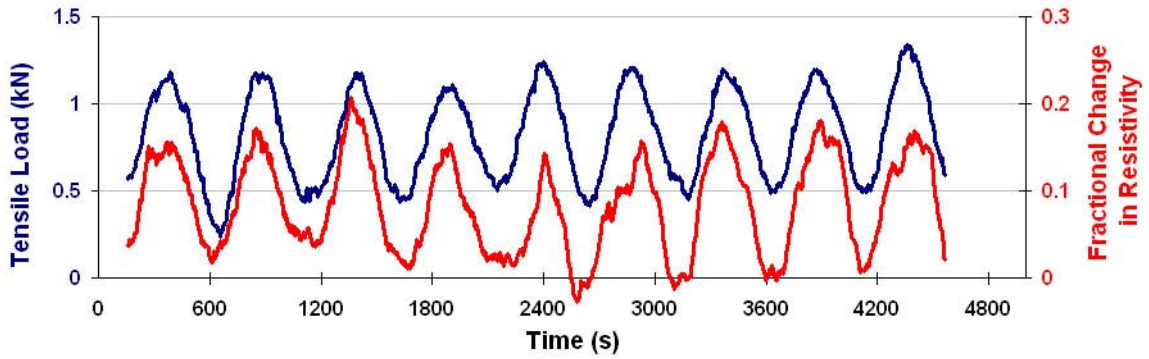


Figure 13- 4: FCR response of 15% CF sensors to tensile cyclic loading with 1kN amplitude

### 13.3.2 Cement-based sensors with 20% CF

Once again, the specimens were cyclically loaded to amplitude of 1kN. The results, shown in Figure 13-5, indicate that yet again there is a reversible relationship between changes in electrical resistivity of the sensors and the cyclic tensile loading.

The resistivity values increase very slightly with an increase in tensile load (FCR values reach 0.15%), and decrease when the unloading branch of the cycle takes place.

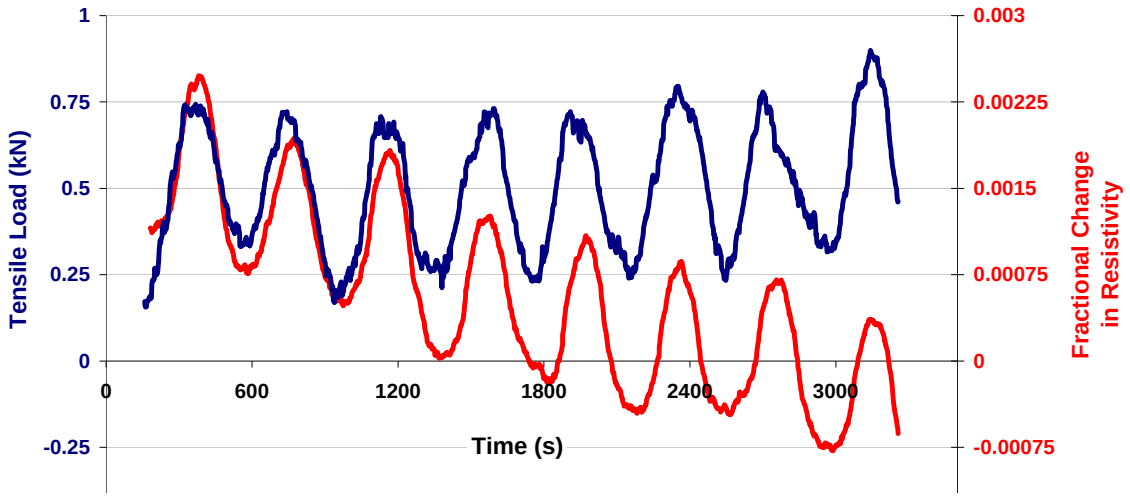


Figure 13- 5: FCR response of 20% CF sensors to tensile cyclic loading with 1kN amplitude

The hysteresis appears more pronounced in the FCR plots of the 20% CF sensors. However, the unloaded resistivity value decreased from 4.053 ohm-cm to 4.045 ohm-cm and this shift corresponds to a temperature increase of only 0.00023°C. Figure 13-6 displays the FCR response with the temperature correction applied (see Appendix B for the resistivity response). The amplitude of FCR, nevertheless, remained more or less constant (at 0.15%) throughout the test, analogous to the 1kN amplitude of the cyclic loading.

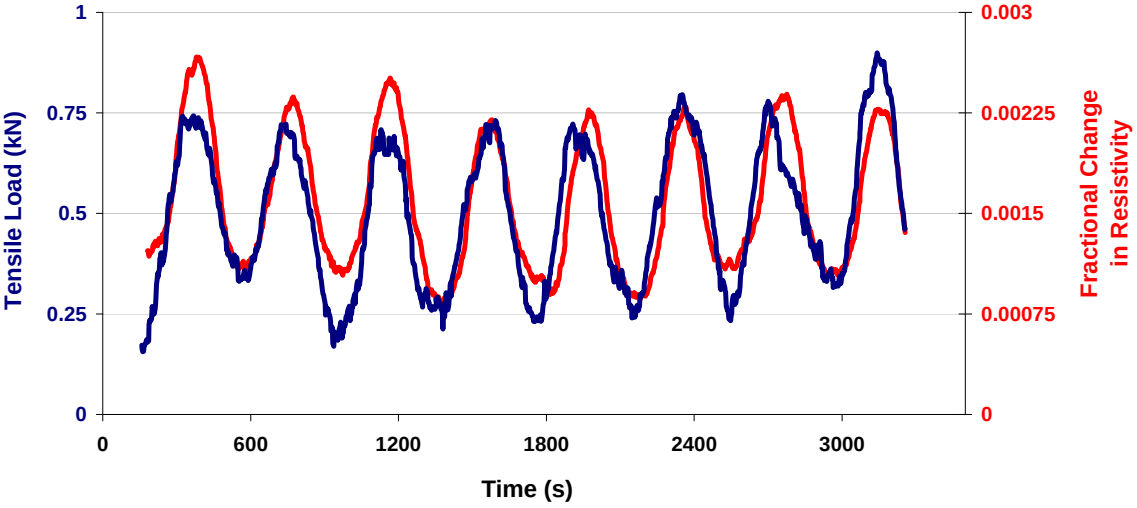


Figure 13- 6: FCR response of 20% CF sensors to tensile cyclic loading with 1kN amplitude after applying the temperature correction

10mm electrical strain gauges were also attached to either side of these samples to compare the results. The FCR and strain measurements are compared in Figure 13-7 (see Appendix B for the strain versus resistivity plot). It is clear that the FCR measurements demonstrate an excellent correlation with strain. The gauge factor for these 20% CF cement-based sensors is estimated at 20-25 (see Figure 13-8), which is still well above that of strain gauges (in the order of 2-3). Comparing the results from 20% CF and 15% CF sensors, implies that sensors with higher fibre content (more conductive) have smaller gauge factors.

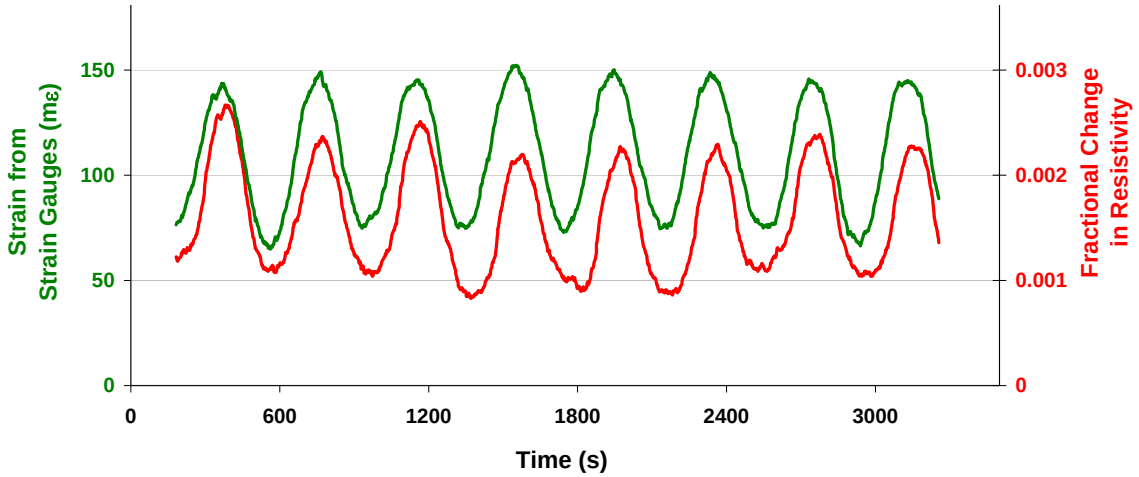


Figure 13- 7: Comparing the FCR response of 20% CF sensors to strain gauge measurements under tensile cyclic loading with 1kN amplitude

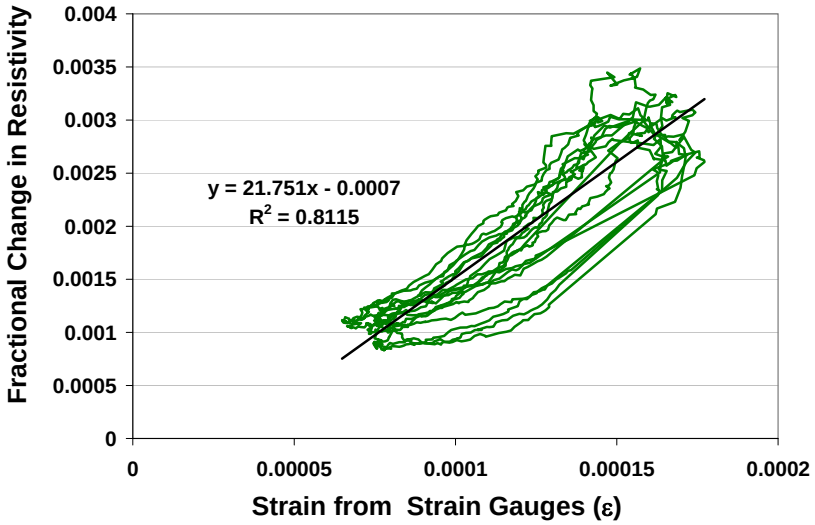


**Figure 13- 8:** Strain and FCR correlation of 20% CF sensors under cyclic tensile loading

An interesting observation was made when one of the 20% CF sensors was loaded in tension until failure. The resistivity values increased ever so slightly (from 4.035 ohm-cm to 4.055 ohm-cm) as the tensile load in creased from 0kN to just more than 1kN. Then as the load increased, the resistivity values suddenly jump to 8 ohm-cm, which may be a sign of the appearance of more micro-cracks and maybe some minor macro-cracks. The resistivity then continues to increase slightly to reach 9 ohm-cm at the ultimate load of approximately 1.5kN, at which point failure occurred and the resistivity values fluctuated drastically in the range of ±20000 ohm-cm, which is basically showing that the specimen has fractured in half. These trends are displayed in Figure 13-9-a.

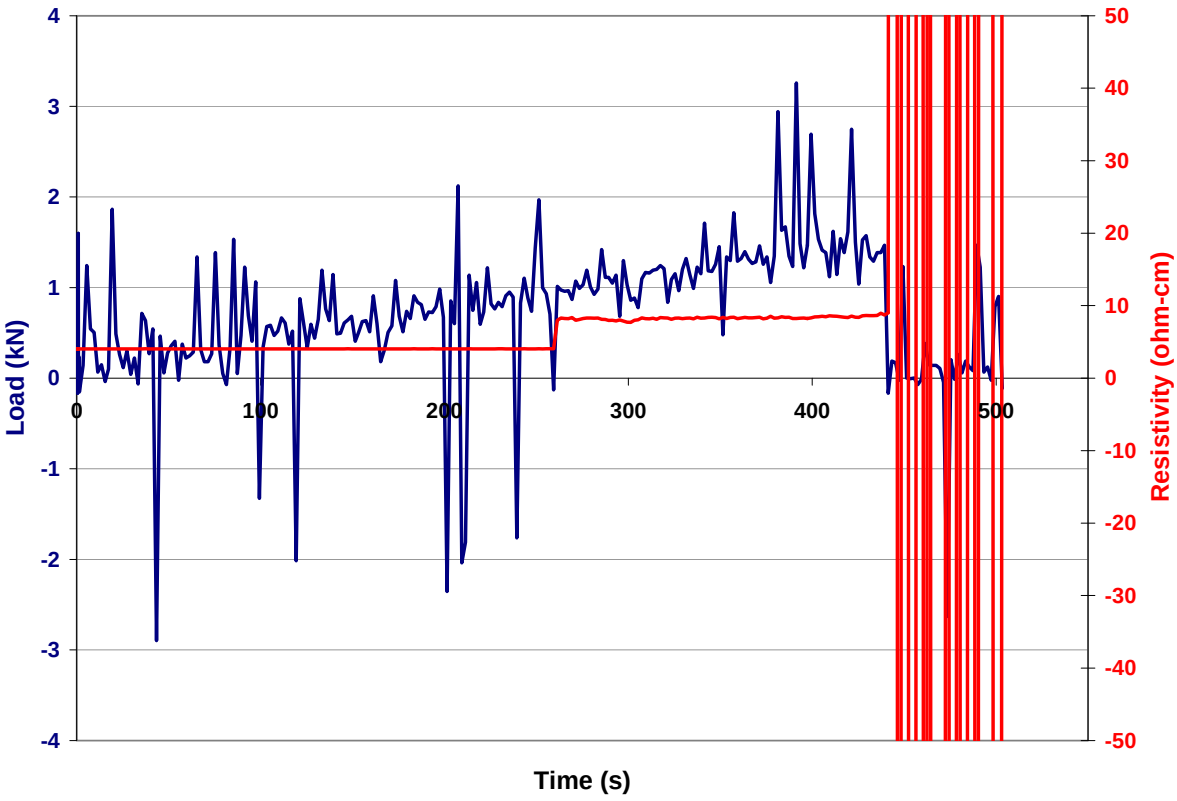


**(a)**

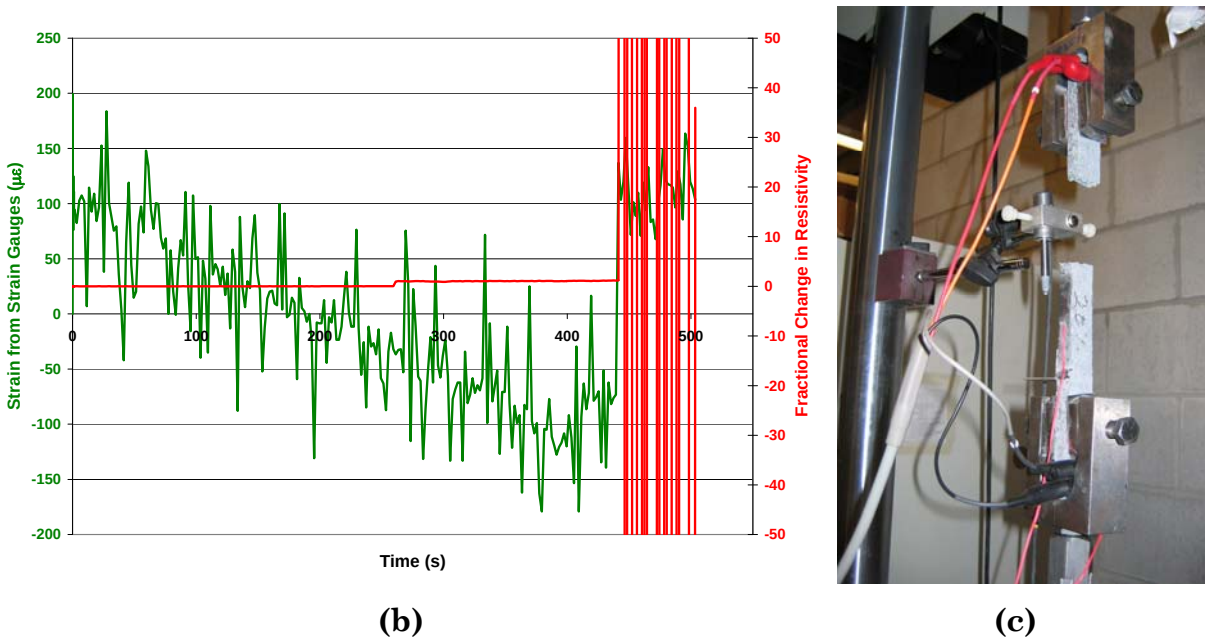


**(b)** **(c)**

Figure 13- 9: Response of 20% CF cement-based sensors to failure at ultimate tensile load: (a) resistivity and variation over time; (b) FCR and strain variation over time; (c) failed specimen.

Figure 13-9-b, illustrates the variation of FCR and strain measurements obtained from the strain gauges (fluctuations in load and strain data indicate gripping problems). Note that the strain values do not provide any indication of micro-crack abundance and the upcoming failure as the FCR jump does. It is only when the loads are very close to failure point that the strain values start to change direction. This may be due to the fact that failure did not occur at the mid-point of the specimen length, where the strain gauges where installed (Figure 13-9-c); therefore the strain gauges were not able to detect the strain at the location of failure. The cement-based sensor, on the other hand, provided more detailed information as to how the material was handling the tensile load.

# CHAPTER 14

# Flexural Loading

Two sets of experiments were conducted to examine the behaviour of cement-based sensors under flexural loading. The purpose of these tests was to attain a somewhat reasonable idea of how these sensors react to flexural loading. Instron FastTrack 8802 Servo-hydraulic Mechanical Testing System was the loading device used for these experiments.

## 14.1 Sensors under Direct Flexural Loading

As shown in Figure 14-1, 150mm x 15mm x 25mm specimens with 5% $V_f$ of petroleum pitch-based carbon fibres (PPCF) were set up such that they would act as a simply supported beam with a point load applied at the mid-span. The vertical displacement was measured by an LVDT located at the underside of the specimens. The resistivity measurements were made using the hand-made device from the preliminary experiments, thus the two-probe method was employed.

Load, displacement and resistance values were recorded using a laptop with DASY Lab 8.0. Figure 14-2 displays the variation of electrical resistivity with an increase in the vertical displacement.

As the applied point load and hence the displacement increased, there was initially a sharp decrease in the resistivity, then as the displacement values reached 0.3mm, the resistivity reduction became slower and eventually stopped decreasing at 0.35mm of vertical displacement. Beyond this point the resistivity values started to gradually increase with an increase in load and displacement until the specimen failed. The three stages of the sensors' behaviour are denoted in Figure 14-2.

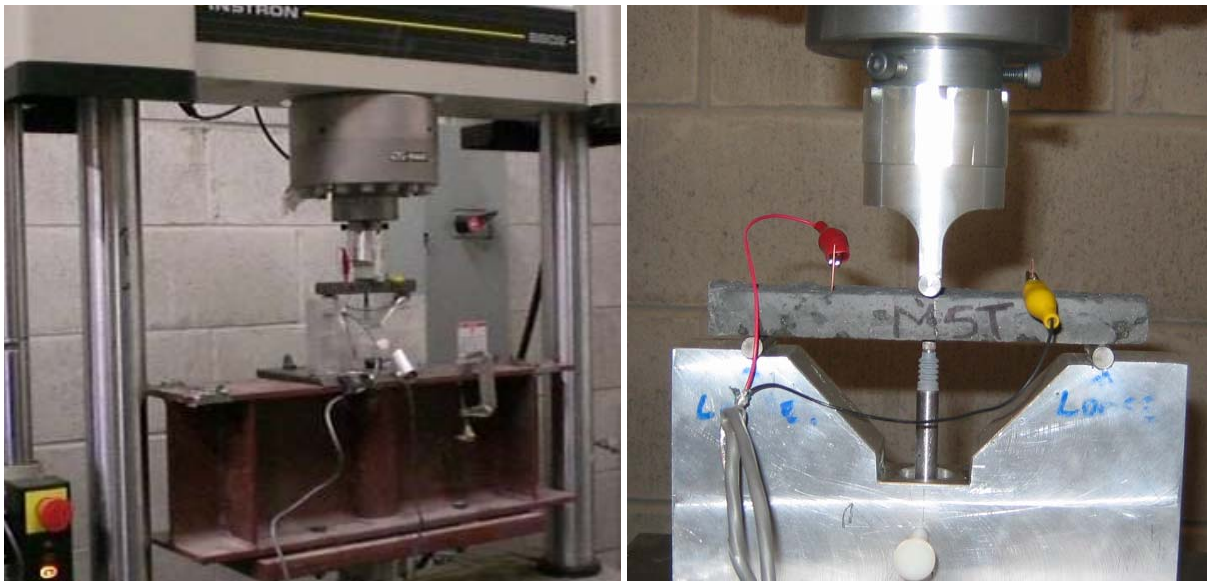

(a) (b)

Figure 14- 1: 5% PPCF cement-based sensors under direct flexure: (a) Test setup; (b) Specimen setup

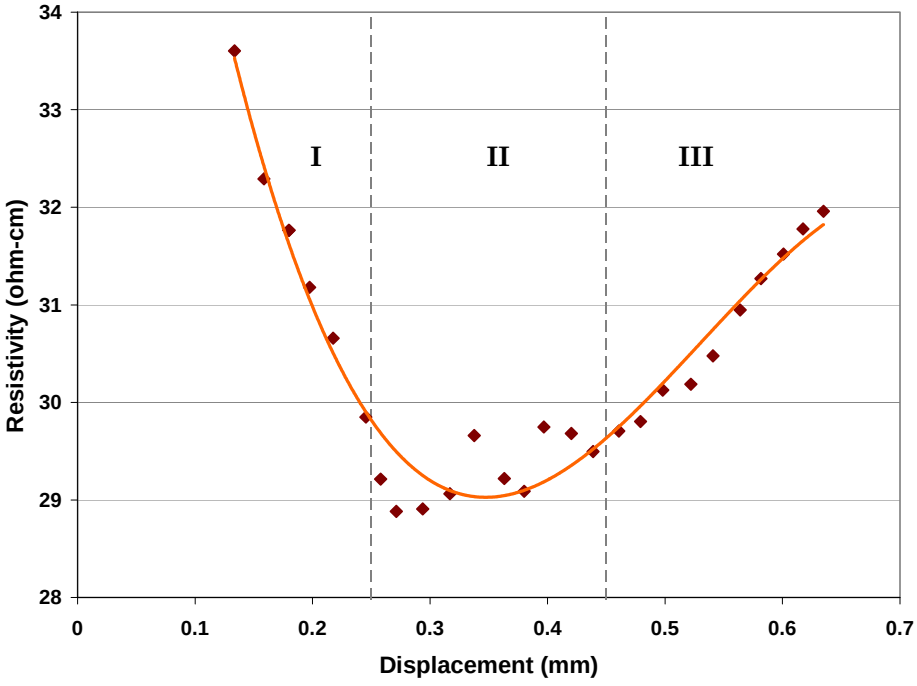


Figure 14- 2: Response of 5% PPCF cement-based sensor to vertical displacement under flexure

The theoretical explanation for this response is as follows:

When the specimen is subjected to flexure, the upper half of the specimen's cross section is compressed and the lower half undergoes tension.

- In the first stage of the test, as the flexural load increases, the fibres in the upper half of the specimen become closer to each other, creating a denser network of fibre, while in the lower half, the fibres become more apart. However, the decrease in electrical resistivity caused by the amplified fibre to fibre connectivity on the top part of the specimen, overpowers the increase in resistivity due to the tension in the bottom half. Therefore as long as the micro-cracks in the specimen were minimal, the resistivity values decreased with flexural load.

- In stage II, the micro-cracks in the bottom of the specimen became more substantial due to tension. In this phase the decrease in resistivity took place at a lower rate until it reached a point where the increase in resistivity at the tensioned half started to control the overall resistivity, increasing it gradually.

- Once the micro-cracks propagated and macro-cracks began to appear, the specimen went through phase III where resistivity values increased at a higher rate. The test was stopped when a major crack occurred at the mid-span (see Figure 14-3).

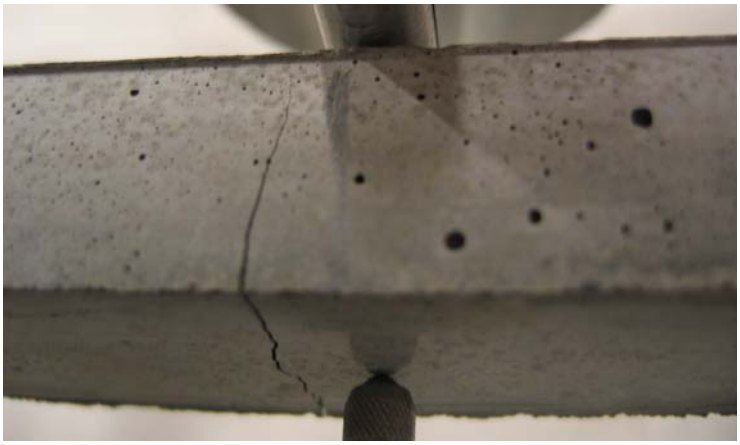

Figure 14- 3: failure of PPCF cement-based sensor under direct flexure

## 14.2 Sensors Embedded in a Beam under Flexure

A 5mm x 5mm x 50mm cement-based sensor with 15% carbon fibre (Figure 14-4-a) was embedded on the underside of a 100mm x 100mm x 350mm beam exactly

at the middle (Figure 14-4-b). The beam was then cyclically loaded in flexure using the four point setup. The load and LVDT data as well as the impedance parameters measured by the LCR meter, were recorded. Figure 14-5 displays the experimental and specimen setup.


**(a)** **(b)**

Figure 14- 4: (a) 15% $V_f$ CFRC sensor embedded on the surface of a (b) flexural beam

**(a)** **(b)**

Figure 14- 5: 15% CFRC sensor attached to a beam under cyclic flexural loading: (a) Test setup; (b) Specimen setup

The amplitude of the cyclic loading was 10kN. Figure 14-6 shows the variation of load and FCR with time. Since with flexural loading, the bottom surface of the beam undergoes tension, the FCR values were expected to be positive. But, even though the FCR trend follows the loading pattern, the response of the sensor corresponds to compression. The explanation for this behaviour may be the fact

that the bond between the sensor and the beam was not adequate. Figure 14-7 displays the cracks in the beam at failure. As mentioned before the purpose of these tests was only to attain a rather reasonable idea of how these sensors response to flexural loading; a more accurate testing procedure along with more efficient attachment of sensors is required to completely understand the behaviour of cement-based sensors under flexural loading.

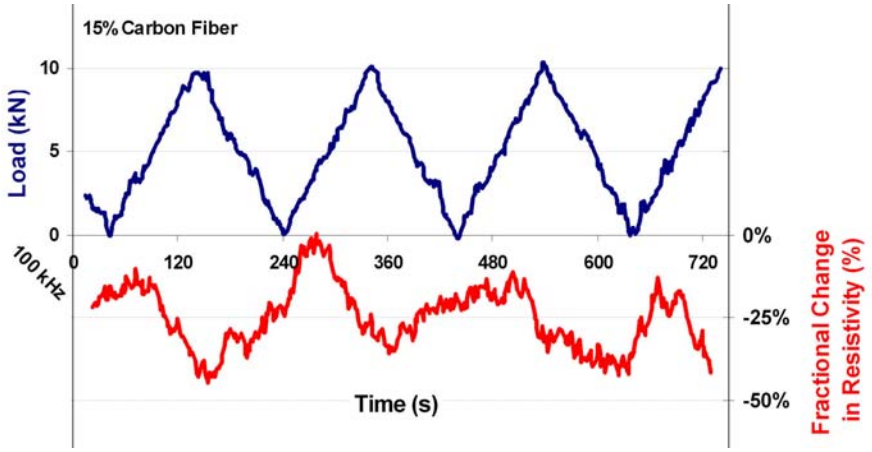


Figure 14- 6: Response of a surface mounted CFRC sensor to cyclic flexure with 10kN amplitude

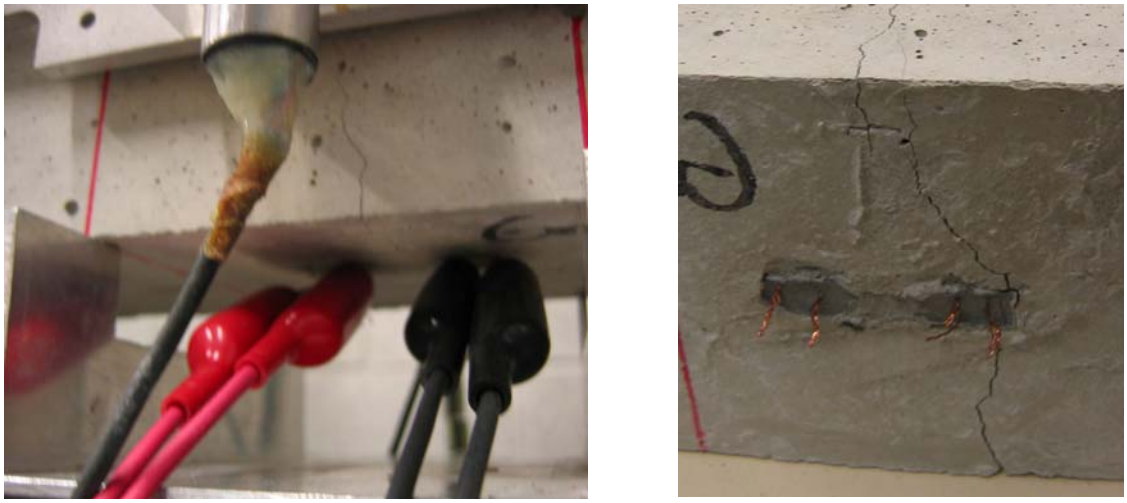

**(a)** **(b)**

**Figure 14- 7:** 15% CFRC sensor attached to a beam under monotonic flexural loading: (a) cracking in the failed beam; (b) the route of the flexural crack at the sensor location

# CHAPTER 15

# Concluding Remarks

The purpose of this study was to develop piezoresistive cement-based sensors capable of sensing stress/strain, temperature and chloride ingression. The possibility of implementing these sensors in structural health monitoring systems as a replacement for conventional strain gauges was investigated.

These cement-based sensors were developed by incorporating two types of carbon fibres, as well as both single-walled and multi-walled carbon nano-tubes in a cement paste matrix. A wide range of experiments were conducted to pinpoint the most efficient fibre content, frequency, electrode type and testing procedure. Next, the response of the sensors to curing time, temperature, moisture and chloride as well as compressive, tensile and flexural loading was explored through monitoring their electrical resistivity.

The following conclusions were obtained from this research:

- Resistivity values of samples with even just 0.5% $V_f$ of carbon fibre dropped considerably (97%) compared to plain samples, which indicates a primary percolation threshold of less than 0.5% $V_f$. The resistivity of the specimens further decreased with the addition of more fibres until a secondary percolation threshold was reached at 5% $V_f$. The electrical conduction in these samples is through the cement paste and the conductive carbon fibres in series. The resistivity values could yet be significantly decreased by adding more fibre to the mix; samples with 20% $V_f$ of CPCF exhibited electrical resistivity values as low as 5 ohm-cm. This is because the electrical conduction in these specimens takes place essentially via a continuous network of carbon fibres. The addition of carbon nanotubes and

creating hybrid samples, also further decreased the electrical resistivity. However, the addition of very high amounts of fibre and CNT reduces the workability of the cementitious composite to a great extent. Specimens with 5% PPCF, 15% CPCF, 15% CPCF + 1%MWCNT and 20% CPCF were selected for the main experiments.

- The cement-based composites were mainly found to be capacitive rather than inductive. Theoretical reasoning along with frequency variation experiments, led to employing the highest current frequency available on the LCR meter, 100 kHz, to be used as the applied current frequency in all of the experiments.

- After comparing different electrode materials, copper mesh was, for the most part, preferred as electrode material for the cement-based sensors. For the cylindrical compression test specimens, though, copper wire and silver paste were the only fitting electrode materials.

- It was also concluded that the two-probe configuration produces very high contact resistance and hence is not suitable for resistivity measurements of cement-based sensors. The four-probe technique was used for the main sets of experiments.

- The electrical resistivity of all the cement-based sensor samples increased with curing time, but, became almost constant after a certain amount of time, depending on the fibre content. This increase is more pronounced in samples with lower amounts of fibre and occurs in consequence of the overall transformation in the microstructure of the specimens during the hydration period. A slight increase in resistivity was also noticed as a result of autoclaving or the addition of methylcellulose and defoamer.

- Temperature was found to have a considerable influence on the electrical resistivity of these sensors. The resistivity values decreased with increasing temperature and increased with the decrease in temperature at a rate of about 22-35 ohm-cm/°C. This rate may be considered as a correction factors in the case of temperature variation during sensing using CFRC sensors.

- Moisture and chloride also influence the resistivity values obtained from CFRC sensors which may affect the accuracy of their stress/strain sensing ability. Thus it is important to take this effect into consideration if and where the sensors are employed in environments subjected to moisture and chloride by installing a sensor merely to detect the effect of moisture and chloride or by coating the sensors with moisture resistant material.

- The piezoresistive quality of the cement-based sensors was confirmed from the results of several monotonic and cyclic compressive and tensile loading experiments; the electrical resistivity of these sensors changed in response to applied mechanical stress.

- Under monotonic compressive loading, the resistivity values of the sensors decreased with the increase in compressive load but as the load reached values close to the ultimate load, the sensor material became inelastic due to the abundance of micro-cracks causing a slight increase in resistivity. As the load exceeded the ultimate load capacity and macro-cracks started to appear, the increase in resistivity became considerable and eventually there was a drastic jump in electrical resistivity, indicating failure.

- Upon cyclic compressive loading, the resistivity values decreased with the increase in compressive load, resulting in negative FCR values, and then increased to the initial value when the unloading branch of each cycle took place. The higher the load, the larger the fractional change in resistivity. The reason for the decrease in resistivity is that when the specimen is compressed, the conduction length between the electrodes decreases, potentially leading to more contact among the conductive fibres. As long as the loading amplitude was such that the sensor material remained in the elastic range, the initial resistivity was regained when the sensor was decompressed.

- The stress/resistivity correlation for the sensors revealed excellent stress sensitivity. The relationships between strain and FCR values obtained from the

cyclic compressive loading tests led to gauge factors estimated at about 300 for the cement-based sensors, which is around 100 times that of conventional strain gauges. The hybrid sensors with 15% CF + 1% MWCNT exhibited an even better stress/strain sensitivity than the sensors with 15% CF alone.

- When subjected to monotonic tensile loading, the resistivity values of the cement-based sensors at first increased slightly, but at the event of failure, the FCR values fluctuated dramatically. Comparing the resistivity variation in the 20% CF sensor with the strain obtained from electrical strain gauges attached to its sides, indicated that the cement-based sensors are potentially more effective in provide an early prediction of an upcoming failure.

- Upon cyclic tensile loading, the resistivity values increased with an increase in tensile stress, resulting in positive FCR values, and then decreased to the initial value when the unloading branch of each cycle took place. The reason for the increase in resistivity is that the tensile strain in the specimen, potentially leads less contact among the conductive fibres. As long as the sensor material remained in the elastic range and the micro-cracking was insignificant, this increase in resistivity was reversible and the sensor regained its initial resistivity when the tension was removed. For the 20% CF sensors, a temperature correction had to be made because the effect of temperature increase in the material was of the same order of magnitude as the fractional change in resistivity in response to the cyclic loading.

- The FCR and strain measurements from the cyclic tensile tests were compared against each other; the FCR measurements demonstrated an excellent correlation with strain. The gauge factor for the 20% CF cement-based sensors was estimated at 20-25 which is well above that of conventional strain gauges.

- Comparing the results from 20% CF and 15% CF sensors, implies that sensors with higher fibre content (more conductive) have smaller gauge factors.

- Upon direct flexural loading, the resistivity of the cement-based sensors went through three stages. First as the applied flexural load increased, the decrease in resistivity due to compression in the upper half of the sensor led to an overall decrease in resistivity. Then when the tension in the bottom half of the sensor caused considerable micro-cracking, the rate of resistivity reduction decreased and then resistivity gradually increased when the micro-cracking became more substantial. Beyond this point the resistivity values started to increase at a higher rate with the increase in load and the appearance of macroscopic cracks until the specimen failed with a single large crack propagating from the bottom of the specimen.

- A small-sized cement-based sensor was near-surface mounted (NSM) on the bottom side of a flexural test beam. The FCR variation of this sensor during the cyclic flexural loading of the beam indicated that the sensor was subjected to compression rather than tension, probably due to insufficient bonding. Nevertheless, the response of the sensor was relatively compatible with the loading cycles. It is suggested that with proper embedding procedure and adequate bonding, these cement-based sensors could be effectively used to sense stress/strain and cracking of a structure under flexural loading.

Overall, the results from this study have shown that that electrical resistivity of the developed cement-based sensors increases reversibly upon tension and decreases reversibly under compression provided that substantial cracking does not occur and the sensor remains in the elastic range. Once a dense field of micro-cracking followed by macro-cracking occurs, these sensors respond distinctly, possibly even prior to the appearance of visible cracks.

These sensors, also known as smart (self-monitoring) structural materials can be used in structures to provide both structural capability and response to applied stress/strain and damage. They can be the future alternative for conventional sensors for monitoring stress/strain and detecting cracks in concrete structures.

# CHAPTER 16

# Suggestions for Future Research

Implementing Structural Health Monitoring (SHM) has recently become a significant consideration in the construction and maintenance of civil engineering structures. Recently developed cement-based sensors may become a prospective alternative to conventional stress/strain sensors on account of their numerous advantages, including:

- Low cost;
- Simplicity in installation and implementation;
- Structural properties;
- Superior durability;
- Excellent sensitivity

Having conducted various experiments to study the sensing ability of cement-based sensors, the necessity for further research on this issue became abundantly clear. Recommendations for future work are as follow:

- Consistency in resistivity values of cement-based sensors with the same composition and exposure conditions is a must is these sensors are to be used in practice. Therefore effort should be made in developing a fabrication procedure enabling uniform fibre dispersion and stable bond between the electrodes and the composite, hence producing sensors with identical properties.

- Further exploration is required to come up with specific guidelines for parameters such as W/C ratio, volume fraction of carbon fibre and/or CNT for creating the most effective sensor. The sensor size, strength and elastic modulus are also factors that need to be taken into consideration allowing for different applications. The experimental results from this study suggest that reducing the

thickness of the sensor may contribute to an improved sensitivity. High strength enables the sensor to remain sound at extreme loading condition. However, a low elastic modulus is preferred so that the fractional change in resistivity is more prominent in response to strain.

- Developing an accurate calibration model that can assess the sensitivity, accuracy, linearity and repeatability of the data obtained from the cement-based sensors. This model must be able to interpret the FCR signals and convert them into strain values. Detecting and quantifying cracks and damage should also be integrated into the interpretation process.

- In order to filter out environmental conditions from the strain data, precise temperature, moisture and chloride presence corrections are required. Differentiating between the sources of the signals is a challenge.

- Cement-based sensors also have the potential to be used as multi-purpose sensors, with the ability to detect both stress/strain and environmental conditions such as temperature variation and chloride content. This requires very accurate calibration procedures.

- Another issue that need to be taken into consideration is the presence of steel rebar in the vicinity of these sensors and their effect on the acquired resistivity data. Simple laboratory experiments would be very helpful in investigating this matter.

- Different embedding and near surface mounting methods need to be explored to determine the most efficient technique of attaching these sensors to the host structure. Bonding properties should especially be examined.

- In order to actually prove the efficacy of the cement-based sensors, they ought to be tested on a real full-scale structure. Once the practicality of using these sensors in real life is verified, feasibility studies should commence, possibly

leading to an ingenious SHM system. Figure 16-1 schematically shows the prospect of testing cement-based sensors on a bridge deck.

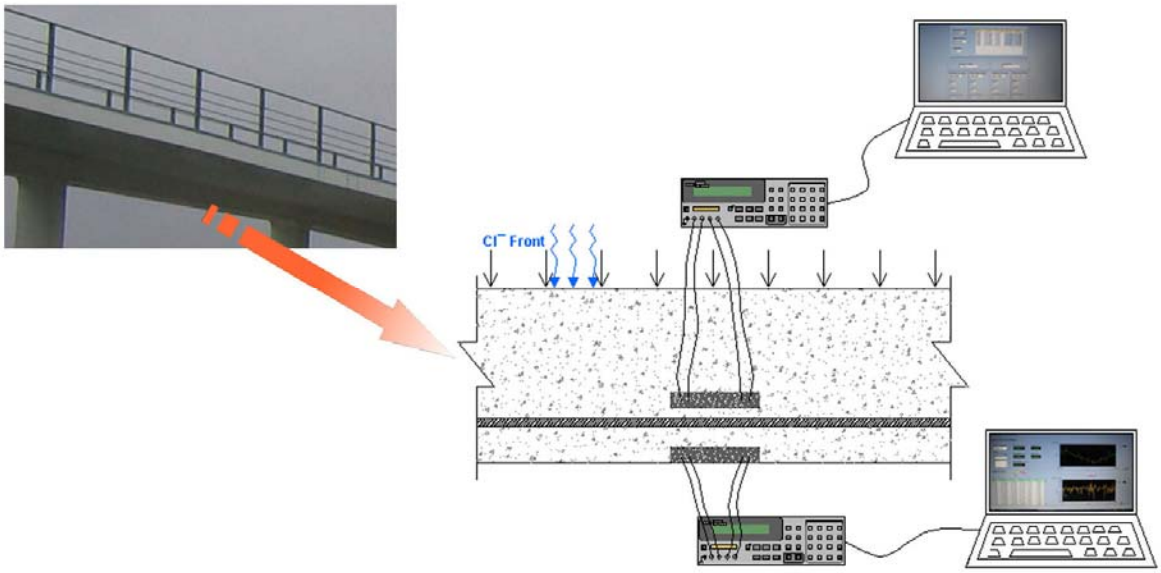


Figure 16- 1: A schematic display of testing cement-based sensors on a bridge deck

- Developing a wireless communication system would be the ultimate step in integrating cement-based sensors into a real-time structural health monitoring system.

# Bibliography

Ahwahnee Technology. (2007). "Image Gallery: Computer model of Multi-walled CNT generated from Nanotube Modeler." http://www.ahwahneetech.com.

Banthia, N., Djeridane, S., and Pigeon, M. (1992). "Electrical resistivity of carbon and steel micro-fiber reinforced cements." *Cem.Concr.Res.,* 22(5), 804-814.

Banthia, N., Nandakumar, N., and Boyd, A. J. (2002). "Sprayed fiber reinforced polymers for repair and strengthening." *International SAMPE Symposium and Exhibition (Proceedings)*, Long Beach, CA, United States , 964-977

Chacko, R. M., Banthia, N., and Mufti, A. A. (2007). "Carbon-fiber-reinforced cement-based sensors." *Canadian Journal of Civil Engineering,* 34(3), 284-290.

Chen, P., and Chung, D. D. L. (1996). "Concrete as a new strain/stress sensor." *Compos.Part B:Eng.,* 27(1), 11-23.

Chen, P., and Chung, D. D. L. (1993). "Carbon fiber reinforced concrete as an electrical contact material for smart structures." *Part 2 (of 2),* SAMPE, Covina, CA, USA, Anaheim, CA, USA, 2067-2076.

Chen, P., and D.D.L, C.,. (1993). "Carbon fiber reinforced concrete for smart structures capable of non-destructive flaw detection." *Smart Mater Struct,* 2(1), 22-30.

Chiarello, M., and Zinno, R. (2005). "Electrical conductivity of self-monitoring CFRC." *Cement and Concrete Composites,* 27(4), 463-469.

Dragos-Marian, B., D.D.L, C., and G.C, L.,. (2000). "Damage in carbon fiber-reinforced concrete, monitored by electrical resistance measurement." *Cem.Concr.Res.,* 30(4), 651-659.

Farhad, R., B, B., Gordon, A, Y., Jerry, and S, L., Jong. (2001). "Volume electrical resistivity of carbon fiber cement composites." *ACI Mater.J.,* 98(1), 25-35.

Gengying, L., and Peiming, W. (2005). "Microstructure and mechanical properties of carbon nanotubes-cement matrix composites." *Journal of the Chinese Ceramic Society,* 33(1), 105-8.

Gjørv, O.E., Vennesland, Ø , and El-Busiady, A.H.S., "Electrical Resistivity of Concrete in the Oceans," Proceedings – 9th Annual Offshore Technology Conference, Houston, Texas, pages 581 to 588, May 2-5, 1977.

Han, B., Guan, X., and Ou, J. (2007). "Electrode design, measuring method and data acquisition system of carbon fiber cement paste piezoresistive sensors." *Sens Actuators A Phys,* 135(2), 360-369.

Han, B., and Ou, J. (2007). "Embedded piezoresistive cement-based stress/strain sensor." *Sens Actuators A Phys,* 138(2), 294-298.

Hou, T., and Lynch, J. P. (2005). "Monitoring Strain in Engineered Cementitious Composites Using Wireless Sensors." *Proceedings of the International Conference on Fracture (ICF XI),* .

Iijima, S. (1991). "Helical microtubules of graphitic carbon." *Nature,* 354(6348), 56-8.

Klowak, C., Rivera, E., and Mufti, A. (2005). "Implementation of civionics in a second generation steel-free bridge deck." *Proceedings- SPIE The International Society For Optical Engineering,* 5767 195.

Li, . (2001). "Cement matrix 2-2 piezoelectric composite—Part 1. Sensory effect." *Materials and Structures,* 34(8), 506.

Li, Z., and Yang, X. (2005). "Cement-based piezoelectric sensing system for structural health monitoring." *Proceedings of ConMat'05 and Mindess Symposium,* The University of British Columbia, .

Li, G. Y., Wang, P. M., and Zhao, X. (2007). "Pressure-sensitive properties and microstructure of carbon nanotube reinforced cement composites." *Cement and Concrete Composites,* 29(5), 377-382.

Li, Z., Yang, X., and Li, Z. (2006). "Application of cement-based Piezoelectric sensors for monitoring traffic flows." *J.Transp.Eng.,* 132(7), 565-573.

Li, Z., and Dong, B. (2003). "0-3 cement-based piezoelectric composites." *Smart Nondestructive Evaluation and Health Monitoring of Structural and Biological Systems II,* SPIE-Int. Soc. Opt. Eng, San Diego, CA, USA, 219-30.

Loh, K. J., Lynch, J. P., and Kotov, N. A. (2006). "Nanoengineered Inductively Coupled Carbon Nanotube Wireless Strain Sensor." *4th World Conference on Structural Control and Monitoring.*

Loh, K. J., Lynch, J. P., and Kotov, N. A. (2005). "Conformable Single-Walled Carbon Nanotube Thin Film Strain Sensors for Structural Monitoring. "*Proceedings of the 5th International Workshop on Structural Health Monitoring.*

Lynch, . (2006). "A Summary Review of Wireless Sensors and Sensor Networks for Structural Health Monitoring." *The Shock and Vibration Digest,* 38(2), 91.

Lynch, J. P., Law, K. H., Kiremidjian, A. S., Carryer, E., Farrar, C. R., Sohn, H., Allen, D. W., Nadler, B., and Wait, J. R. (2004). "Design and performance validation of a wireless sensing unit for structural monitoring applications." *Struct. Eng. Mech.,* 17(3-4), 393-408.

Makar, J. M., and Beaudoin, J. J. (2003). "Carbon Nanotubes and their application in the construction industry. "*Proceedings of 1st International Symposium on Nanotechnology in Construction, .*

Makar, J., Margeson, J., and Luh, J. (2005). "Carbon nanotube/cement composites – early results and potential applications." *Proceedings of 3rd International Conference on Construction Materials: Performance, Innovations and Structural Implications, .*

McCarter, W. J., Starrs, G., Chrisp, T. M., and Banfill, P. F. G. (2007). "Activation energy and conduction in carbon fibre reinforced cement matrices." *J.Mater.Sci.,* 42(6), 2200-3.

Mo, L. T., Wu, S. P., Liu, X. M., and Shui, Z. H. (2005). "Study on the piezoresistivity character of electrically conductive asphalt concrete." *Proceedings of ConMat'05 and Mindess Symposium,* The University of British Columbia.

Monfore, G.E. “The Electrical Resistivity of Concrete,” *Journal of the PCA Research andDevelopment Laboratories,* Vol. 10, No. 2, pages 35 to 48, May 1968.

Mufti, A. A. (2001). "Guidelines for Structural Health Monitoring." *Design Manual no.2.*

Mufti, A. A., Bakht, B., Tadros, G., Horosko, A. T., and Sparks, G. (2007). "Civionics - A new paradigm in design, evaluation, and risk analysis of civil structures." *J Intell Mater Syst Struct,* 18(8), 757-763.

Ou, J. (2006). "Research and practice of intelligent sensing technologies in civil structural health monitoring in the mainland of China." *Nondestructive Evaluation and Health Monitoring of Aerospace Materials, Composites, and Civil Infrastructure V,* International Society for Optical Engineering, Bellingham WA, WA 98227-0010, United States, San Diego, CA, United States, 61761.

Park, . (2000). "Impedance-Based Health Monitoring of Civil Structural Components." *Journal of Infrastructure Systems,* 6(4), 153.

Reza, F., Yamamuro, J. A., Batson, G. B., and Lee, J. S. (2003a). "Smart behaviour of carbon fiber cement composites in compact tension." *16th ASCE Engineering Mechanics Conference.*

Reza, F., Batson, G. B., Yamamuro, J. A., and Lee, J. S. (2003b). "Resistance changes during compression of carbon fiber cement composites." *J.Mater.Civ.Eng.,* 15(5), 476-483.

Rivera, E., and Mufti, A. A. (2004). "Civionic Specifications." *Design Manual no.6.*

Rivera, E., Mufti, A. A., and Thomson, D. J. (2007). "Civionics for structural health monitoring." *Canadian Journal of Civil Engineering,* 34(3), 430-437.

Robbins, A., and Miller, W. C. (2003). *Circuit Analysis: Theory and Practice.* Thomson Delmar Learning.

Robinson, N., and Saafi, M. (2006). "Nanotechnology and MEMS-based systems for civil infrastructure safety and security: Opportunities and challenges." *Smart Structures and Materials 2006 - Sensors and Smart Structures Technologies for Civil, Mechanical, and Aerospace Systems,* International Society for Optical

Engineering, Bellingham WA, WA 98227-0010, United States, San Diego, CA, United States, 61742.

ScienceProg. (2006). "Characteristics of sensors and transducers." http://www.scienceprog.com.

Senturia, S. D. (2001). *Microsystem Design.* Kluwer Academic Publishers, Boston.

Shen, B., Yang, X., and Li, Z. (2006). "A cement-based piezoelectric sensor for civil engineering structure." *Materials and Structures/Materiaux Et Constructions,* 39(285), 37-42.

Shi, C. (2004). "Effect of mixing proportions of concrete on its electrical conductivity and the rapid chloride permeability test (ASTM C1202 or ASSHTO T277) results." *Cem.Concr.Res.,* 34(3), 537-545.

Shifeng, H., Dongyu, X., Jun, C., Ronghua, X., Llngchao, L., and Xin, C. (2007). "Smart properties of carbon fiber reinforced cement-based composites." *J.Composite Mater.,* 41(1), 125-31.

Tsung-Chin Hou, and Lynch, J. P. (2005). "Conductivity-based strain monitoring and damage characterization of fiber reinforced cementitious structural components." *Smart Structures and Materials 2005: Sensors and Smart Structures Technologies for Civil, Mechanical, and Aerospace Systems,* SPIE-Int. Soc. Opt. Eng, San Diego, CA, USA, 419-29.

Wang, C. S., Wu, F., and Chang, F. -. (2001). "Structural health monitoring from fiber-reinforced composites to steel-reinforced concrete." *Smart Mater Struct,* 10(3), 548-552.

Wang, Y., Swartz, R. A., Lynch, J. P., Law, K. H., and Loh, C. (2007). "Performance evaluation of decentralized wireless sensing and control in civil structures." *Nondestructive Characterization for Composite Materials, Aerospace Engineering, Civil Infrastructure, and Homeland Security 2007,* SPIE, Bellingham WA, WA 98227-0010, United States, San Diego, CA, United States, 653113.

Wansom, S., Kidner, N. J., Woo, L. Y., and Mason, T. O. (2006). "AC-impedance response of multi-walled carbon nanotube/cement composites." *Cement and Concrete Composites,* 28(6), 509-519.

Wen, . (2006). "The role of electronic and ionic conduction in the electrical conductivity of carbon fiber reinforced cement." *Carbon,* 44(11), 2130.

Wen, S., and Chung, D. D. L. (2007). "Piezoresistivity-based strain sensing in carbon fiber-reinforced cement." *ACI Mater.J.,* 104(2), 171-179.

Wen, S., and Chung, D. D. L. (2006). "Model of piezoresistivity in carbon fiber cement." *Cem.Concr.Res.,* 36(10), 1879-1885.

Wen, S., and Chung, D. D. L. (2005). "Self-sensing characteristics of carbon fiber cement." *Proceedings of ConMat'05 and Mindess Symposium,* The University of British Columbia, .

Wen, S., and Chung, D. D. L. (2001). "Electric polarization in carbon fiber-reinforced cement." *Cem.Concr.Res.,* 31(2), 141-147.

Whiting, D. A., and Nagi, M. A. (2003). "Electrical Resistivity of Concrete – A Literature Review." *Rep. No. Report Serial No. 2457,* Portland Cement Association (PCA).

Xie, P., Gu, P., and Beaudoin, J. J. (1996). "Electrical percolation phenomena in cement composites containing conductive fibres." *J.Mater.Sci.,* 31(15), 4093-7.

Yakovlev, G., Keriene, J., Gailius, A., and Girniene, I. (2006). "Cement based foam concrete reinforced by carbon nanotubes." *Materials Science,* 12(2), 147-51.

Zallen, R. (1983), "Physics of Amorphous Solids", Wiley, New York, 135-204.

Zeng-Qiang, S., and D.D.L, C.,. (1999). "Carbon fiber-reinforced concrete for traffic monitoring and weighing in motion." *Cem.Concr.Res.,* 29(3), 435-439.

Zhang, D., Li, Z., and Wu, K. (2002). "2-2 Piezoelectric cement matrix composite: Part II. Actuator effect." *Cem.Concr.Res.,* 32(5), 825-830.

Zhu, S., and Chung, D. D. L. (2007). "Theory of piezoresistivity for strain sensing in carbon fiber reinforced cement under flexure." *J.Mater.Sci.,* 42(15), 6222-6233.

# Appendix A

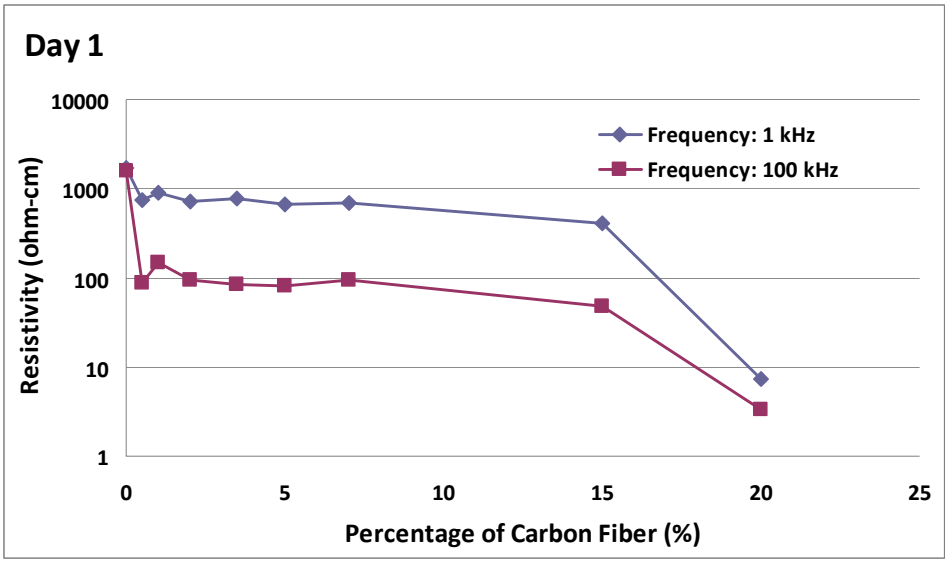


Figure A- 1: Effect of fibre (CPCF) content on electrical resistivity at day 1

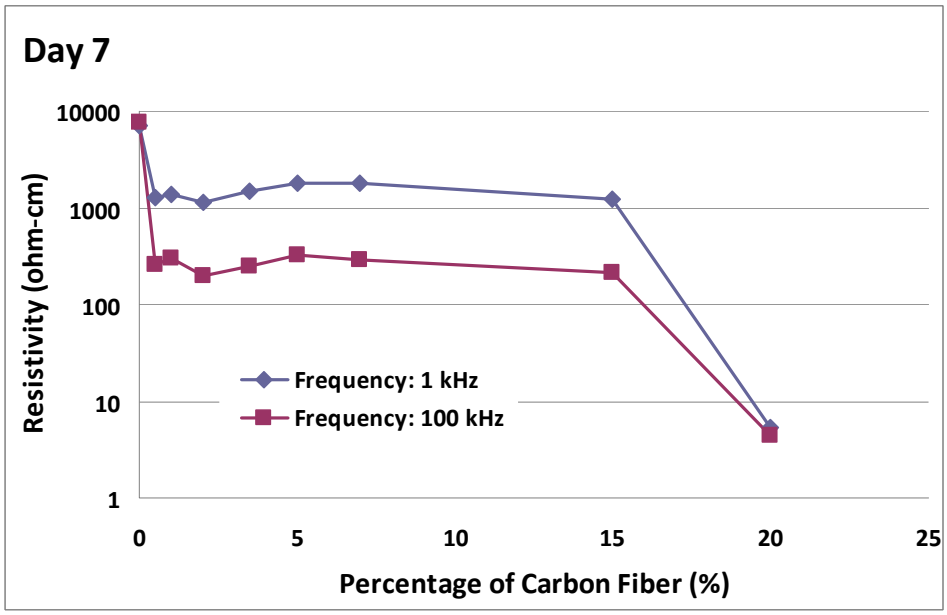


Figure A- 2: Effect of fibre (CPCF) content on electrical resistivity at 7 days

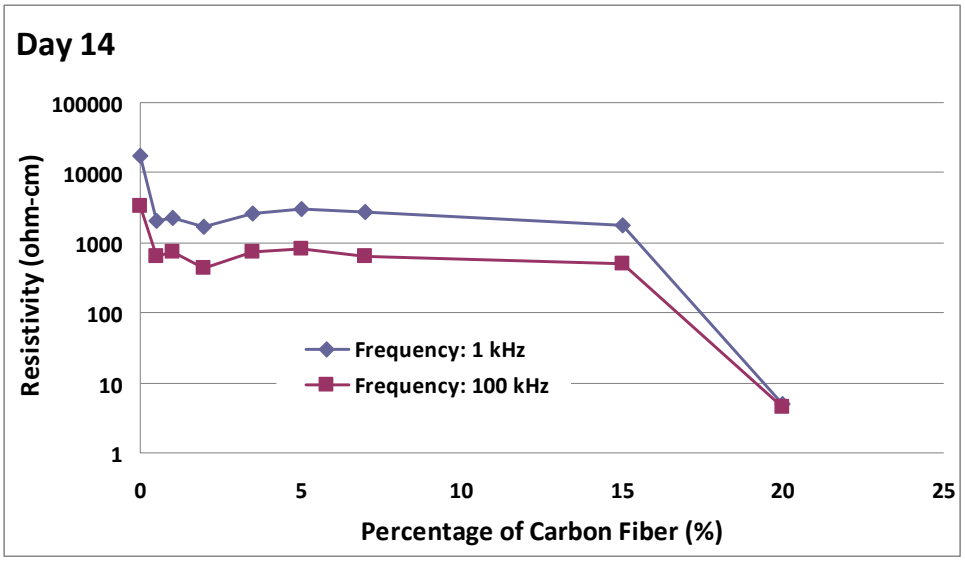


Figure A- 3: Effect of fibre (CPCF) content on electrical resistivity at 14 days

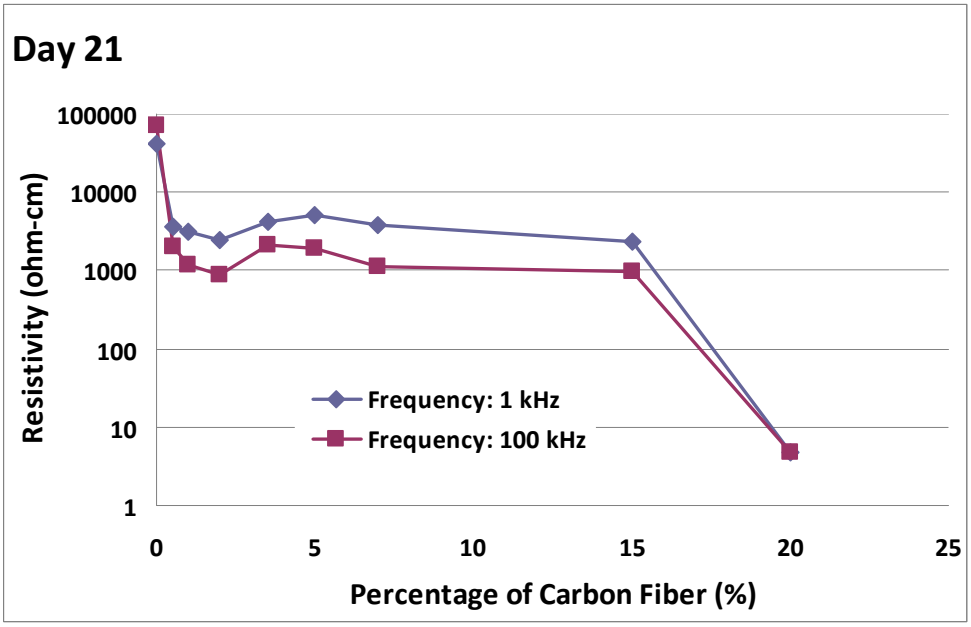


Figure A- 4: Effect of fibre (CPCF) content on electrical resistivity at 21 days

# Appendix B

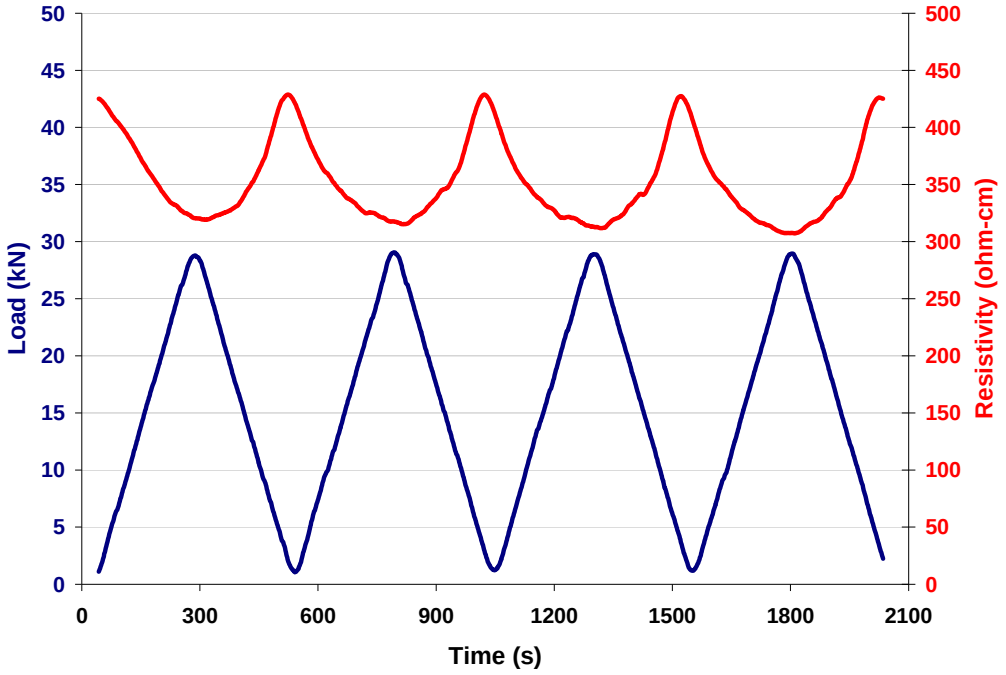


Figure B- 1: Resistivity response of 15% CF sensors to compressive cyclic loading

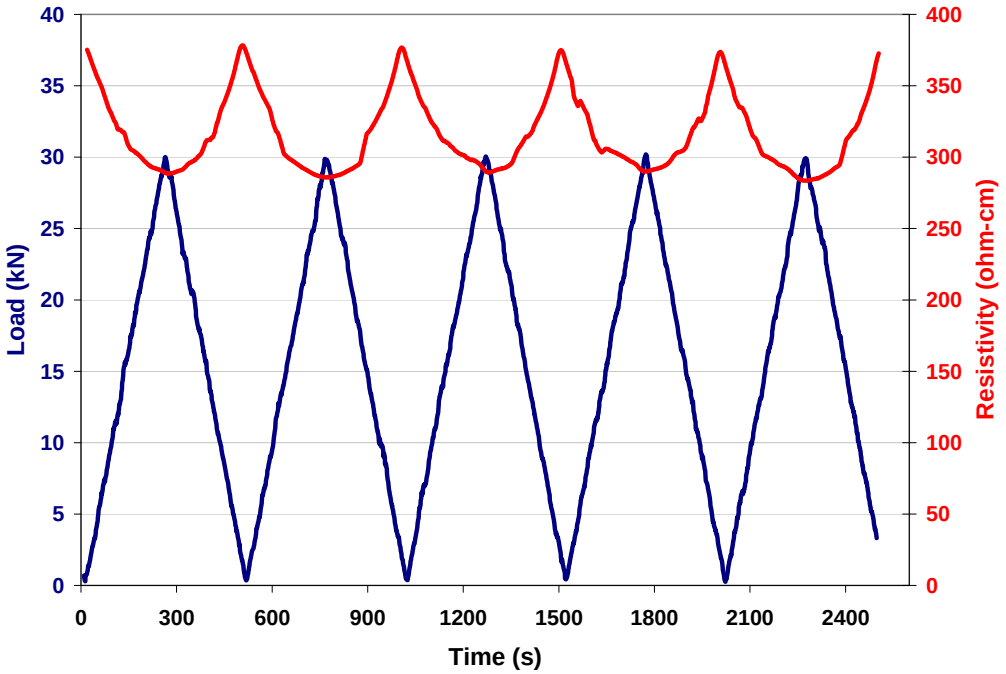


Figure B- 2: Resistivity response of 15% CF + 1% MWCNT sensors to compressive cyclic loading

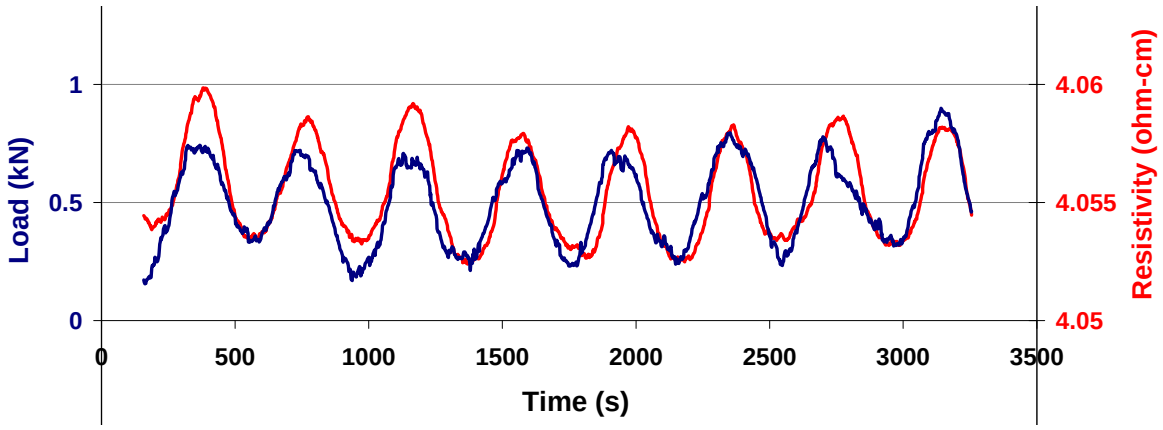


Figure B- 3: Resistivity response of 20% CF sensors to tensile cyclic loading

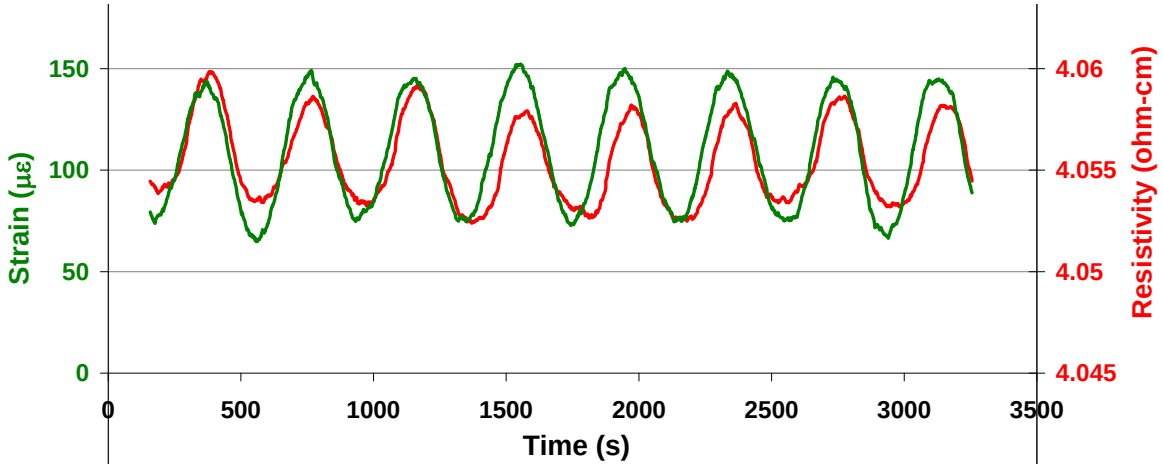


Figure B- 4: Resistivity response of 20% CF sensors to cyclic tensile strain

# Appendix C

# C.1 Material Safety Data Sheet

**1 - Identification of substance:**

Chemical Name: Carbon Nanotubes
Formula: Carbon
Chemical Family: Synthetic Graphite
Synonyms: Carbon Nanotubes
CAS Number: 7782-42-5 (Graphite)

- **Manufacturer/Supplier:**

**Cheap Tubes Inc.**
112 Mercury drive
Brattleboro VT, 05301
802.254.6969

www.cheaptubesinc.com

Revision Date: June 21, 2007

**2 - CNT Composition/Data on components:**

- **Chemical characterization:**
  **Description: (CAS#)**
  Graphite (CAS# 7782-42-5 , 95%)

| Component | % | OSHA/PEL | ACGIH/TLV |
|---|---|---|---|
| Synthetic graphite | Up to 100% | 15 mg/m3 (total dust)<br>5 mg/m3 (respirable fraction) | 2 mg/m3 TWA |
| Metallic impurity | Balance | | |

**3 - CNT Hazards identification**

**Potential CNT Health Effects**

Eye Contact: May cause eye irritation
Skin Contact: No known hazards, but may be mildly irritating
Inhalation: May cause irritation to respiratory tract
Ingestion: No known hazards, but may irritate gastrointestinal tract
Acute and Chronic High concentration of dusts may be irritating to eyes, skin,
Health Effects: mucus membranes and respiratory tract.

- **Information pertaining to particular dangers for man and environment**
  R 36/37 Irritating to eyes and respiratory system.

**4 - CNT First aid measures**

- **After inhalation**
  Remove to fresh air. If required, provide artificial respiration. Keep patient warm. Seek immediate medical advice.

- **After skin contact**
  Immediately wash with water and soap and rinse thoroughly.
  Seek immediate medical advice.

- **After eye contact**
  Rinse opened eye for several minutes under running water. Then consult a doctor.

- **After swallowing** Seek immediate medical advice.

**5 - CNT Fire fighting measures**

Flash Point: Not applicable.
Explosion Limits: Unknown
Extinguisher Medium: Water, Carbon Dioxide, Dry Chemical, or Foam
Special Procedures: None
Decomposition Products: Carbon Monoxide, Carbon Dioxide

Unusual Hazards: Thermal decomposition or combustion may produce dense smoke.

- **Suitable extinguishing agents**

CO2, extinguishing powder or water spray. Fight larger fires with water spray.

- **Special hazards caused by the material, its products of combustion or resulting gases:**

In case of fire, the following can be released:
Carbon monoxide (CO)

- **Protective equipment:**

Wear self-contained respirator.
Wear fully protective impervious suit.

**6 - <u>Accidental CNT release measures</u>**

- **Person-related safety precautions:**

Wear protective equipment. Keep unprotected persons away.
Ensure adequate ventilation

- **Measures for environmental protection:**

Do not allow material to be released to the environment.

- **Measures for cleaning/collecting:** Ensure adequate ventilation.

- **Additional information:**

See Section 7 for information on safe handling
See Section 8 for information on personal protection equipment.
See Section 13 for disposal information.

**7 - <u>CNT Handling and storage</u>**

- **Handling**

- **Information for safe handling:**

Keep container tightly sealed.
Store in cool, dry place in tightly closed containers.
Ensure good ventilation at the workplace.

- **Information about protection against explosions and fires:**

Keep away from bright flashes of light. Flashes of light can cause spontaneous combustion.

- **Storage** – store in light proof packaging

- **Requirements to be met by storerooms and receptacles:**
No special requirements.

- **Information about storage in one common storage facility:**
Store away from oxidizing agents.
Store away from halogens.
Do not store together with acids.

- **Further information about storage conditions:**
Keep container tightly sealed.
Store in cool, dry conditions in well sealed containers.

**8 - CNT Exposure controls and personal protection**

- **Additional information about design of technical systems:**
Properly operating chemical fume hood designed for hazardous chemicals and having an average face velocity of at least 100 feet per minute.

**Components with limit values that require monitoring at the workplace:**

Graphite

| | mg/m3 |
|---|---|
| ACGIH TLV | 2 |
| Belgium TWA | 2.5 |
| Finland TWA | 5 |
| France VME | 2 |
| Germany MAK | 6 |
| Ireland TWA | 5 |
| Korea TLV | 2 |
| Netherlands MAC-TGG | 2 |
| Poland TWA | 2 |
| Sweden NGV | 5 (dust) |
| Switzerland MAK-W | 2.5 |
| United Kingdom | 5-LTEL |
| USA PEL | 15 mppcf |

- **Additional information:** No data

- **Personal protective equipment**

- **General protective and hygienic measures**
  The usual precautionary measures for handling chemicals should be followed.
  Keep away from foodstuffs, beverages and feed.
  Remove all soiled and contaminated clothing immediately.
  Wash hands before breaks and at the end of work.
  Avoid contact with the eyes.
  Avoid contact with the eyes and skin.

- **Breathing equipment:**
  Use suitable respirator when high concentrations are present.

- **Protection of hands:** Impervious gloves

- **Eye protection:** Safety glasses

- **Body protection:** Protective work clothing.

**9 - CNT Physical and chemical properties:**

- **General Information**

- **Form:** Powders

- **Color:** Black

- **Odor:** Odorless

**Value/Range Unit Method**

- **Change in condition**

- **Melting point/Melting range:** 3652-3697 ° C (subl/vac)

- **Boiling point/Boiling range:** Not determined

- **Sublimation temperature / start:** Not determined

- **Flash point:** Not applicable

- **Ignition temperature:** Not determined

- **Decomposition temperature:** Not determined

- **Danger of explosion:**
  Product does not present an explosion hazard.

- **Explosion limits:**

- **Lower:** Not determined

- **Upper:** Not determined

- **Vapor pressure:** Not determined

- **Density:** at 20 ° C ~ 2.1 g/cm³

- **Solubility in / Miscibility with**

- **Water:** Insoluble

**10 - <u>CNTs Stability and reactivity</u>**

- **Thermal decomposition / conditions to be avoided:**
  Decomposition will not occur if used and stored according to specifications.

- **Materials to be avoided:**
  Oxidizing agents
  Acids
  Halogens
  Interhalogens Alkali metals

- **Dangerous reactions** No dangerous reactions known

- **Dangerous products of decomposition:** Carbon monoxide and carbon dioxide

**11 - <u>CNTs Toxicological information</u>**

- **Acute toxicity:**

- **Primary irritant effect:**

- **on the skin:** Irritant to skin and mucous membranes.

- **on the eye:** Irritating effect.

- **Sensitization:** No sensitizing effects known.

- **Subacute to chronic toxicity:**
  The inhalation of graphite, both natural and synthetic, has caused pneumoconiosis in exposed workers. The pneumoconiosis found is similar to coal worker's pneumoconiosis.

- **Additional toxicological information:**
  To the best of our knowledge the acute and chronic toxicity of this substance is not fully known.
  No classification data on carcinogenic properties of this material is available from the EPA, IARC, NTP, OSHA or ACGIH.

**12 - <u>CNTs Ecological information:</u>**

- **General notes:**

Do not allow this material to be released to the environment.

**13 - <u>CNTs Disposal considerations</u>**

- **Product:** Carbon Nanotubes

- **Recommendation**

Consult state, local or national regulations to ensure proper disposal. Specific care should be taken to insure that no carbon nanotubes or carbon nanotube packaging is released into the environment.

- **Uncleaned packagings:**

Consult all state, local or national regulations to ensure proper disposal. Specific care should be taken to insure that no carbon nanotubes or carbon nanotube packaging is released into the environment.

- **Recommendation:**

Disposal must be made according to official regulations.

**14 - <u>CNTs Transport information</u>**

Not a hazardous material for transportation.

- **DOT regulations:**

- **Hazard class:** None

- **Land transport ADR/RID (cross-border)**

- **ADR/RID class:** None

- **Maritime transport IMDG:**

- **IMDG Class:** None

- **Air transport ICAO-TI and IATA-DGR:**

- **ICAO/IATA Class:** None

- **Transport/Additional information:**

Not dangerous according to the above specifications.

**15 - <u>CNTs Regulations</u>**

- **Product related hazard informations:**

This material is listed on the US Toxic Substances Control Act (TSCA) Inventory and the following chemical inventories: Canadian Domestic Substances List (DSL), European Inventory of Existing Commercial Chemical Substances (EINECS), Korean Existing Chemicals List (ECL), Australian Inventory of Chemical Substances (AICS), the Philippines Inventory of Chemicals and Chemical Substances (PICCS), and the Swiss Giftliste 1 Inventory of Notified New Substances. In addition, this substance is not regulated in Japan and excluded from the Japanese Chemical Substances Control Law according to the Japanese Ministry of Economy, Trade and Industry, formerly the Ministry of International Trade and Industry (MITI).

- **Hazard symbols:** Eye Irritant

- **Risk phrases:** 36/37 Irritating to eyes and respiratory system.

- **Safety phrases:**

26 In case of contact with eyes, rinse immediately with plenty of water and seek medical advice.

- **National regulations**
  All components of this product are listed in the U.S. Environmental Protection Agency Toxic Substances Control Act Chemical Substance Inventory.

- **Information about limitation of use:**
  For use only by technically qualified individuals.

**16 - Other CNTs information:**

Employers should use this information only as a supplement to other information gathered by them, and should make independent judgement of suitability of this information to ensure proper use and protect the health and safety of employees. This information is furnished without warranty, and any use of the product not in conformance with this Material Safety Data Sheet, or in combination with any other product or process, is the responsibility of the user.

HAZARDOUS MATERIALS IDENTIFICATION SYSTEM (HMIS)
Health Flammability Reactivity BASIS
1 0 0 Synthetic graphite powder

NATIONAL FIRE PROTECTION ASSOCIATION (NFPA)
Health Flammability Reactivity BASIS
1 0 0 Synthetic graphite powder
**Label Precautions:**
Do not get in eyes, on skin or on clothing.
Do not breathe dust.
Wash thoroughly after handling.
Keep container closed.
Use with adequate ventilation.

**Label First Aid:**
If inhaled, remove to fresh air. If breathing difficulties persist, get medical attention. In
case of contact, immediately flush eyes or skin with plenty of water for at least 15
minutes. If irritation develops or persists, get medical attention.

**Disclaimer:** Cheap Tubes Inc. provides the information contained herein in good faith and makes no representation as to its comprehensiveness or accuracy.

This document is intended only as a guide to the appropriate precautionary handling of the material by a properly trained person using this product. Individuals receiving the information must exercise their independent judgment in determining its appropriateness for a particular purpose. Cheap Tubes Inc. makes no representations or warranties, either express or implied, regarding the suitability of the material for any purpose or the accuracy of the information contained within this document. Accordingly, Cheap Tubes Inc. will not be responsible for damages resulting from use of or reliance upon this information.

Read more: cheaptubes.com carbon nanotubes msds - http://www.cheaptubesinc.com/cntmaterialsafetydatasheet.htm#ixzz0CPd32qJe

# C.2 Inhalation Toxicity Risk of Carbon Nanotubes

*Source: Lam CW, James JLt, McCluskey R and Hunter RL. "Pulmonary toxicity of single-wall carbon nanotubes in mice 7 and 90 days after intratracheal instillation." ToxSci Advance Access published 26, 2003.*

An entire molecular electronics industry is poised to take off, much of it on the back of carbon nanotubes. But new research is raising alarm. Nanotubes are highly damaging to the lungs of mice. Dr. Mae-Wan Ho calls for a moratorium until proper safeguards can be put in place.

Molecular electronics is making headlines. Much of it is based on single-wall carbon nanotubes, which have many other potential applications as strong, lightweight material in the aerospace and defence industries. Nanotubes are now manufactured in bulk. Dr. Smalley (Nobel laureate and a pioneer in carbon nanotube research) predicted that hundreds of thousands of tons of the stuff could be produced in 5 to 10 years and "in time, millions of tonnes of nanotubes will be produced worldwide every year". But enthusiasm for research and development has run way ahead of safety precaution.

Unprocessed nanotubes are very light, and could become airborne and potentially reach the lungs. Researchers in the Space and Life Sciences of NASA Johnson Space Center, Wyle Laboratories, and the Department of Pathology and Laboratory Medicine, University of Texas Medical School, in Houston, Texas,

USA, investigated the toxicity of carbon nanotubes to the lungs, by introducing them into the trachea of mice under anaesthesia.

The results are alarming. Five of the mice treated with high dose of one kind of nanotubes died within 7 days. All nanotube products induced epitheliod granulomas – tumour-like nodules of bloated white blood cells in the lining of the lungs - and in some cases inflammation of the lungs at 7 days. These persisted and became more pronounced in animals that were sacrificed at 90days. The lungs of some animals also showed inflammation around the bronchi, and extensive necrosis (tissue death).

Carbon nanotubes, the researchers conclude, are "much more toxic than carbon black and can be more toxic than quartz, which is considered a serious occupational health hazard in chronic inhalation exposures."

The researchers had used nanotubes produced under different conditions containing different heavy metals. Samples of 'raw' and 'purified' nanotubes both contained iron, while a third nanotube product contained nickel and yttrium.

A suspension containing 0, 0.1 or 0.5 mg of carbon nanotubes was introduced into the trachea of the mice. As added controls, groups of mice were given a suspension of carbon black or of quartz. The mice were killed at 7days or 90days after the single treatment, in order to examine the lungs.

Nanotubes are neither water-soluble nor wettable, and all the products were extremely difficult to disperse; and ultrasound as well as heat-inactivated mouse serum had to be used.

Graphite – the most similar form of carbon to nanotubes - does not possess the electrical properties and fibrous structure of the nanotubes, and its permissible inhalation exposure limit set by the occupational safety and health administration (OSHA) is 15mg/m3 of total dust and 5mg/m3 for the 'respirable' (capable of being inhaled) fractions. It is well known that the geometry and surface chemistry of particulates can play an important role in causing lung toxicity.

All animals treated with 0.1mg per mouse of nickel-yttrium containing nanotubes showed no overt clinical signs. But 5 of 9 mice treated with 0.5mg died: 2/4 within the 7day group and 3/5 in the 90day group. All deaths occurred 4 to 7 days after receiving the nanotubes. Deaths generally preceded by lethargy, inactivity and body-weight losses. These symptoms were also seen in the high dose mice that survived. Mice in the 90day group lost 27% of their body weight by the first week. Symptoms in the two surviving mice disappeared after one week and the animals started to gain weight.

The iron-containing nanotubes (both raw and purified) did not cause deaths in the mice. Mild signs of inactivity, hypothermia, and occasionally shivering were most noticeable 8 to 12h after treatment with the raw nanotubes, and symptoms disappeared soon after this time. There were no body weight losses with the raw or purified iron-containing nanotubes.

Under the microscope, the lungs of dead animals in the high dose group showed large aggregates of particles in macrophages (large white blood cells that 'eat' foreign particles) in the alveolar space (air sac), some of the aggregates were also found in spaces between cells, forming granulomas (tumour-like nodules consisting of the bloated white blood cells). There were also signs of inflammation. Granulomas were not detected in mice given the low dose of the nickel-yttrium nanotubes. The lungs of mice given high dose of either raw or purified iron-containing nanotubes showed prominent granulomas at 7days. Most of these nodules were located beneath the bronchial epithelium (lining) and were present throughout the lung fields. Some appeared to extend into the bronchi as polyps (irregular growths) .

The granulomas consisted of macrophages laden with black particles, and had very few other white blood cells. Some of the lungs from mice given high doses of the nanotubes appeared grossly abnormal at 90 days. The lung lesions were generally more pronounced than those given the high dose at 7 days; some also had necrosis (tissue death), and extensive inflammation. Granulomas and other

pulmonary lesions were also seen in some of the mice given the lose doses of nanotubes, but to a milder degree.

Heat inactivated serum did not produce any clinical signs, nor gross or microscopic lesions. The mice of the carbon black or quartz treated controls also did not show any clinical signs that could be attributed to treatment. Quartz at high dose (0.5 mg) induced an increase in the number of macrophages in the lungs, and some of these cells contained particles. Quartz also produced mild to moderate inflammation. The results for the 7day and 90day groups were generally similar. One mouse in the 7day group had a low-grade granuloma reaction; and the mice in the high dose 90day group had increased clusters of lymphocytes surrounding the bronchi (sign of inflammation).

Purified nanotubes contained only a small amount of metal (2% by weight). Insoluble iron and iron compounds are low in toxicity, so the results strongly indicate that the nanotubes themselves induced the granulomas. Another research group had found similar results previously in rats. The deaths of 5 mice may have been caused by nickel and yttrium in the nanotube sample, as they did not occur in the other samples of nanotubes.

One of the major effect of nanotubes is that they moved rapidly through the walls of the air sacs, in contrast to carbon black. Nanotubes are totally insoluble and nonbiodegradable fibres, and it is well known that the pathogenicity of a fibre in the lungs directly correlates with its persistence.

Graphite toxicity is known as graphite pneumoconiosis, characterized by granulomas, emphysema, tissue death and hardening of the blood vessels, among other symptoms, and has been long recognized in a large number of workers involved in mining and processing graphite. But theses nanotube samples did not contain graphite.

These results show that a single exposure is enough to trigger serious effects including deaths. No safety tests have yet been carried out, especially in the longer-term, on a range of other nanoparticles used, some of them in intended

medical procedures. Civil society watchdogs such as the ETC Group have called for a moratorium on nanotechnology research and development.

The present findings certainly justify a moratorium on research involving nanotubes, if not all nanoparticles, until proper safeguards can be put in place, and safety tests carried out in the meantime.